University of Stavanger

Faculty of Science and Technology

MASTER'S THESIS

Study program/Specialization: Petroleum Geosciences Engineering	Spring semester, 2017 Open
Author: Eirik Oppedal	(Author's signature)
Faculty supervisor: Chris Townsend	
Title of thesis: Rift Segmentation: structural mapping of syn-rift successions between the Kerpini-Tsivlos and Mamoussia-Pirgaki Faults, Greece	
Credits (ECTS): 30	
Keywords: Greece Corinth Rift Syn-rift Kerpini-Tsivlos Fault Mamoussia-Pirgaki Fault Half-graben Structural Geology Transfer Faults	Number of pages: …… + enclosure: …… Stavanger, 15.06.2017

Rift Segmentation: structural mapping of syn-rift successions between the Kerpini-Tsivlos and Mamoussia-Pirgaki Faults, Greece

By

Eirik Oppedal, BSc.

Master's Thesis

Presented to the Faculty of Science and Technology

The University of Stavanger

The University of Stavanger

June 2017

Acknowledgements

I would like to express my sincere gratitude to my supervisor Chris Townsend for his continuous support and guidance. His knowledge of the Corinth Rift and experience in the field has been invaluable during the field trips. I would also like to thank my co-supervisor Alejandro Escalona for his feedback during the semester. Further thanks go to my colleagues, Asbjørn Veiteberg and Herman Birkeland, for their company and encouragement throughout the entire project.

Abstract

Rift Segmentation: structural mapping of syn-rift successions between the Kerpini-Tsivlos and Mamoussia-Pirgaki Faults, Greece

Eirik Oppedal

The University of Stavanger

Supervisor: Chris Townsend

The Corinth Rift of Central Greece is currently active in the Gulf of Corinth. A series of rotated fault blocks from the early rift stages are preserved onshore in the southern part of the rift. These are well-exposed in incised river valleys, allowing detailed studies of normal faulting and associated syn-rift sedimentation. The study area for this project is limited between the Kerpini-Tsivlos and Mamoussia-Pirgaki Faults. This is an area where lateral correlation of faults and sedimentary packages is challenging, evident by a great variety in previous interpretations. Several major faults cannot be traced directly across the river valleys, and there is an ongoing debate about whether these faults terminate or are displaced laterally by relay or transfer structures. Through detailed structural mapping assisted by 3D modelling software, this study has investigated the along-strike continuity of faults and depocentres. Furthermore, it has investigated the relative age relationships between faulting and sedimentation in order to contribute to the understanding of the rift evolution.

Extensive NNE-SSW trending intervals of miscorrelation are identified in three different river valleys, indicating the presence of underlying transfer faults which are perpendicular to the graben-bounding faults. The transfer faults are segmenting the rift, and significant variations in bedding geometry/dip and fault throw between individual segments suggest that they have evolved individually. The structural evolution of the Corinth Rift is thus more complex than previously assumed. Fault activity in the early rift stages was broadly distributed across a number of faults, and the southern rift margin has generally migrated northwards through time.

Table of Contents

List of figures

List of tables

Chapter 1 – Introduction

The interaction between the African and Anatolian tectonic plates initiated back-arc extension in the Oligocene (Jolivet *et al.*, 1994; Le Pichon & Angelier, 1979), which resulted in the development of several active rifts. The Corinth Rift of Central Greece is one of them. It is among the world's most active rifts, and initiated some 5 million years ago (Doutsos & Piper, 1990; Leeder *et al.*, 2008; Ori, 1989). A series of ESE-WNW striking rotated fault blocks from the early stages of this rift is preserved in the northern Peloponnese Peninsula, south of the Gulf of Corinth. Incisive north-trending river valleys provide exposures of these fault blocks, as they cut near perpendicular to strike of the main structures. This allows for detailed studies of normal faulting and associated syn-rift sedimentation, and it provides a unique opportunity to understand the development of ancient rift systems. Furthermore, this area can be used as an extensional basin analogue for hydrocarbon exploration (e.g. on the Norwegian Continental Shelf). The northern Peloponnese has thus been studied and mapped in various detail (Collier & Jones, 2004; Dahman, 2015; Ford *et al.*, 2013; Hadland, 2016; Rohais *et al.*, 2007; Sigmundstad, 2016; Skourtsos & Kranis, 2009; Stuvland, 2015; Syahrul, 2014; Wood, 2013), and as a result, several different interpretations of the evolution and current structural-stratigraphic configuration of the rift system have developed.

The study area for this project is limited between the Vouraikos and Krathis River Valleys. Approximate southern and northern boundaries are the Kerpini-Tsivlos and Mamoussia-Pirgaki Faults respectively. This is an area where outcrops and elevated viewing points are not easily accessible, and it is yet to be mapped in detail. Lateral correlation of faults and sedimentary packages is challenging, evident by a great variety in previous interpretations. Several major faults cannot be traced directly across the river valleys, and there is no wide agreement on whether individual faults simply terminate in the valleys, or are linked to parallel faults by relay or transfer structures. Even though most recent publications acknowledge the presence of fault-linking structures in the Corinth Rift, there has been little emphasis on understanding how abundant and extensive the structures are (some exceptions: Dahman (2015); Ford *et al.* (2016); Ford *et al.* (2013); Wood (2013)).

The purpose of this study is firstly to investigate the E-W continuation of faults and depocentres in the study area through detailed structural mapping combined with 3D modelling software. Secondly, it aims to present evidence for the relative age relationships between faulting and sedimentation in order to contribute to the understanding of the rift evolution.

1.1 Geological framework

1.1.1 Regional geology

The tectonic setting in the Eastern Mediterranean Sea is influenced by the interaction of the African, Anatolian, Eurasian and Arabian Plates (Figure 1). The Gulf of Corinth is located in the north-western part of the Anatolian Plate. This plate is bounded by the Hellenic Trench in the southwest (where the African Plate is subducting below the Anatolian Plate), by the right lateral North Anatolian Fault in the north (which separates it from the Eurasian Plate), and by the left lateral East Anatolian Fault in the east (which separates it from the Arabian Plate). The Anatolian Plate can be subdivided into the smaller Aegean and Anatolian Plates (Jackson, 1994), but the boundary between them is not entirely agreed upon. Papazachos (1999) defines it in Western Turkey, while (Scott, 1981) infers it below the Mediterranean Sea.

The tectonic evolution of the Eastern Mediterranean Sea is dominated by two main factors:

1. North-eastward subduction of the African Plate at the Hellenic Trench
2. Northward continental collision of the Arabian Plate into the Anatolian Plate in Eastern Turkey (Taymaz *et al.*, 2007)

The continental collision forces an anti-clockwise rotation of the Anatolian Plate along the East and North Anatolian Faults, pushing it west-southwest towards the Hellenic Trench. Back-arc extension in the Aegean Sea and Southern Greece is a result of slab pull related to the Hellenic subduction, and the anti-clockwise rotation of the Anatolian Plate. The back-arc extension initiated in the Oligocene (Gautier *et al.*, 1999; Jolivet *et al.*, 1994; Le Pichon & Angelier, 1979), while the rotation of the Anatolian Plate initiated in the Pliocene (Armijo *et al.*, 1996).

Within the Anatolian extensional system, the Corinth Rift is the most active among a number of WNW-ESE trending rifts. Based mainly on micropaleontological dating, its initiation is estimated to be at around 5 Ma (Doutsos & Piper, 1990; Leeder *et al.*, 2008; Ori, 1989). The Corinth Rift was superimposed on Hellenide thrust sheets which where emplaced westwards during the Cretaceous to Miocene (Richter, 1976).

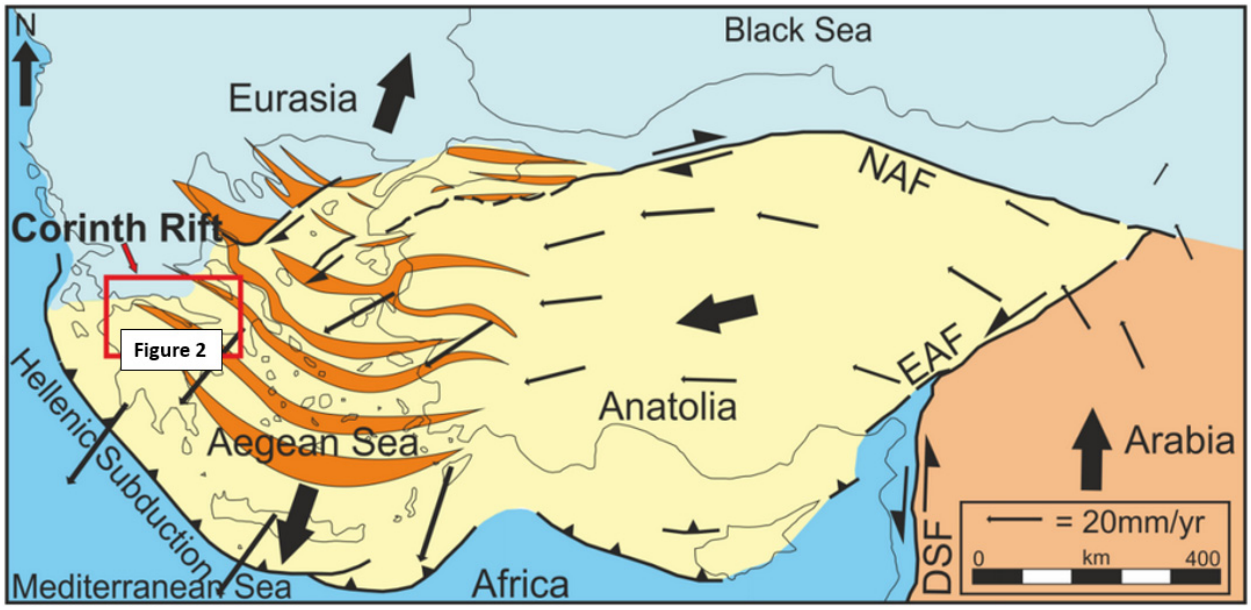

Figure 1: Tectonic plate configuration in the Eastern Mediterranean Sea. Black arrows indicate the direction of plate movement. Modified after Wood (2013).

1.1.2 Structural and stratigraphic overview

The Gulf of Corinth is a 115 kilometre WNW-ESE oriented elongated graben, separating the Peloponnese Peninsula in the south from mainland Greece in the north (Figure 2). Its northern margin is dominated by south-dipping faults, and its southern margin by north-dipping faults. The rift system is currently active in the Gulf of Corinth, while inactive faults from the early rift stages are preserved onshore in the northern Peloponnese Peninsula (Figure 3). The early rift is characterized by a series of rotated fault blocks with associated (syn-rift) sedimentary infill in half-grabens (Figure 4). Incised river valleys (trending SSW-NNE) provide excellent exposures of these fault blocks, as they cut perpendicular to the strike of the main structures. This allows for detailed studies of the entire southern rift margin, from the town of Kalavryta in the south to the Gulf of Corinth in the north. All the major graben bounding faults are north-dipping, with dip angles in the range of 40-60°.

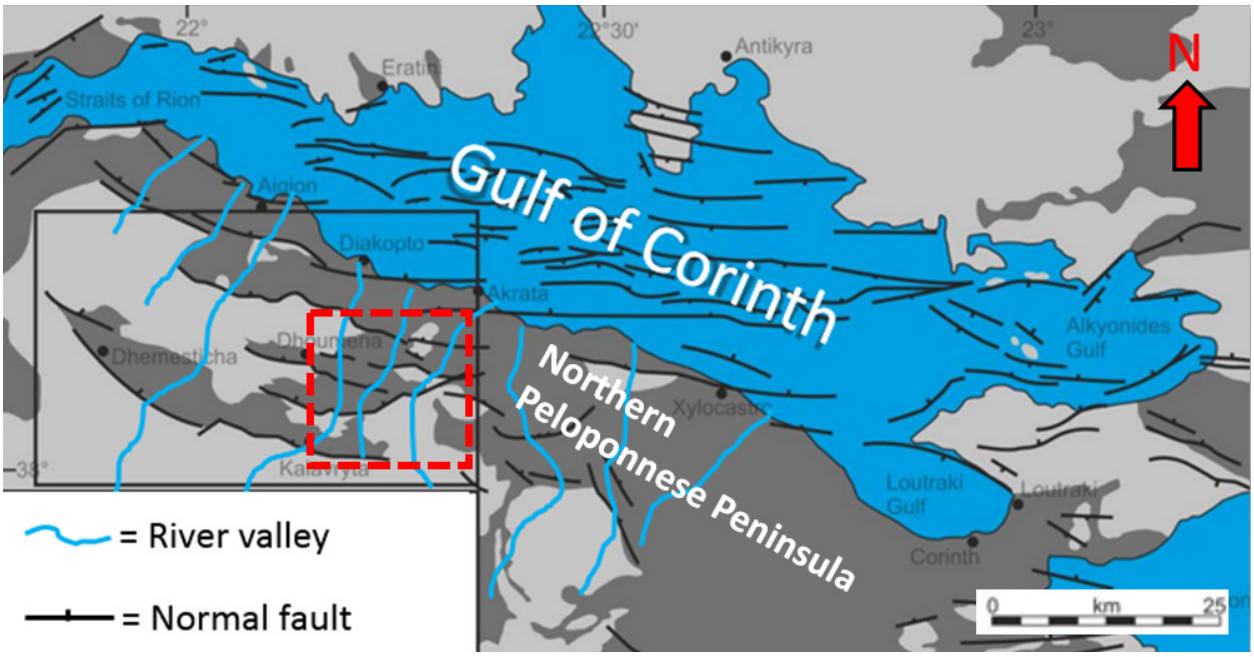

Figure 2: Structural overview of the Corinth Rift and its southern margin. The study area is marked with a red box. Modified after Wood (2013).

In the Kalavryta area, the so-called Pindos thrust sheet constitutes the dominant pre-rift stratum. It is mostly composed of Upper Triassic-Jurassic, highly deformed, metamorphosed carbonates (Skourlis & Doutsos, 2003), and is one of several Hellenide thrust sheets which were emplaced westwards during the Cretaceous to Miocene. The younger syn-rift infill is described in various detail by several researchers. A publication by Ford *et al.* (2013) describes the southern rift margin

as a whole, with the aim to understand the tectono-sedimentary evolution of the Western Corinth Rift. They have classified three main stratigraphic groups (Figure 5) within the syn-rift deposits:

Lower Group: The Lower Group is dominant in the southern part of the rift, extending from the Kalavryta Fault Block in the south to the Mamoussia-Pirgaki Fault Block in the north. It consists generally of (terrestrial) coarse conglomeratic fluvial/alluvial to fine-grained lacustrine successions.

Middle Group: While the Lower Group is characterized by terrestrial deposits, the Middle Group consists of alluvial and Gilbert-type fan deltas that have prograded northwards into a brackish/marine environment. Laterally equivalent distal turbidites and hemipelagic suspension deposits can be found alongside the prograding deltas. The Middle Group is separated from the Lower Group by an erosional unconformity, and it is dominantly confined to the Mamoussia-Pirgaki Fault Block. Smaller portions of the hemipelagic and turbiditic deposits extend northwards to the Helike Fault Block.

Upper Group: The Upper Group is mainly deposited offshore, and it includes the sediments currently being deposited in the active part of the rift. Onshore it is characterized by conglomeratic Gilbert-type deltas, concentrated along the hangingwall of the Helike Fault where they unconformably overlie the Middle and Upper groups and build into the Gulf of Corinth.

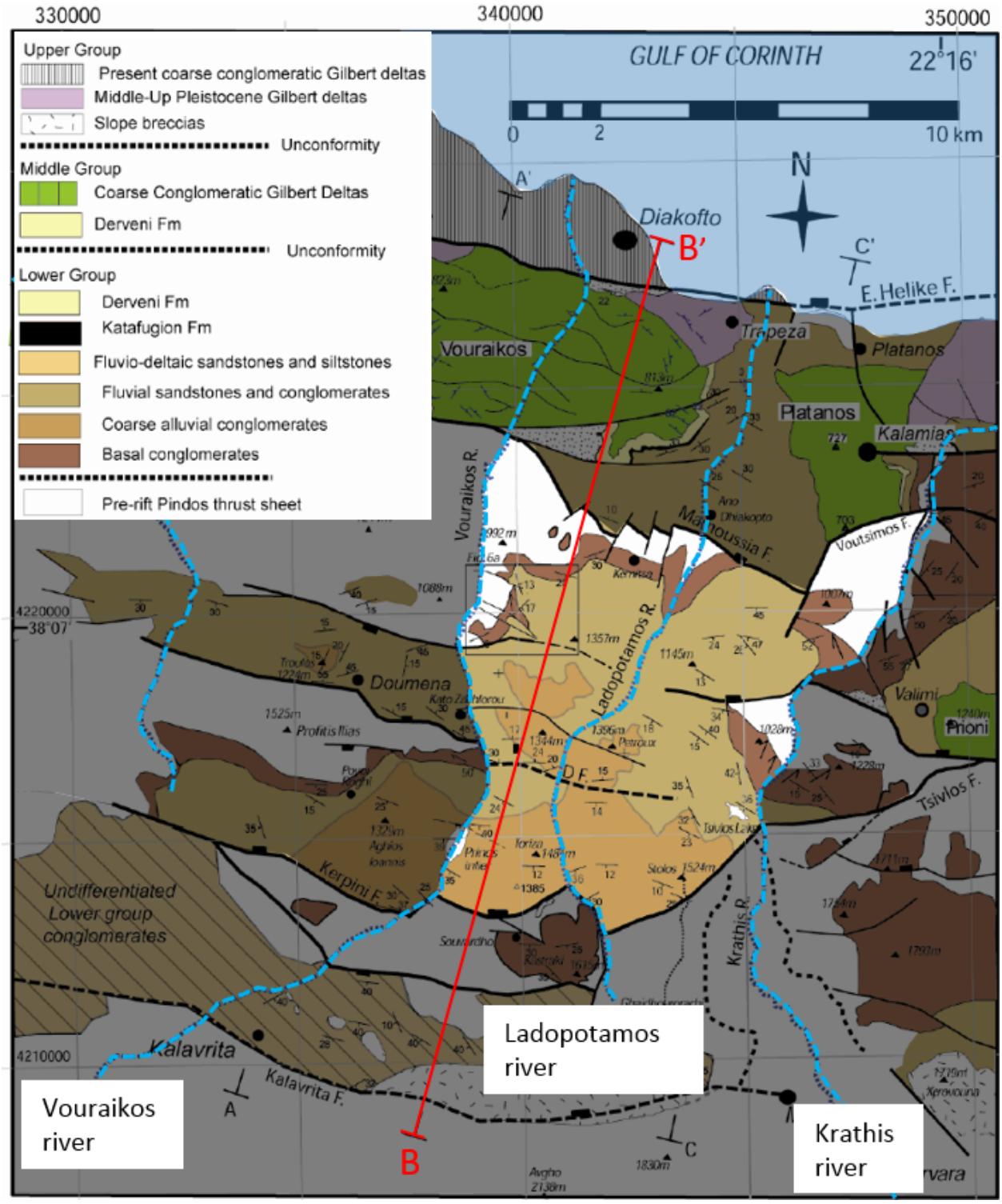

Figure 3: Structural map of the central northern Peloponnese Peninsula. The study area is highlighted in brighter colours. Cross section B-B` is displayed in Figure 4. Modified after Ford et al. (2010).

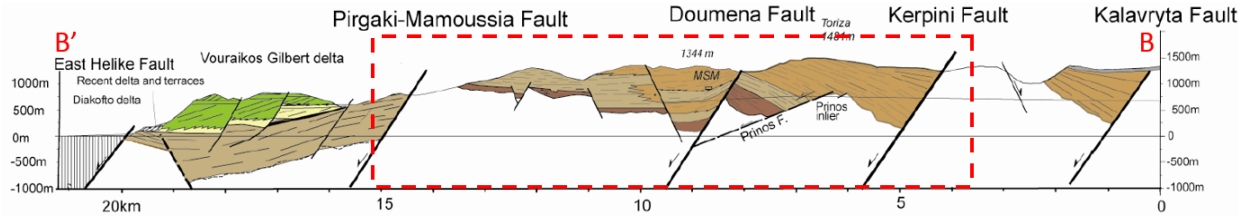

Figure 4: Cross section B-B`from Figure 3. The study area is marked with a red box. Modified after Ford et al. (2010).

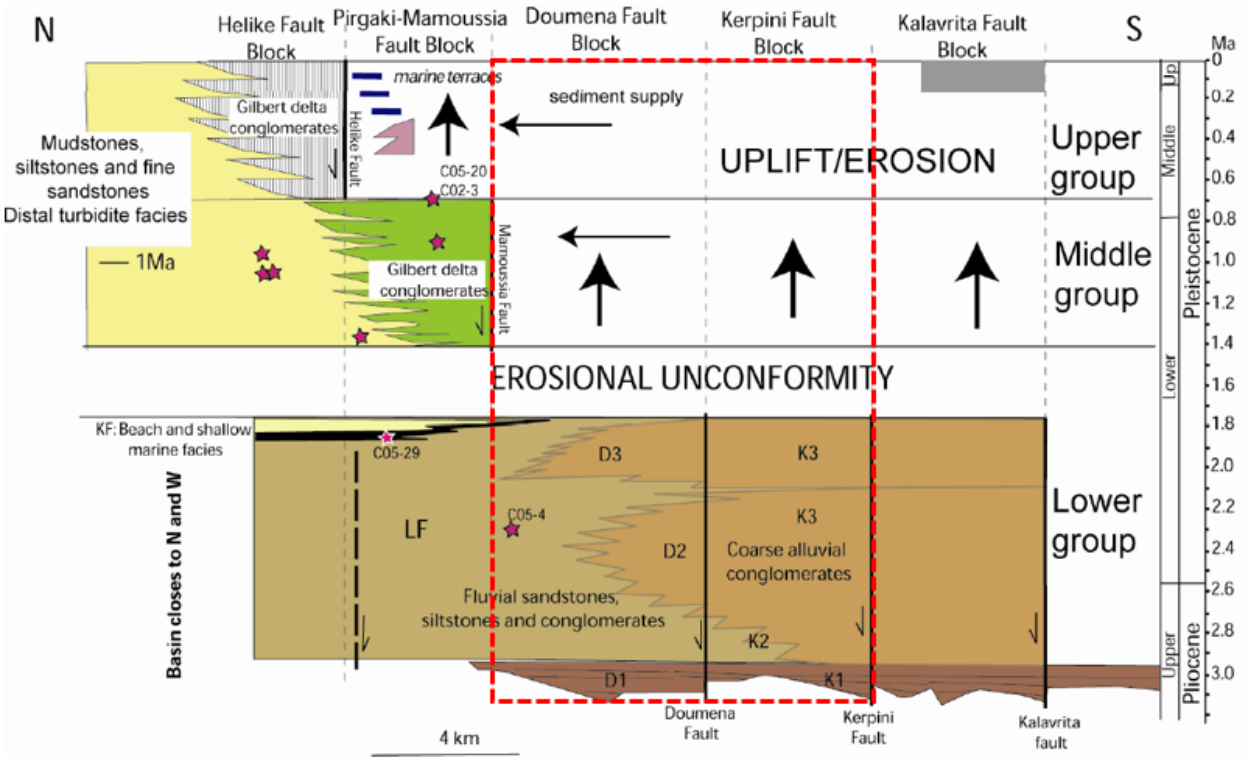

Figure 5: Wheeler diagram showing the stratigraphic correlations along the N-S profile in Figure 4. The study area is marked in a red box. Modified after Ford et al. (2010).

1.2 Previous work

The geometry of the Corinth Rift has been subject to debate for decades. Doutsos and Piper (1990) proposed that the normal faults in the Peloponnese Peninsula are of a listric nature, but the lack of evidence supporting such a model have seen most researchers favour a planar fault model (e.g. Ford *et al.* (2013); Moretti *et al.* (2003); Rohais *et al.* (2007); Westaway (2002)). Doutsos and Poulimenos (1992) suggested that the normal faults at the surface link to an underlying major low-angle normal fault. Later, Flotté and Sorel (2001) and Chery (2001) developed on that idea, and proposed that the rift is underlain by a north-dipping crustal detachment fault which is exposed in the southernmost part of the rift system (Chelmos Fault, Figure 6). Studies of focal mechanisms (Rietbrock *et al.*, 1996) from the Aigion earthquake in 1995 have also been used to support a model involving an active low-angle crustal detachment, as the cluster of recorded micro earthquakes show a north-dipping zone of seismicity below the gulf. A dominance of north-dipping faults and the suggested detachment has raised the question as to which the rift is symmetrical or asymmetrical (e.g. Jolivet *et al.* (2010); McNeill *et al.* (2005); Moretti *et al.* (2003))

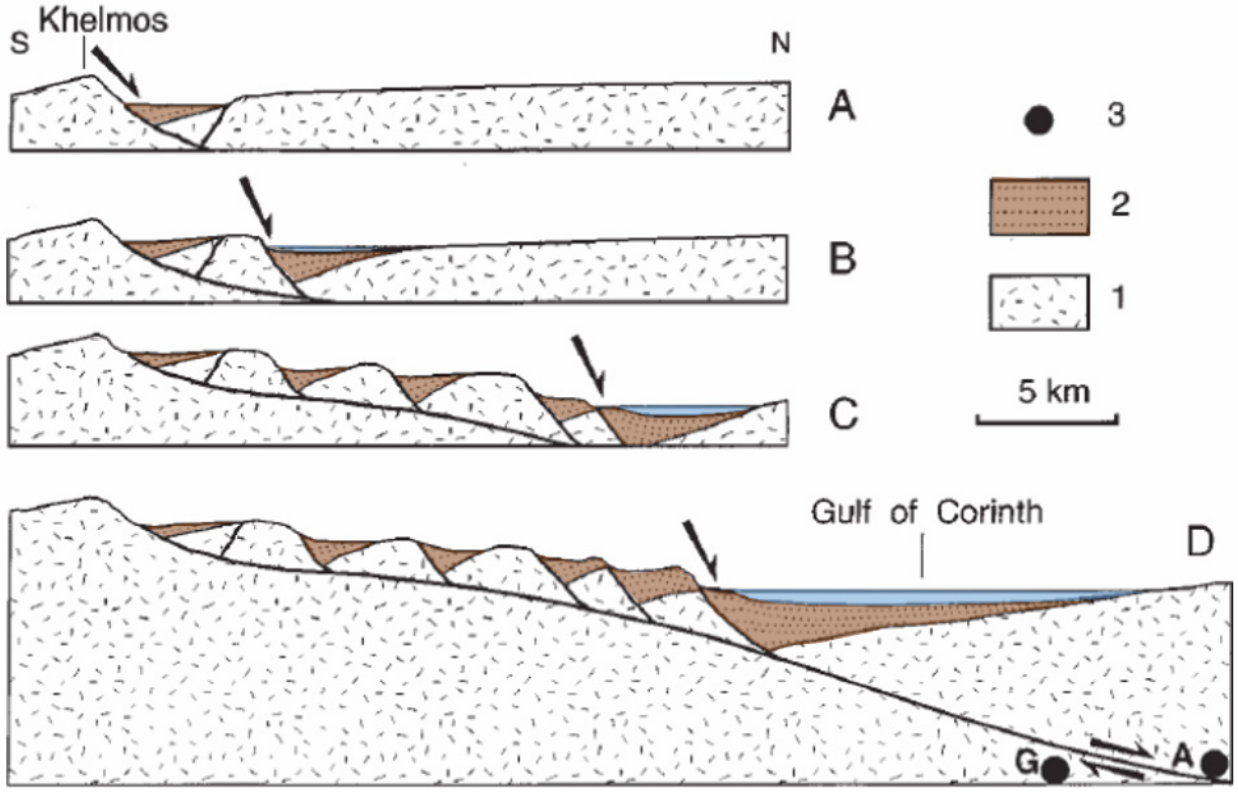

Figure 6: Evolution of the Corinth Rift in four steps, showing a northward fault propagation and the proposed linkage to the Chelmos detachment fault. 1: Basement rock. 2: Syn-rift sediments. 3: Micro earthquakes from Rietbrock et al. (1996), recorded 15 km west of this cross section. Modified after Sorel (2000).

The Corinth Rift system is segmented, evident by large (up to kilometre-scale) steps of major faults along approximately N-S trends. Ghisetti and Vezzani (2005) suggest that the rift segmentation is controlled by pre-existing structures in the underlying pre-rift Pindos Basement. Steps are especially prominent in river valleys, where several faults cannot be directly correlated across. There is so far no wide agreement on whether individual faults simply terminate in the valleys, or are linked to parallel faults by relay or transfer structures (conceptual models: Figure 7 and Figure 8). Both structures are identified in other rift systems, e.g. the Rio Grande Rift (Mack & Seager, 1995), the Reconcavo Graben (Milani & Davison, 1988), the Suez Rift (Moustafa, 1996) and the East African Rift (Morley *et al.*, 1990).

Ford *et al.* (2013) propose that each fault step is caused by an individual cross fault (e.g. in their Kerpini and Mamoussia Faults, Figure 3) or relay zone. The latter is supported by Wood (2013). Dahman (2015) identified an extensive N-S interval of miscorrelation in Vouraikos River, and prefers a model involving several kilometres long transfer faults (Figure 9).

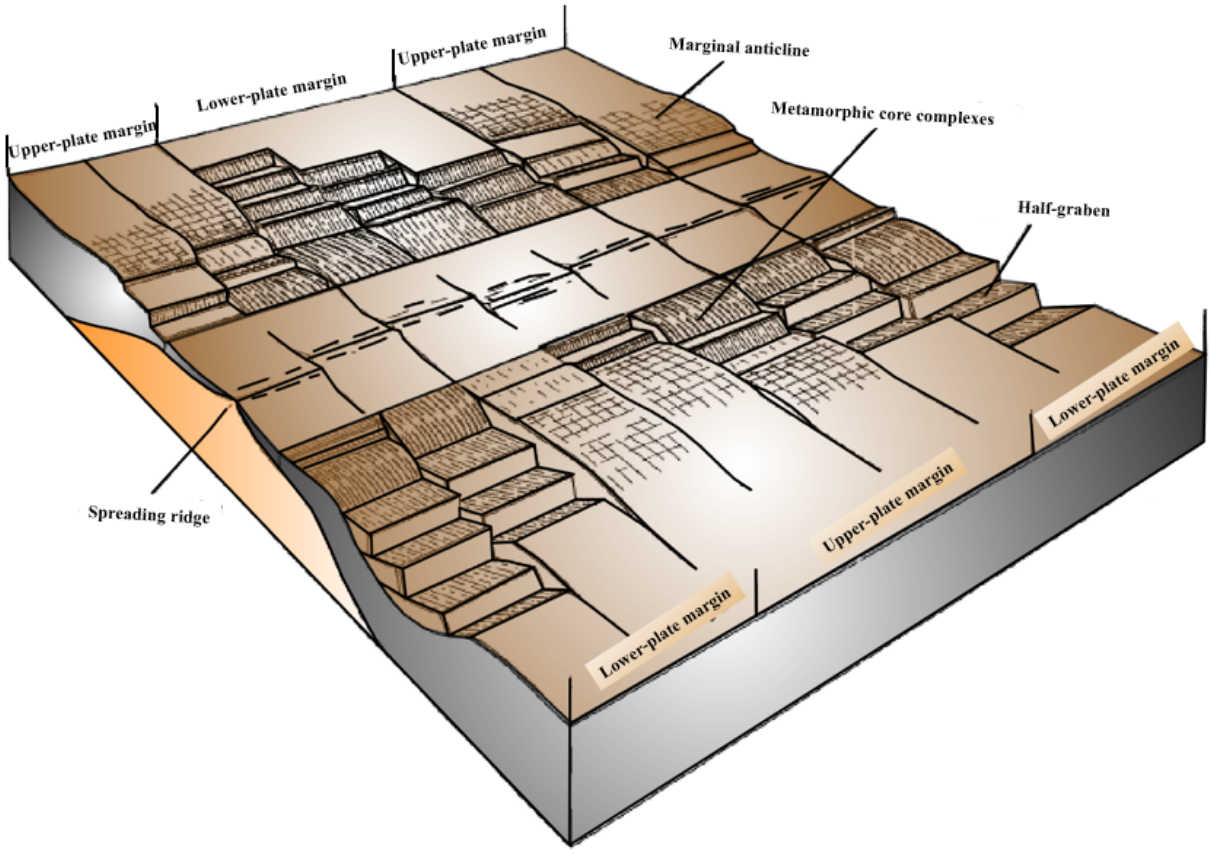

Figure 7: Conceptual model of transfer faults in a developing rift. Modified after Lister et al. *(1986).*

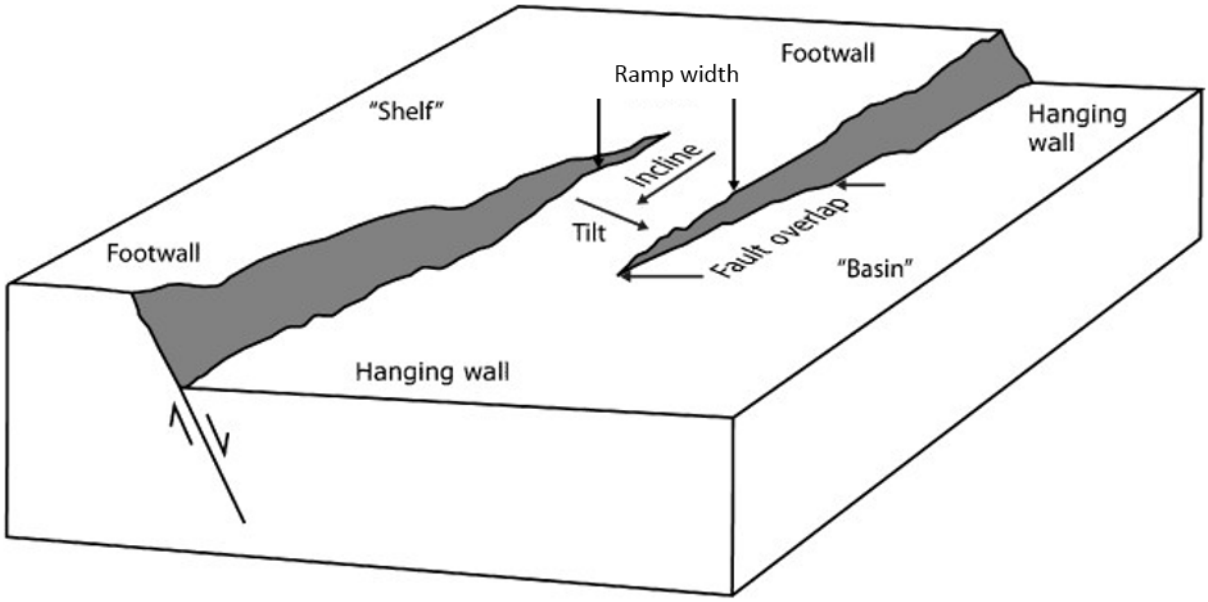

Figure 8: Conceptual model of a relay ramp. Modified after Athmer et al. *(2010).*

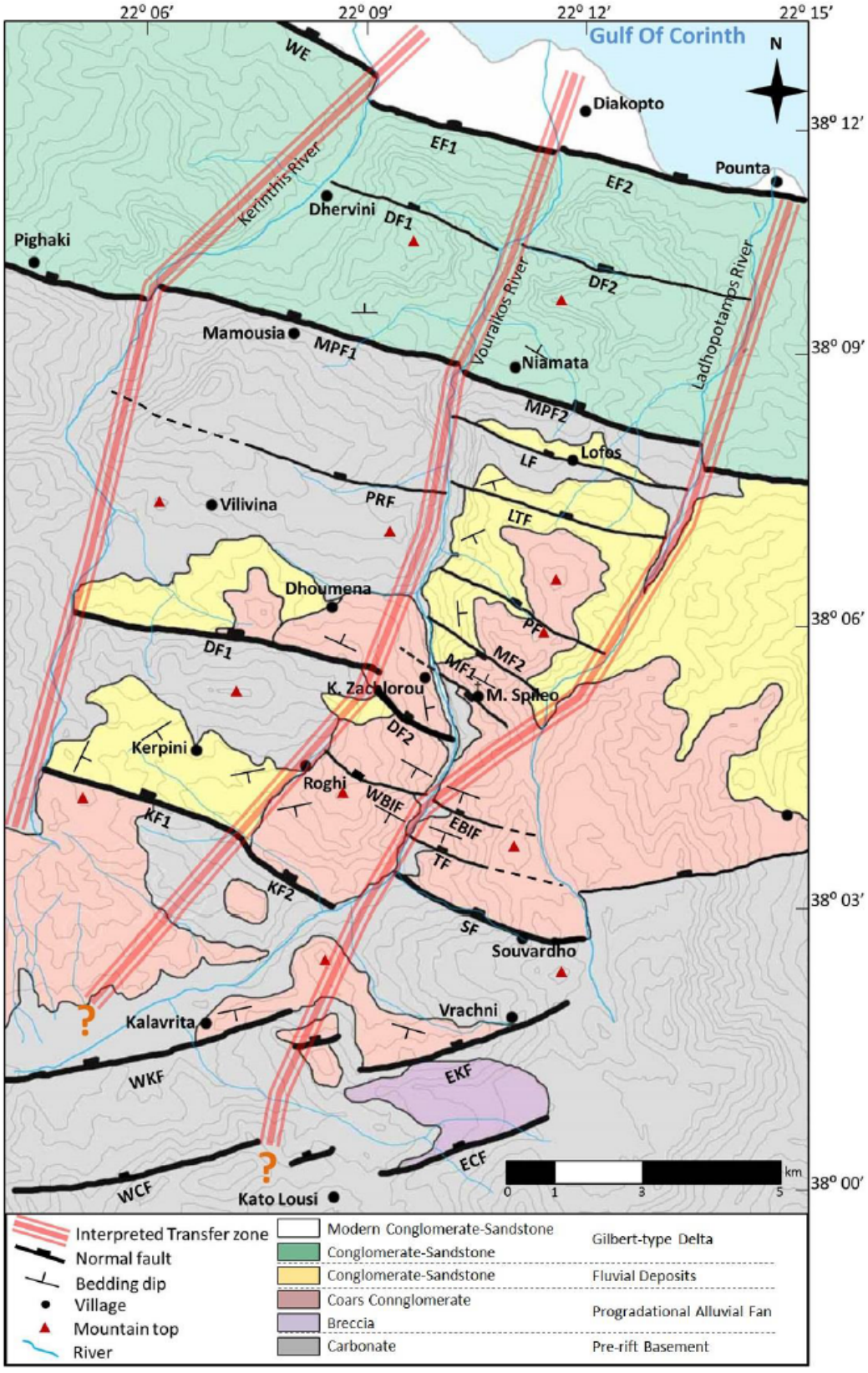

Figure 9: Structural map by Dahman (2015) with extensive N-S transfer faults.

A general consensus has been reached on the idea of northward migration of fault activity (Ori, 1989; Sorel, 2000; Collier and Jones, 2003; Flotté *et al.*, 2005; Ford *et al.*, 2013), from presently inactive faults south of the town of Kalavryta to the active rift in the Gulf of Corinth. This implies that the syn-rift sediments are progressively younger towards the Gulf of Corinth. Although the general northward migration is agreed upon, the relative timing between individual faults remains unclear.

Sorel (2000) suggests a sequential northward fault migration, where the displacement of an abandoned fault is always transferred to a fault further north (Figure 6). This is disputed by other authors (Collier & Jones, 2004; Rohais *et al.*, 2007) who propose a model where fault activity is distributed across several active faults (Figure 10), where the "zone" of active faults propagate northwards. This model involves simultaneous syn-rift deposition in different half-grabens. Based on U/Th dating, Causse *et al.* (2004) suggest that the Dhoumena Fault was active at around 0.125 Ma. This is significantly out of sequence with the model by Sorel (2000), and potentially supports the model by Collier & Jones (2004) and Rohais *et al.* (2007).

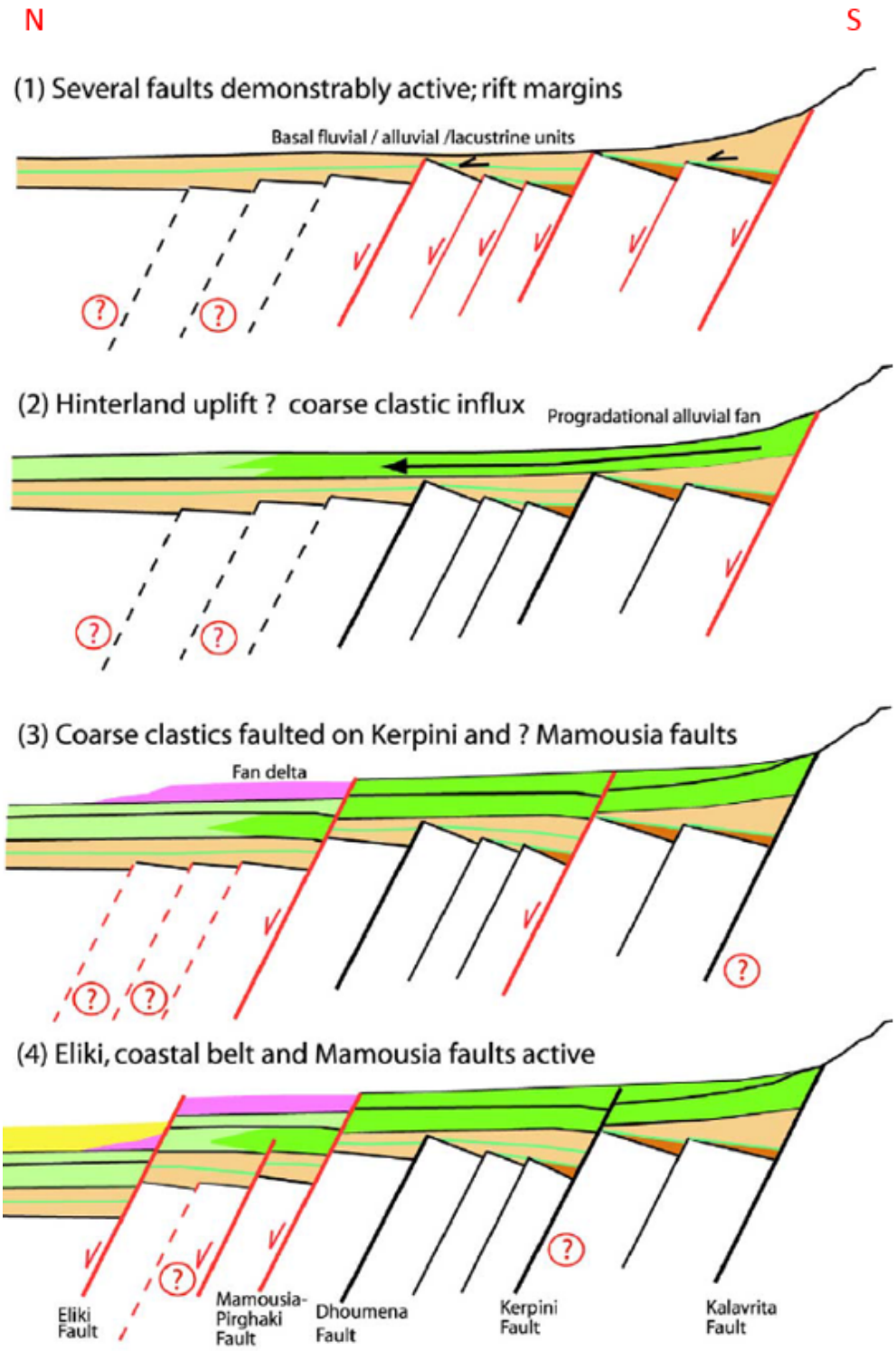

Figure 10: Evolution of the southern margin of the Corinth Rift. Modified after Collier and Jones (2004).

1.3 Thesis motivation and objectives

The Corinth rift serves as an important analogue for structural uncertainty in hydrocarbon exploration (in extensional basins, e.g. on the Norwegian Continental Shelf). The geometries of faults and the linkages between them control the distribution of hanging wall reservoirs. The way a fault is extrapolated along strike heavily influences reservoir volumes and the distribution of facies. Fault discontinuities (i.e. steps), as seen in the northern Peloponnese Peninsula, are not easily identifiable on 2D seismic during exploration. When not identified, the volumes of a prospect can be overestimated as displacement minima related to relay and transfer structures often define structural spill points. Being able to predict/identify along-strike discrepancies would thus have significant implications for the economic viability of a prospect. Furthermore, insight in the evolution of rift systems is critical for understanding the timing of petroleum system elements in an exploration setting.

The purpose of this study is firstly to investigate the E-W continuation of faults and depocenters in the study area through detailed structural mapping. Secondly, it aims to present evidence for the relative age relationships between faulting and sedimentation in order to contribute to the understanding of the rift evolution. All the objectives for the thesis are defined as follows:

- Make a detailed interpretation of 5 valley sections, and investigate the correlation between them.
- Determine the direction of sediment transport (paleo flow) within different lithologies, and consider their source area and down-stream rock equivalents.
- Compile structural and stratigraphic evidence in order to establish relative age relationships.
- Construct a 3D structural-stratigraphic model describing the present day configuration.
- Propose a structural-sedimentary evolution model of the study area.

Chapter 2 – Methodology

The methodology for this project can be divided into three parts; pre-fieldwork, fieldwork and post-fieldwork.

2.1 Pre-fieldwork

In order for the field trips to be as rewarding as possible, and for the objectives to be met, thorough preparations were made. Published literature was review in order to identify locations of particular interest, and to get a general understanding of the different existing interpretations. A preliminary structural map based on the reviewed literature was made prior to the first field trip in July/August, providing an overview of what should be investigated. Hiking and driving routes for each day were also prepared, ensuring no time was wasted in the field. Prior to the second field trip (April, 2017) an evaluation of the data from the first trip was done, uncovering lacking data and new areas of interest.

2.2 Fieldwork

The fieldwork was carried out over a total of 25 days, and consisted of collecting data in the form of:

• Sedimentological descriptions of outcrops.

• Photos and sketches of valley exposures (including use of a DJI Phantom 3 Drone equipped with camera).

• Locations of faults and lithological contacts.

• Strike and dip measurements of faults, bedding planes and unconformities.

• Paleo current measurements from imbrication, cross bedding and channel geometries.

The main focus during the first field trip was to describe the valley exposures as detailed as possible, in order to have a solid initial framework of the study area. The second field trip consisted of mapping specific areas between the valleys in greater detail, to test the theories developed in the months after the first trip.

The syn-rift sediments were briefly described, and differentiated based on sedimentological characteristics such as bed thickness, clast size, roundness, sphericity, sorting, grading and

preferred clast orientation. The clast size is estimated by measuring the long axis of the 10 largest clasts within a square metre which is representative for the unit being described. The average measurement of 5-10 square metres is the clast size presented in this thesis. The clast sphericity and roundness are described according to the definition in Figure 11.

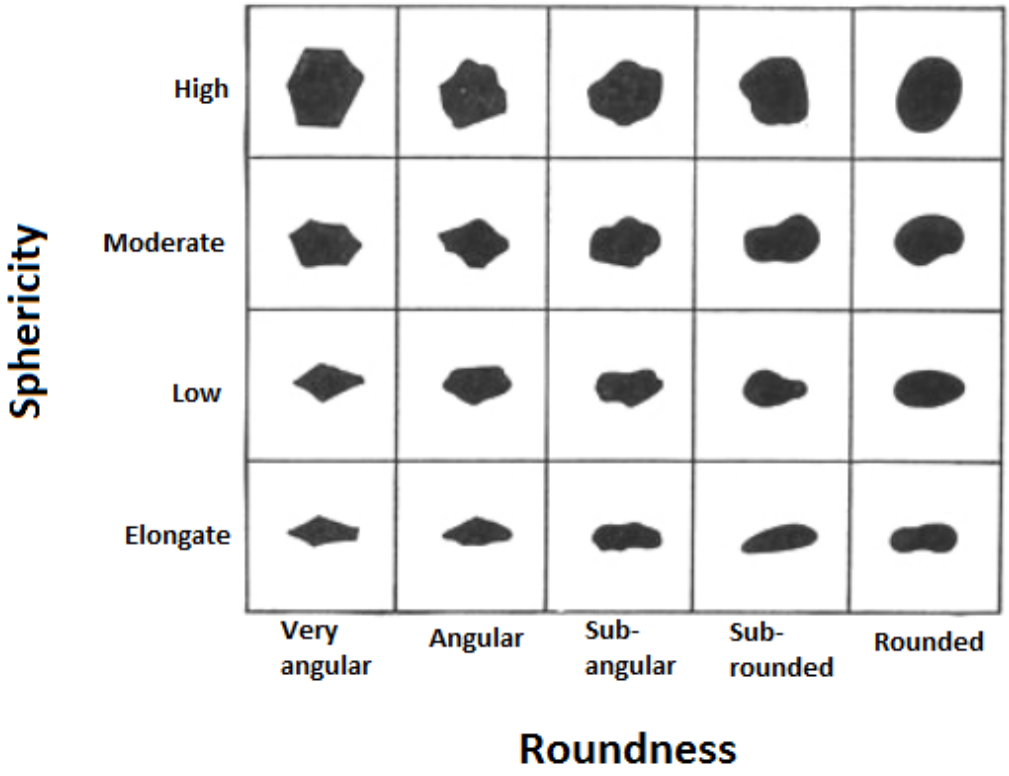

Figure 11: Definition of roundness and sphericity used for field descriptions. Modified after Krumbein and Sloss (1956).

2.3 Post-fieldwork

The first step after both field trips was to organize the collected data, making them easily accessible for interpretation. GPS points were imported to a geographic information system (GIS) database, in order to geo-reference all the collected data on a map. The numerous photos of the valley exposures were merged into larger composite photos and interpreted in CorelDraw.

Interpretation of fault continuation between valleys (wherever challenging terrain prevented tracing in the field) were done by combining Google Earth and 3D structural modelling in Petrel. The strike of faults observed in the field is often unknown, but some faults are clearly visible on

satellite images. Other structures are less visible, but several of the faults observed in the field tend to be located on boundaries between sparsely and densely vegetated areas, or simply on a small groove in the topography. During modelling in Petrel, it was tested how planar fault surfaces intersect a digital elevation model (DEM), and how those intersections compared to the features observed in Google Earth.

Chapter 3 – Field observations and interpretations

3.1 Introduction

The structure of the study area (Figure 12) is characterized by a majority of north-dipping faults, exposed in the Vouraikos, Ladopotamos, Potamia and Krathis River Valleys. Six major faults are here identified; the Kalavryta, Kerpini-Tsivlos, South Graben (not a previously used name), Dhoumena, Valimi and Mamoussia-Pirgaki Faults. The South Graben Fault might be considered as the eastward continuation of the Dhoumena Fault after a right-step in the Vouraikos River, but it is here interpreted as an individual fault. Although the Kalavryta and Dhoumena Faults with respective hangingwall lithologies are added to the map, they have not been studied in detail in this thesis.

The pre-rift metamorphosed carbonate (Pindos Basement) is well exposed in the eastern and north-western part of the study area, but thick successions of syn-rift sediments make up most of the exposed lithologies. The syn-rift sediments here correspond to the Lower Group by Ford *et al.* (2013) which is characterized by terrestrial alluvial and fluvial conglomerates. The study area can roughly be divided into three different segments from south to north (Figure 13 and Figure 14), based on their exposed lithologies:

1. A southern segment dominated by coarse alluvial conglomerates. Two different alluvial units are identified (Basal and Upper Alluvial Conglomerates), separated by an unconformity. The Basal Alluvial Conglomerates are overlying the Pindos Basement. There are also local exposures of a minor unit (Grey Breccia/conglomerate) which stands out from all the other lithologies because of its great amount of angular clasts.
2. A central segment characterized by a thick (>600 m) fluvial succession (Fluvial Conglomerates) with a buried base. It is conformable overlain by a massive unit of Upper Alluvial Conglomerates. The Pindos Basement is not exposed here.
3. A northern segment with well-exposed Pindos Basement. It is onlapped by an 80 metre thick unit of Basal Alluvial Conglomerates, followed by 300 metres of Fluvial Conglomerates.

The sediments in Segment 1 dip southwards towards the Kerpini-Tsivlos Fault, which is characteristic for the majority of fault blocks in the southern margin of the Corinth Rift. In

Segments 2 and 3 anomalous northward dips are observed, particularly to the west of Ladopotamos River.

The identified lithologies and structural features are described in more detail throughout this chapter. The structural features in five valley sections will be presented, captured by photos (both original and interpreted ones) from a number of different viewpoints. The photos are marked with key letters, where each letter has an associated description in bullet point format. The colour legend from Figure 12 is consistently used for the lithologies throughout this thesis.

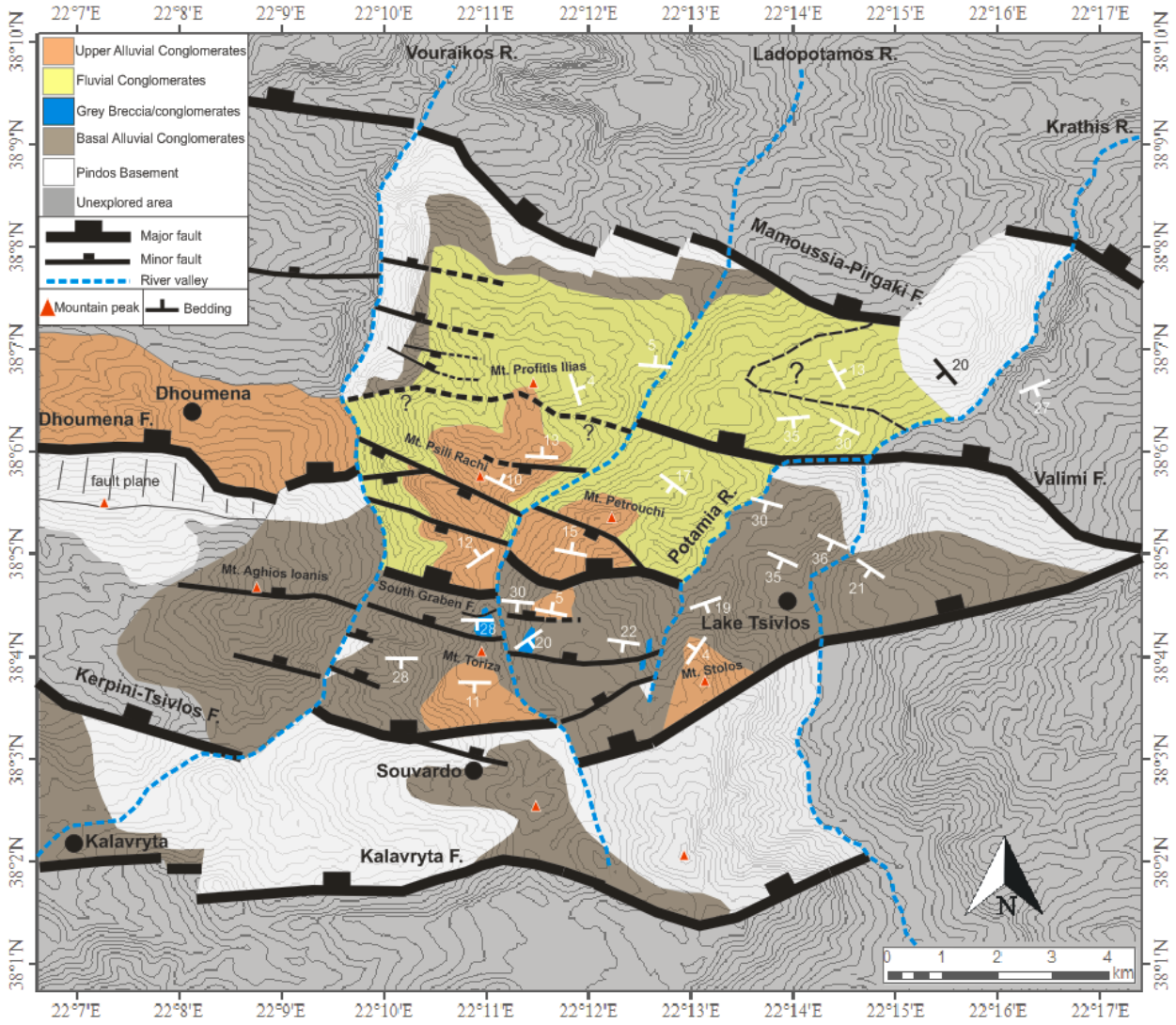

Figure 12: Structural map of the study area.

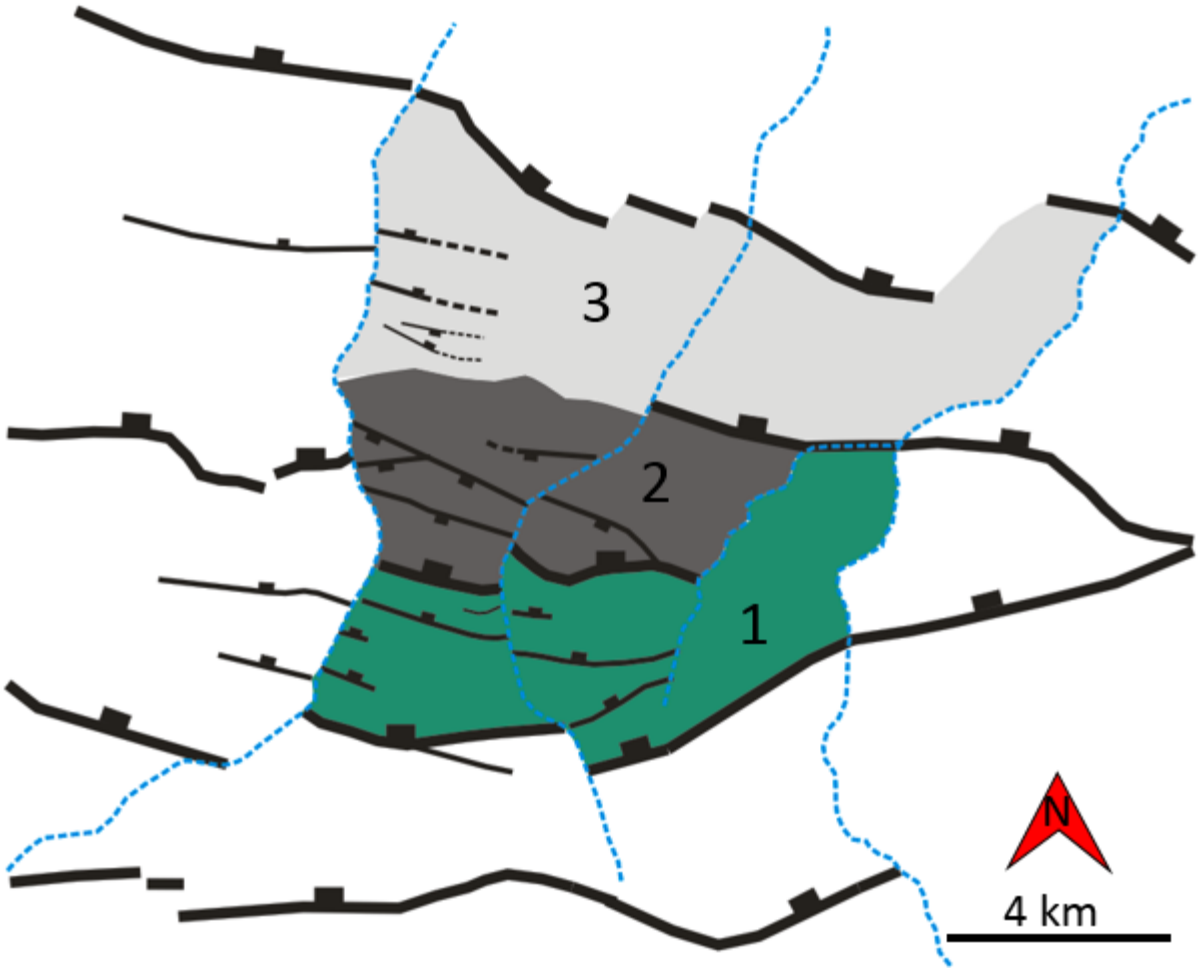

Figure 13: Structural map of the study area, highlighting the 3 main segments into which it can be divided.

3.2 Lithologies

During the field work four lithological units were identified within the syn-rift half graben infill which unconformably overlies the Pindos Basement. They are all terrestrial clastics (dominantly conglomerates) and are differentiated based on brief sedimentological descriptions such as bed thickness, clast size, roundness, sphericity, sorting, grading and preferred clast orientation.

This sub-chapter will present general descriptions of all the observed units, including their stratigraphic relationship with the other units (see Figure 14 for stratigraphic overview) and outcrop photos (outcrop locations are marked on Figure 15).

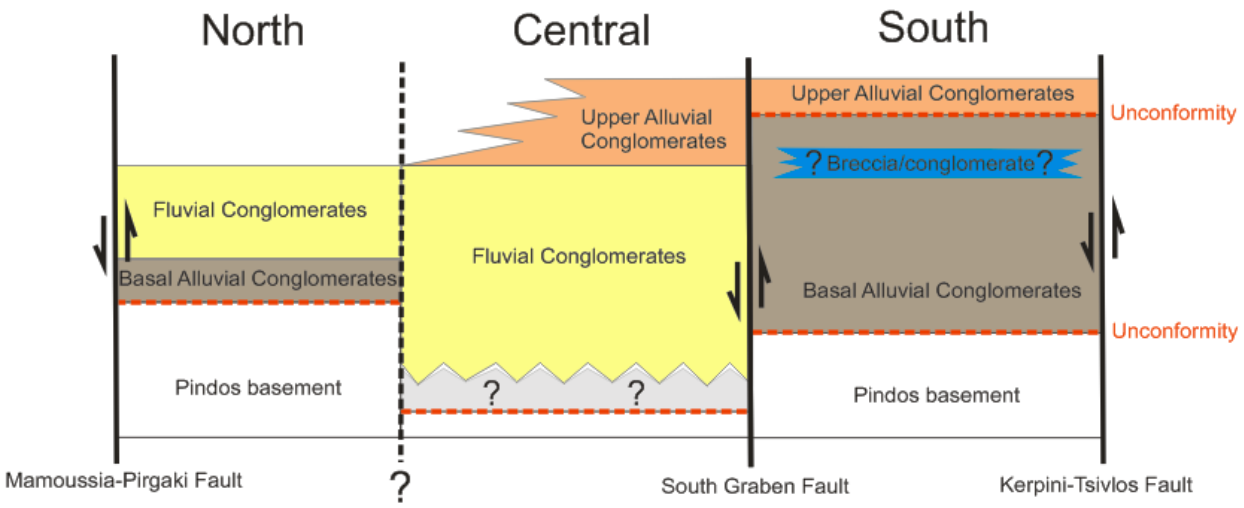

Figure 14: Generalized stratigraphic overview of the study area (roughly divided into 3 segments), illustrating the boundaries between the different units. The base of the Fluvial Conglomerates in the central segment is unexposed, lying in the sub-surface.

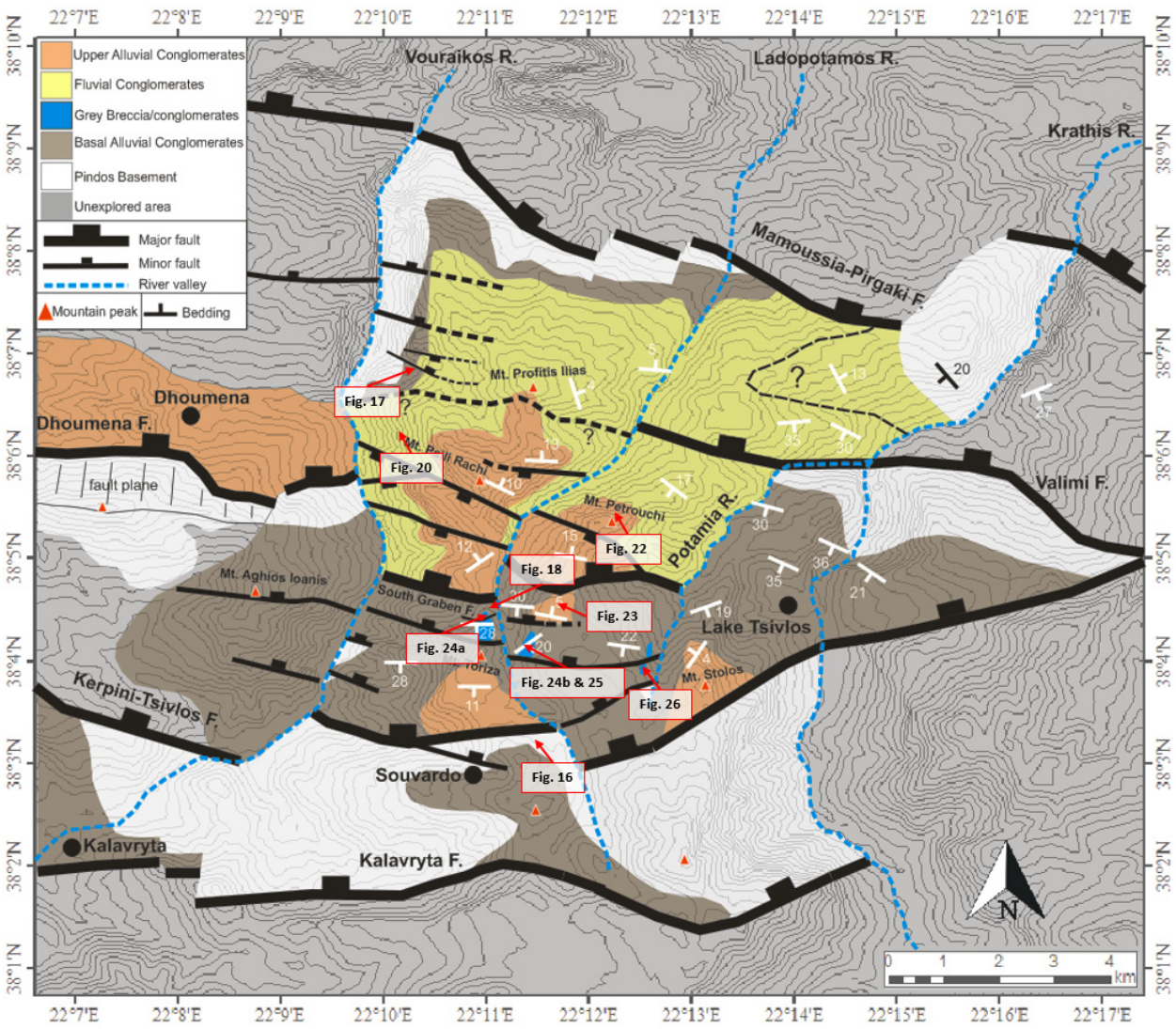

Figure 15: Structural map showing the location of the outcrops presented in Sub-chapter 3.2.

3.2.1 Pindos Basement

The pre-rift basement unit (Figure 16) consists mainly of metamorphosed carbonates, with some local occurrences of shale. It is highly deformed due to the compressional regime under which the Hellenide thrust sheet was emplaced, and there are thus few reliable bedding surfaces for dip measurements. Its down-section extent is estimated by extrapolating the dip of unconformity surfaces separating it from the half graben sedimentary infill. This method relies on the assumption that the unconformity planes are approximately planar, although they may in reality have significant paleo topography.

Figure 16: Pindos Basement. Outcrop location is marked on Figure 15.

3.2.2 Basal Alluvial Conglomerates

Alluvial conglomerates are observed as the lowermost sedimentary infill at two separate locations; in the north-western part of the study area (in the Vouraikos River) and in the hangingwall of the Kerpini-Tsivlos Fault. Stratigraphically, the two successions are not overlain by the same unit, and the southern succession is ~700 metres thicker than the northern one. Thus, it is unclear whether they can be considered as the same unit or not. The southern conglomerates are slightly coarser and poorer sorted, but in general their sedimentological character is similar (described below, Table 1 and 2). In this thesis they are interpreted as the same unit.

Northern Basal Alluvial Conglomerates

In the north-western part of the study area (Vouraikos River) 80 metres of thick, coarse-grained alluvial conglomerates (Figure 17) onlap rotated fault blocks of Pindos Basement. The succession

is cut by low-displacement (< 50 m) faults which is sealed by (or unexposed in) overlying strata. It is overlain by the Fluvial Conglomerates, described in Sub-chapter 3.2.3. The southern boundary of this unit is abrupt, as it terminates laterally towards a 600 metre thick succession of Fluvial Conglomerates. The nature of this boundary will be discussed in Chapter 3.3. The general lithological description of this stratigraphic unit is found in Table 1

Table 1: General characteristics of the northern Basal Alluvial Conglomerates.

Characteristic	**Description**
Clast size	13 cm
Sorting	Moderate --> poor
Grading	None
Bed thickness	10-30 m
Clast roundness	Sub-rounded
Preferred clast orientation	None
Clast sphericity	Low --> moderate

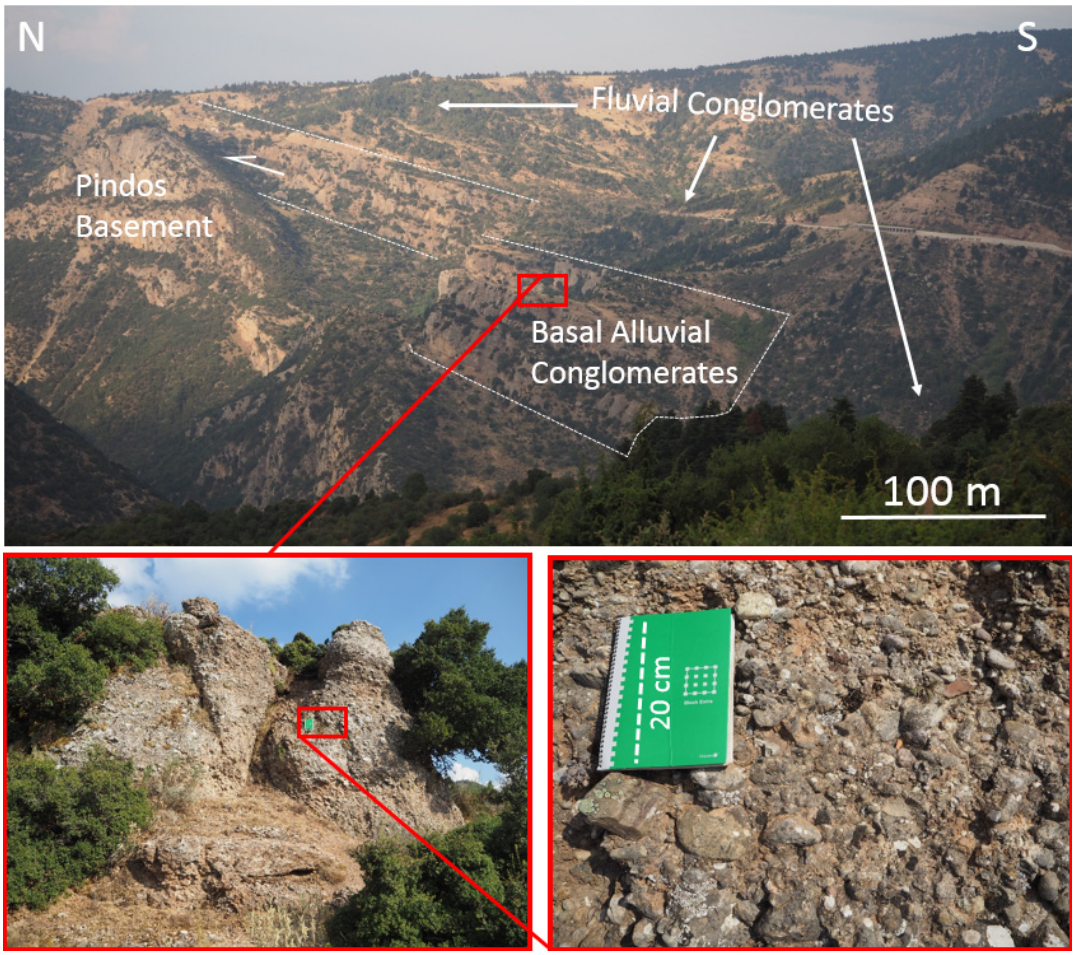

Figure 17: Northern Basal Alluvial Conglomerates. The outcrop location is marked on Figure 15.

Southern Basal Alluvial Conglomerates

In the footwall of the South Graben Fault is an 800 metre succession of alluvial conglomerates overlying the Pindos Basement (Figure 18). Unlike the northern Basal Alluvial Conglomerates, its angular relationship with the basement is ambiguous. It appears to onlap the basement in the Vouraikos River, but the unconformity there is poorly exposed and the relationship can thus not be determined with certainty. To the very east in the study area, in the Krathis River, the beds are parallel to the unconformity. Locally, the Basal Alluvial Conglomerates are unconformably overlain by the Upper Alluvial Conglomerates.

The unit consistently dips 20-30°S towards the Kerpini-Tsivlos Fault, which conforms to the typical south-tilting observed in other fault blocks in the southern rift margin. Its bed thicknesses decrease up-section, suggesting that the unit is retrograding. The beds near its base are similar in thickness to those of the northern Basal Alluvial Conglomerates.

Although not supported by adequate sedimentological observations, the northern Basal Alluvial Conglomerates are here correlated to the lower beds of the southern Basal Alluvial Conglomerates. They are considered as the first and most extensive deposits in a south-retrograding alluvial fan system. The lithological description of the southern Basal Alluvial Conglomerates is found in Table 2.

Table 2: General characteristics of the southern Basal Alluvial Conglomerates.

Characteristic	**Description**
Clast size	15 cm
Sorting	Poor
Grading	None
Bed thickness	5-30 m (decreasing up-section)
Clast roundness	Sub-rounded
Preferred clast orientation	None
Clast sphericity	Low --> moderate

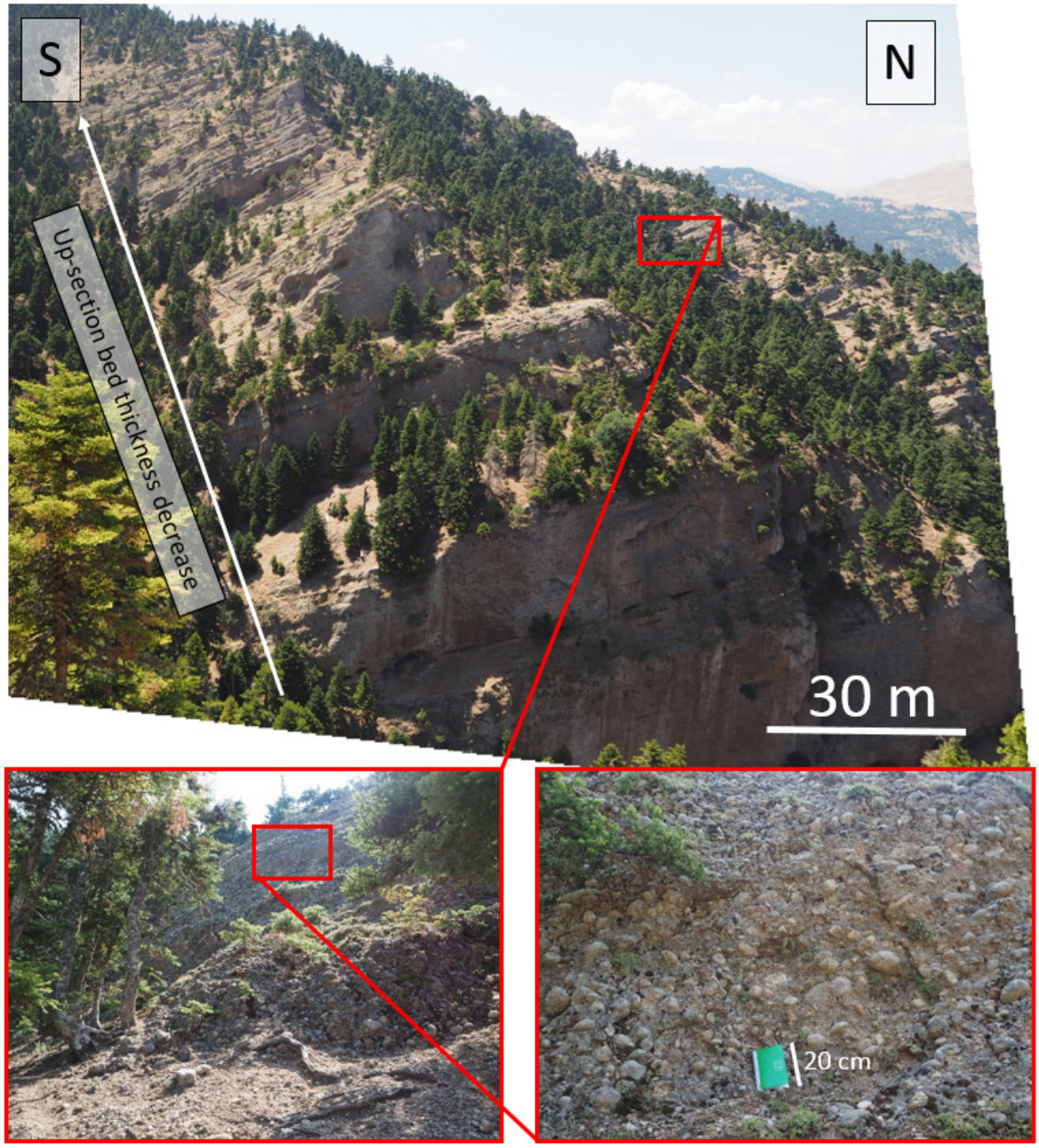

Figure 18: Southern Basal Alluvial Conglomerates. Outcrop location is marked on Figure 15.

3.2.3 Fluvial Conglomerates

In the hangingwall of the South Graben Fault is a thick fluvial succession. The observable part of the succession is 600 metres thick, but as its base is not exposed the thickness of this unit is even greater. It is overlain by the Upper Alluvial Conglomerates (described in Sub-chapter 3.2.4). There

are no observable discordance between the two units, and the contact appears to be conformable. In the north-western part of the study area the lower part of the Fluvial Conglomerates terminates laterally against the Pindos Basement and Basal Alluvial Conglomerates (Figure 20). The upper 300 metres of the succession extend further northwards and overlies the Basal Alluvial Conglomerates. The angular relationship between these two units is not determined with certainty, as there are few well-exposed beds within the Fluvial Conglomerates directly above the contact.

It is comprised of 1-5 metre thick bodies of well sorted matrix-supported conglomerates, and thinner beds of light brown/red silt and fine sand. Channel geometries (typically of a 15-25 m width) are commonly present within the conglomerates, and clast imbrications are often observable in outcrops. The finer sediments are interpreted as sequential floodplain deposits. The clast size variety between individual channels is believed to relate to different levels of flow energy within a braided river system. The succession is fining northwards, both in terms of clast sizes and bed thicknesses. The general lithological description can be seen in Table 3. Clast imbrications and the azimuth of exposed channel bodies indicate a dominant paleo flow towards northeast (Figure 19).

Table 3: General characteristics of the Fluvial Conglomerates.

Characteristic	**Description**
Clast size	5-10 cm (decreasing northwards)
Sorting	Very well (best sorted conglomerates)
Grading	Usually none. Some occasions of normal grading
Bed thickness	1-5 metres
Clast roundness	Sub-rounded --> rounded
Preferred clast orientation	Occasionally imbricated
Clast sphericity	Moderate --> high

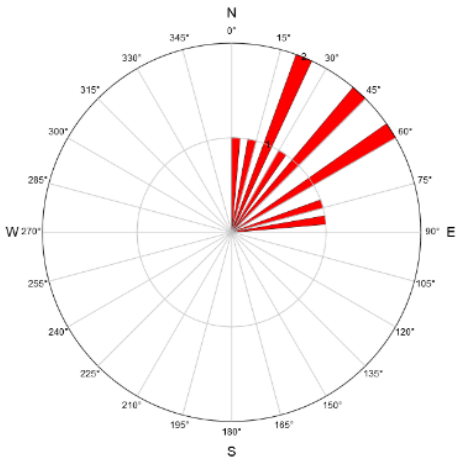

Figure 19: Rose diagram showing paleo flow indicators for the Fluvial Conglomerates.

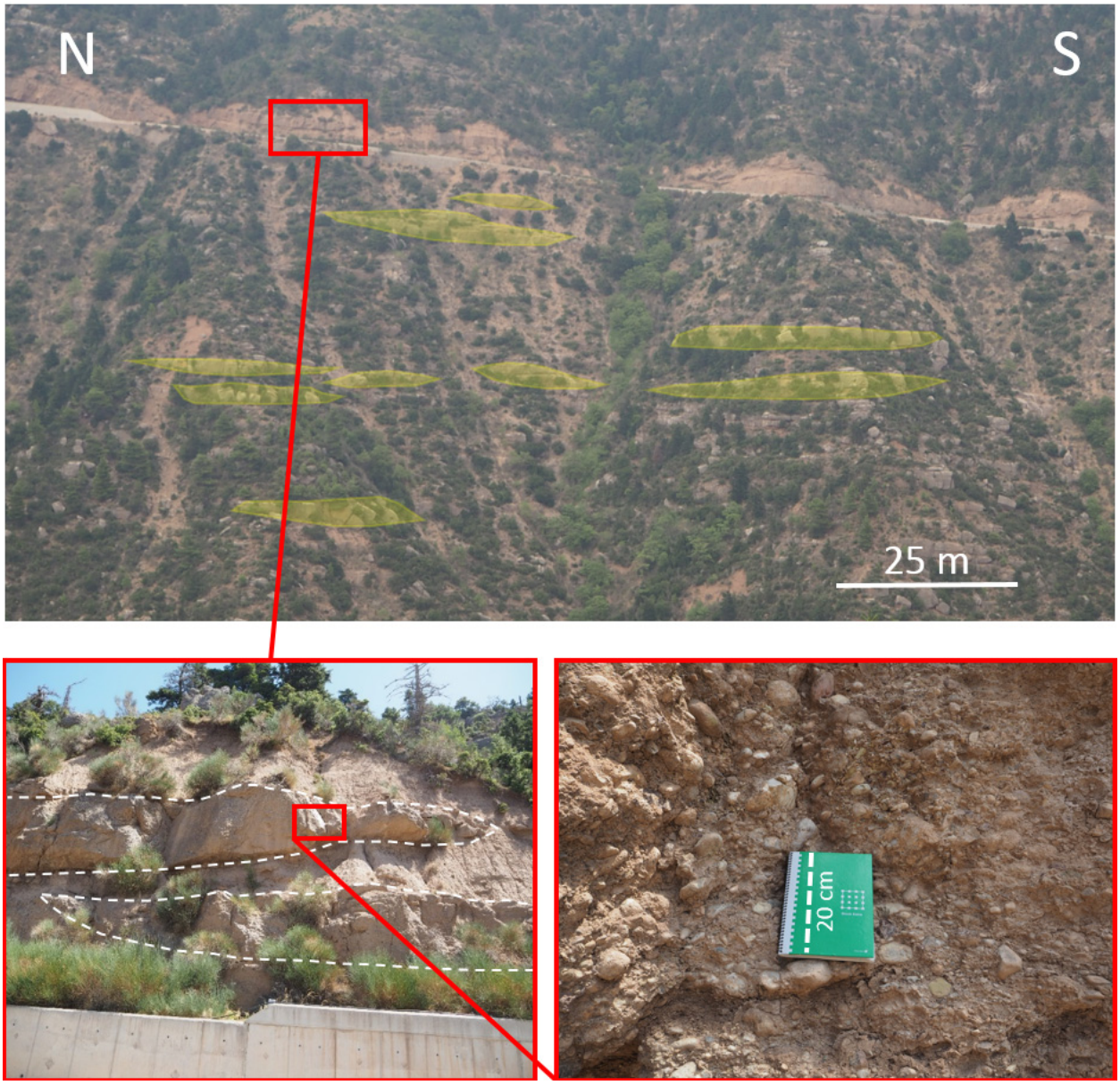

Figure 20: Conglomeratic channel bodies and floodplain deposits. Some (but not all) of the channels are highlighted. The outcrop location is marked on Figure 15.

3.2.4 Upper Alluvial Conglomerates

The uppermost unit is a sharp-based 300 metre thick succession of very massive clast-supported conglomerates with bed thicknesses reaching 30-40 metres. Beds are separated by thin layers of siltstone or sandstone. It is more poorly sorted than the Fluvial Conglomerates, and contains few internal structures (there are some rare occasions of imbrication (Figure 21). It is seen unconformably overlying the Basal Alluvial Conglomerates in the south (Figure 22), and conformably overlying the Fluvial Conglomerates in the central part of the study area (there are no observable discordance between the two) (Figure 23). The unit is interpreted as a significant progradational alluvial fan sourced from the south. Its northern boundary is abrupt, and it is limited either by erosion or a south-dipping fault. The general lithological description of the Upper Alluvial Conglomerates can be seen in Table 4.

Table 4: General characteristics of the Upper Alluvial Conglomerates.

Characteristic	**Description**
Clast size	10-15 cm
Sorting	Moderate --> poor
Grading	Usually none. Inverse grading observed locally.
Bed thickness	10-40 metres. Most massive unit in terms of bed thickness.
Clast roundness	Sub-rounded
Preferred clast orientation	None. Some rare cases of imbrication.
Clast sphericity	Moderate

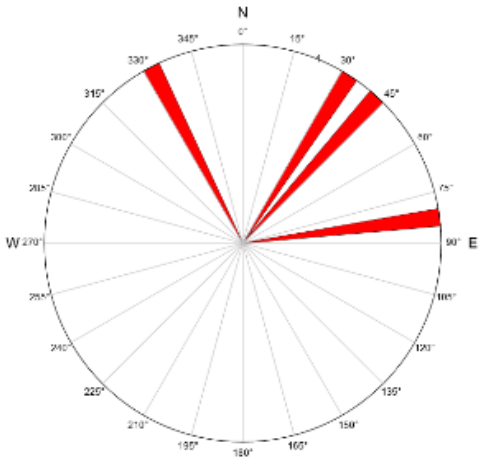

Figure 21: Rose diagram showing paleo flow indicators for the Upper Alluvial Conglomerates.

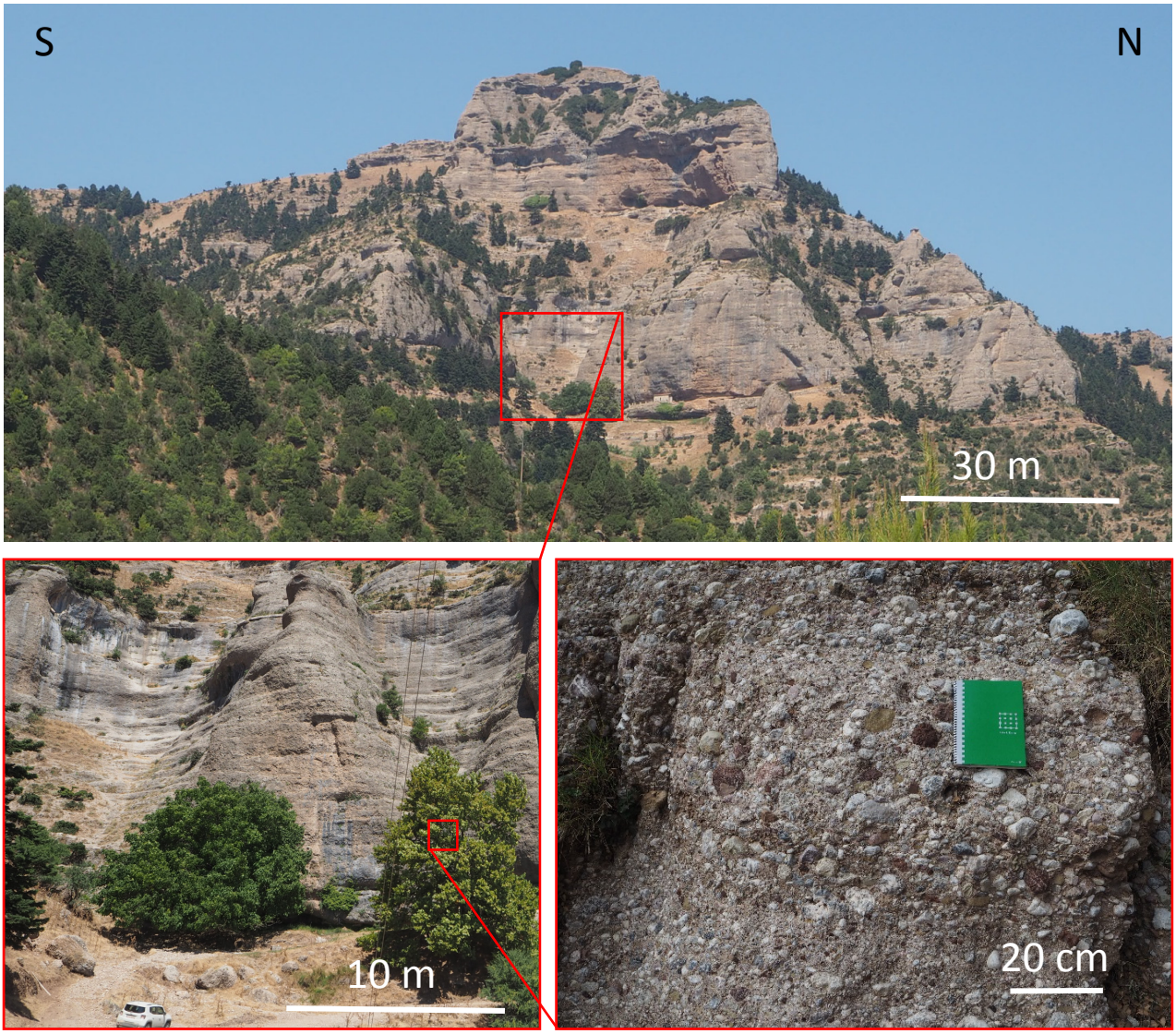

Figure 22: Upper Alluvial Conglomerates at the peak of Mt. Petrouchi. The outcrop location is marked on Figure 15.

Figure 23: Upper Alluvial Conglomerates unconformably overlying the Basal Alluvial Conglomerates (the unconformity is not shown here). The location of the photo is marked in Figure 15.

3.2.5 Grey Breccia/conglomerates (minor unit)

A distinct 10-30 metre thick grey unit of hard, consolidated, matrix-supported breccia to conglomerate is locally exposed in 4 valley sections. It has a sharp top and base (Figure 24a), and a characteristic "sponge-like" surface as pebbles have fallen out of its matrix (Figure 24b). The great variety in clast roundness differentiates this unit from all the others within the study area. It is observed on top of the Basal Alluvial Conglomerates (Figure 25), but a similar looking unit is

also seen *within* the Basal Alluvial Conglomerates (Figure 26). They share the same characteristic matrix, grey colour and variety in clast roundness. The distance between each outcrop is large, and it is unclear whether they can be considered as one single unit or not. However, in this thesis it is presented as such. The general lithological description of this stratigraphic unit can be seen in Table 5.

Table 5: General characteristics of the Grey Breccia/conglomerate.

Characteristic	**Description**
Clast size	10 cm
Sorting	Very poor. Clasts range from pebble to boulder size. Chaotic.
Grading	None
Bed thickness	1-3 m
Clast roundness	Sub-angular. Wide roundness range from angular to rounded.
Preferred clast orientation	None
Clast sphericity	Elongated --> low

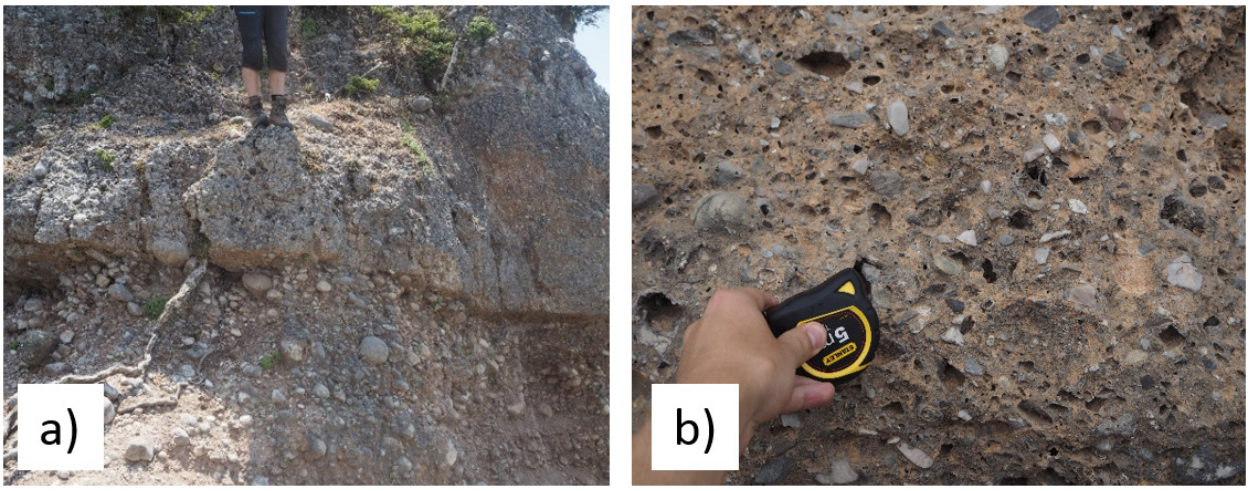

Figure 24: Grey Breccia/conglomerate. a) Sharp contact between Basal Alluvial Conglomerates (base) and Grey Breccia/conglomerates (top). b) Characteristic "sponge-like" matrix. The photo is from the same unit as in Figure 25, in a part with more angular clasts. The locations of the photos are found in Figure 15.

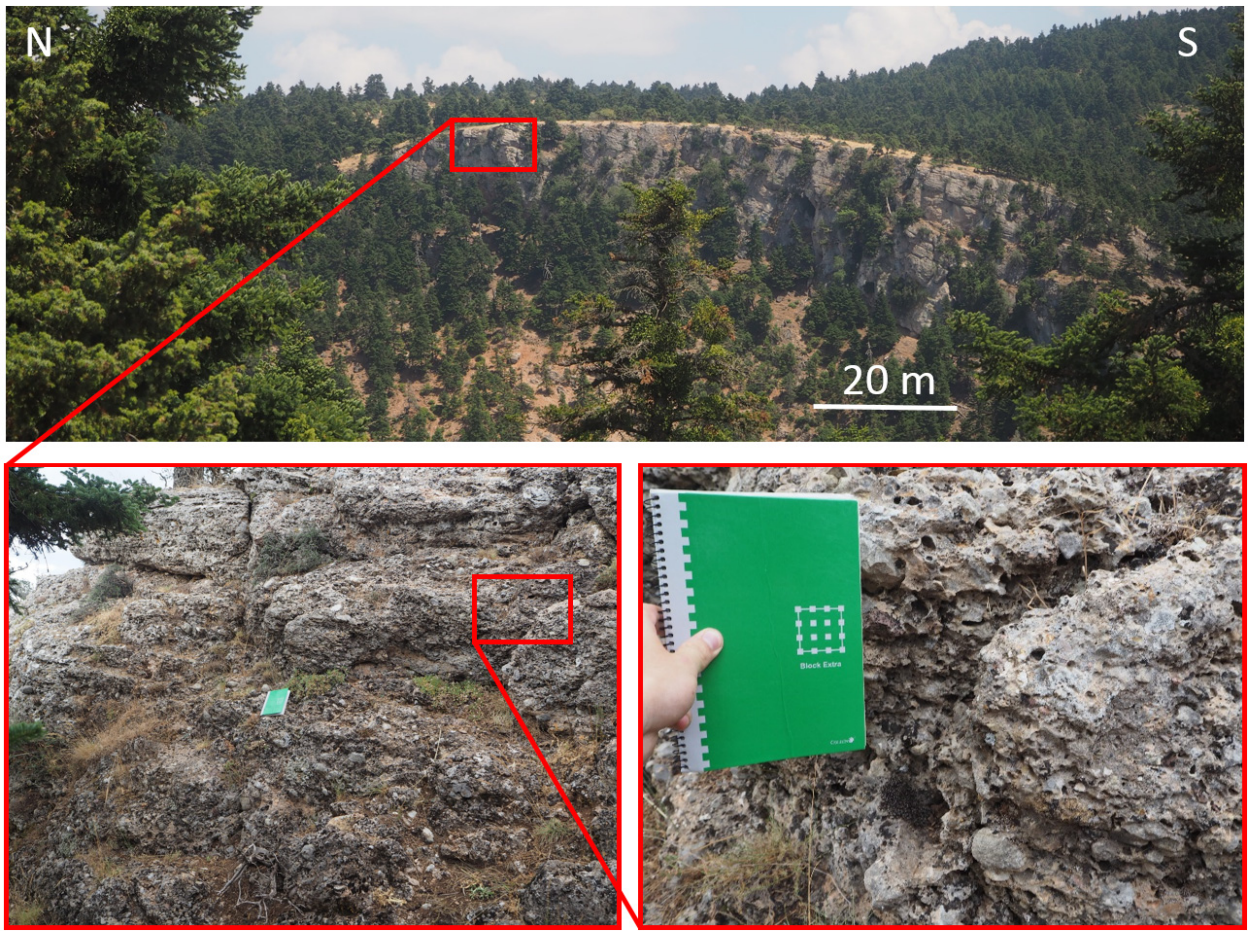

Figure 25: Grey Breccia/conglomerate on top of Basal Alluvial Conglomerates. The outcrop location is marked on Figure 15.

Figure 26: Grey Breccia/conglomerates situated within the Basal Alluvial Conglomerates. The locations of the photos are found in Figure 15.

3.3 Valley section 1: Vouraikos East

The Vouraikos River Valley is among the most studied sections in the Kalavryta area, as several lithologies, including the basement, are very well exposed. This sub-chapter offers photos, both original and interpreted ones, from four different viewpoints in order to capture most of the features in the valley side. All the viewpoints are marked on Figure 27, and the photos are here presented from north to south.

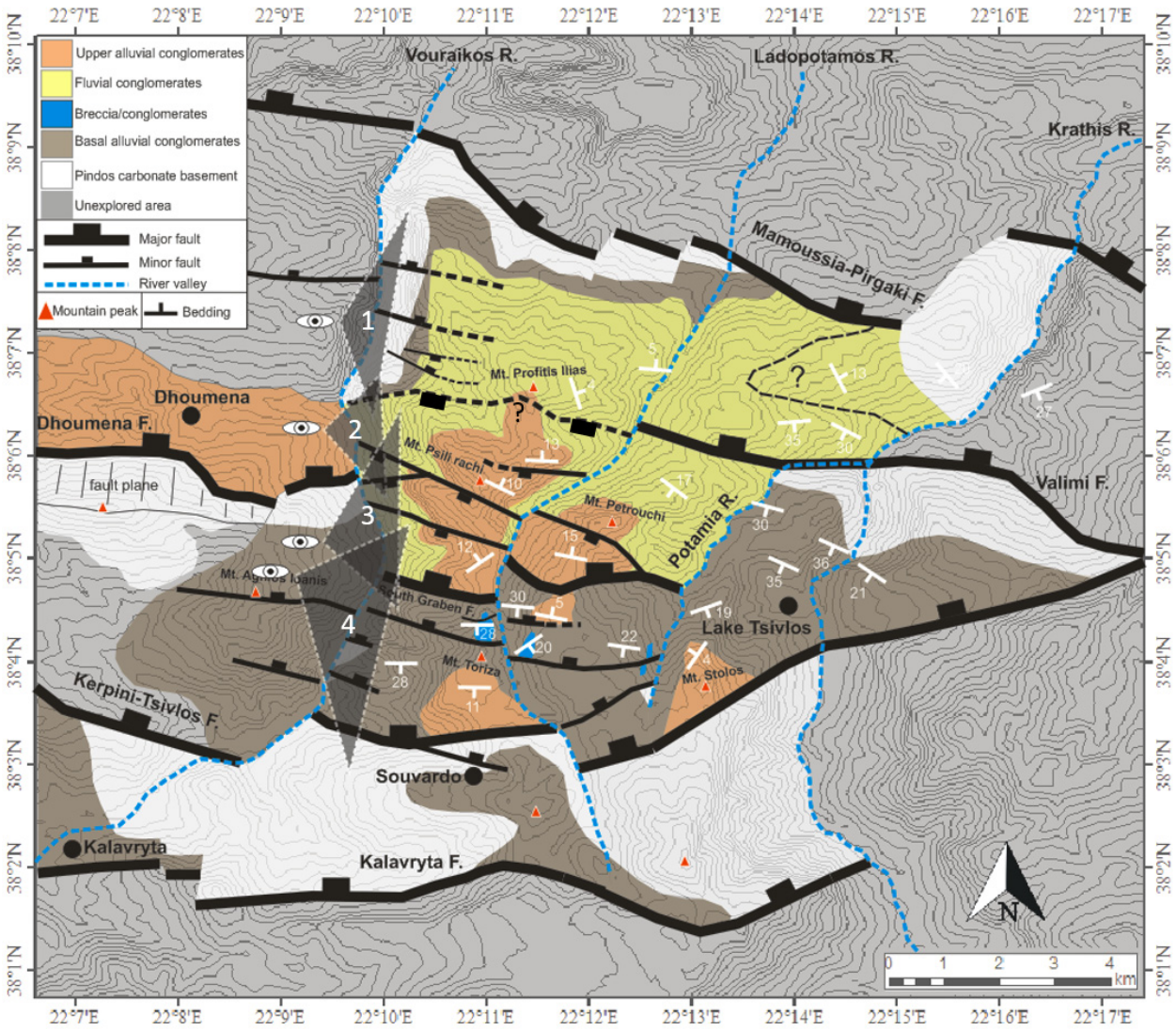

Figure 27: Structural map showing the four different viewpoints from which Section 1 is photoed.

3.3.1 View 1

View 1 (Figure 28) shows the very north-western part of the study area, where a series of south-tilted (domino) basement blocks crop out at the valley bottom. They are overlain by 80-100 metres of Basal Alluvial Conglomerates, followed by a 300 metre succession of Fluvial Conglomerates. To the very south the basement and Basal Alluvial Conglomerates are not exposed, and 600 metres of Fluvial Conglomerates are overlain by a 200 metre package of massive Upper Alluvial Conglomerates.

Observations + interpretation:

a. The Basal Alluvial Conglomerates onlap the basement unconformity. It is here evident that the basement blocks experienced initial rotation prior to deposition of the earliest syn-rift sediments.
b. The Basal Alluvial Conglomerates are cut by low-displacement (<50 m) faults which are either sealed by (or unexposed in) the overlying strata.
c. The basement and Basal Alluvial Conglomerates terminate laterally towards Fluvial Conglomerates in the south. The contact between them dips to the south. Two possible scenarios could explain this:
    1. The southern side is down-thrown (minimum 300 m) by a south-dipping fault, and Basal Alluvial Conglomerates are buried below the thick succession of Fluvial Conglomerates.
    2. The basement and Basal Alluvial Conglomerates are eroded by incised rivers, and the sharp lateral change is an unconformity.

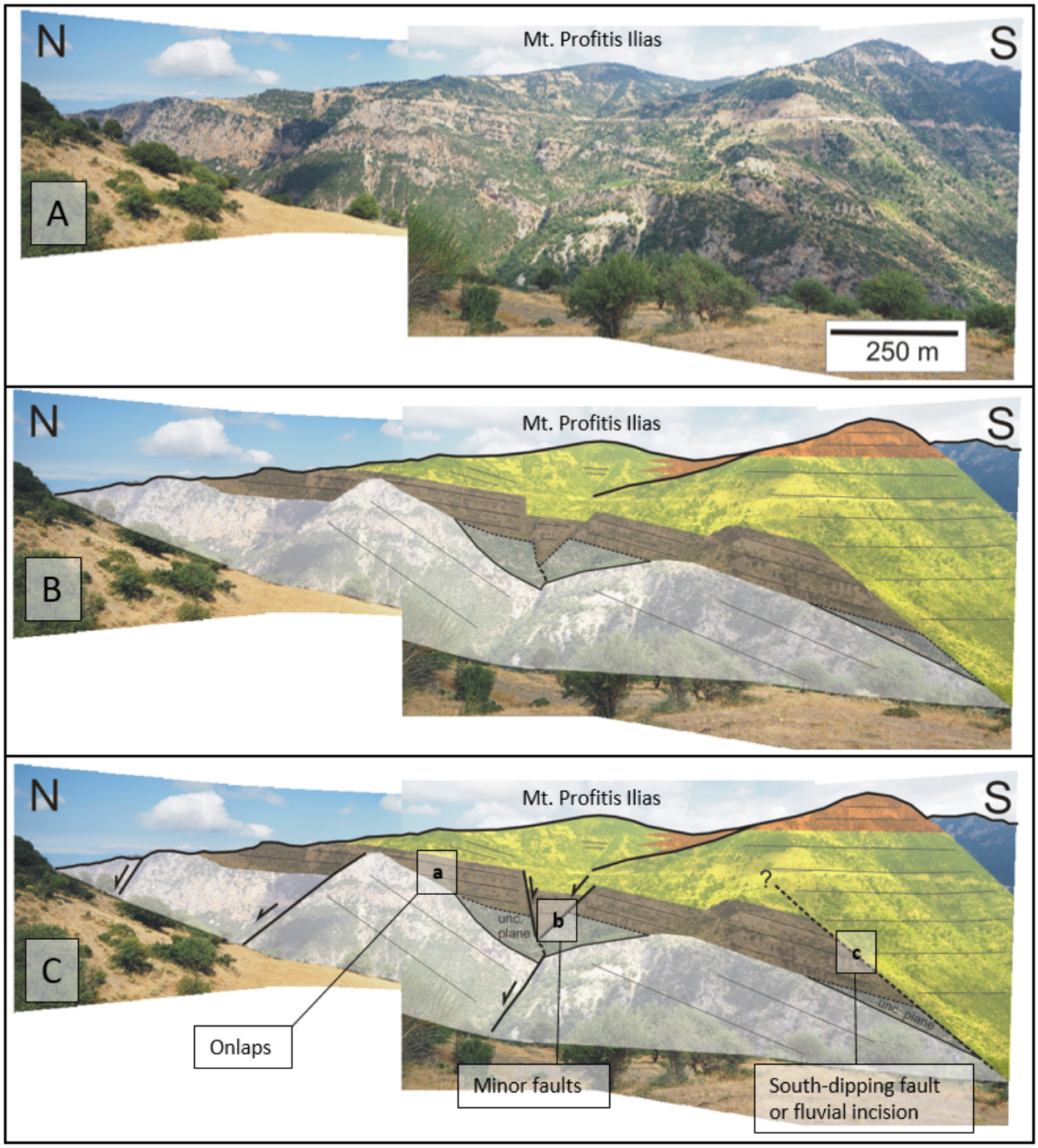

Figure 28: Section 1, View 1. A: original photo, B: observed lithological units and bedding, C: structural interpretation. The location of the photoed section is found in Figure 27.

3.3.2 View 2

From this view (Figure 29) one can observe the Basal Alluvial Conglomerates from a different perspective, and how they terminate towards the thick succession of Fluvial Conglomerates with a buried base. 200 metres of Upper Alluvial Conglomerates are overlying the Fluvial Conglomerates, and they are here clearly differentiated. The contact between them is stepping down to the south.

Observations + interpretation:

a. The northern boundary of the Upper Alluvial Conglomerates is here controlled by erosion, as the unit extrapolates into mid-air.
b. The Upper Alluvial Conglomerates are offset by 2 clear south-dipping faults, previously named Mega Spilio Fault 3 (MSF3) and Mega Spilio Fault 2 (MSF2) by Dahman (2015). Their displacement is 250 metres and 100 metres respectively. MSF2 terminates towards MSF3. A possible third south-dipping fault slightly offsets the uppermost beds.
c. The sharp contact between the Fluvial and Basal Alluvial Conglomerates appears to dip to the north. However, this is implausible as the sediments on the southern side of the contact are younger. The presence of either a south-dipping fault or unconformity both seem likely.

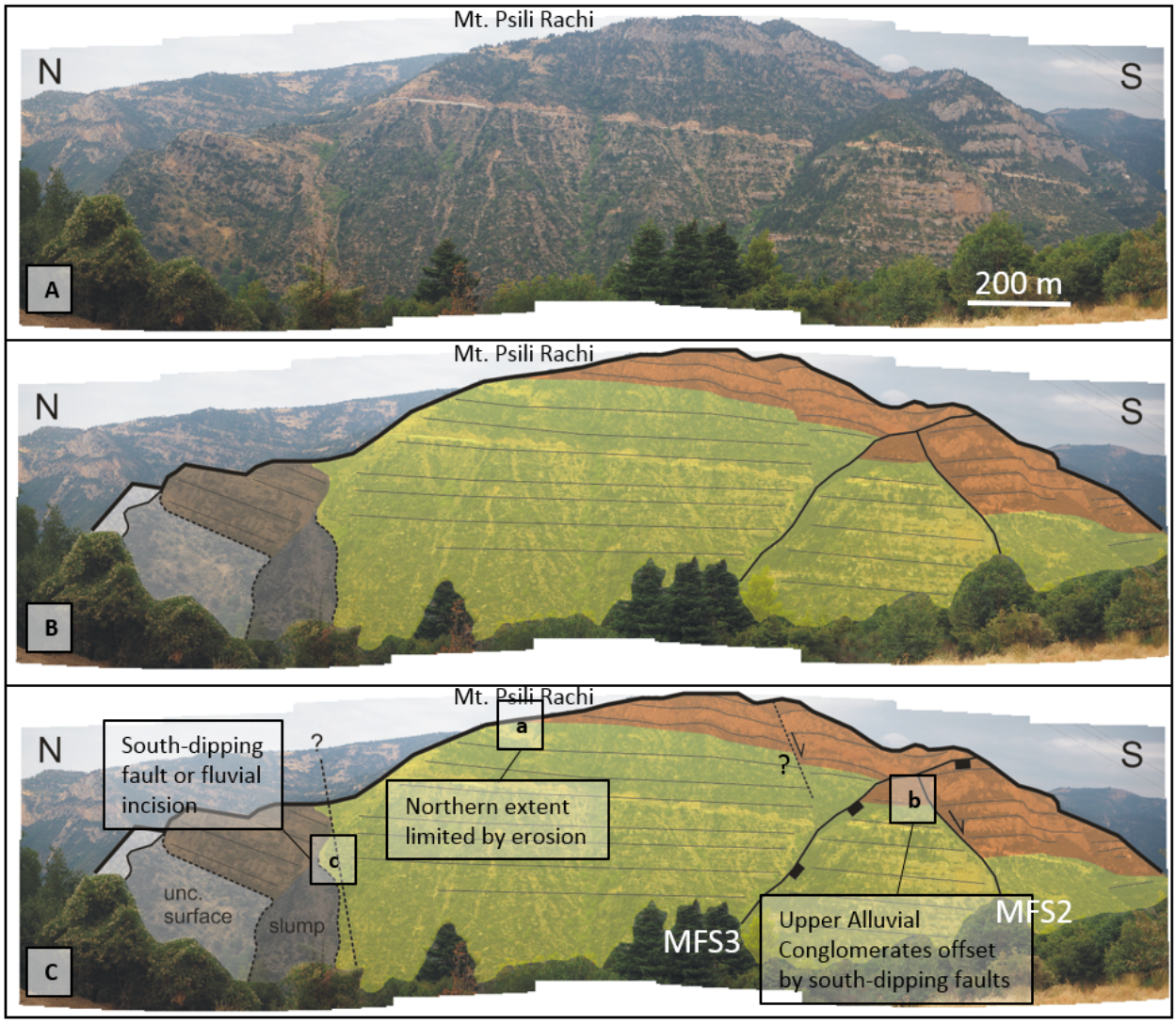

Figure 29: Section 1, View 2. A: original photo, B: observed lithological units and bedding, C: structural interpretation. The location of the photoed section is found in Figure 27.

3.3.3 View 3

This view (Figure 30) offers a better perspective of the faulted Upper Alluvial Conglomerates seen in View 2, and it is highly oblique to the south-dipping Mega Spilio faults. It also captures the southern Basal Alluvial Conglomerates, although covered in vegetation.

Observations + interpretation:

a. The Upper Alluvial Conglomerates in the hangingwall of MSF3 are slightly folded. As the footwall sediments of MSF3 (at the top of Mt. Psili Rachi) are apparently sub-horizontal, the folded beds in the hangingwall might be a result of increasing fault slip along MSF3 towards the northwest (conceptual model, Figure 31). This fold geometry has previously been interpreted as a hangingwall syncline caused by fault-propagation folding or normal drag along a north-dipping fault (Dhoumena fault, Ford *et al.* (2013) and Wood (2013)).
b. There is evidence of a south-dipping fault (Mega Spilio Fault 1 (MSF1), Dahman (2015)), as a thick package of Upper Alluvial Conglomerates is downthrown 100 metres directly south of the Mega Spilio Monastery (marked on Figure 30). The thickness of this package is similar to the package at the top of Mt. Psili Rachi. The monastery is thus believed to sit on the fault plane of MSF1.
c. South of MSF1 is a 600 metre wide zone of dense vegetation and poor exposure. The contact between the Fluvial and Upper Alluvial Conglomerates is here not identified. However, Fluvial Conglomerates are observed at the base, and Upper Alluvial Conglomerates are observed near the mountain top, thus the contact has to be somewhere in between. The outcrops in this zone are generally dipping 10-20°N.
d. South of the vegetated zone (c) is an 800 metre succession of Basal Alluvial Conglomerates with beds consistently dipping 25-30°S all the way to the Kerpini-Tsivlos Fault. No beds are traceable across a small incision in the valley side, and it is interpreted to represent the trace of the major north-dipping South Graben Fault. The displacement of this fault is uncertain, but it is estimated to be in region of 600-1500 metres.
e. On the mountain top, 200 metres south of the inferred South Graben Fault, is a small outcrop of Grey Breccia/conglomerate. It terminates southwards towards a poorly exposed north-dipping fault. A better exposure of this fault will be shown in Section 2.

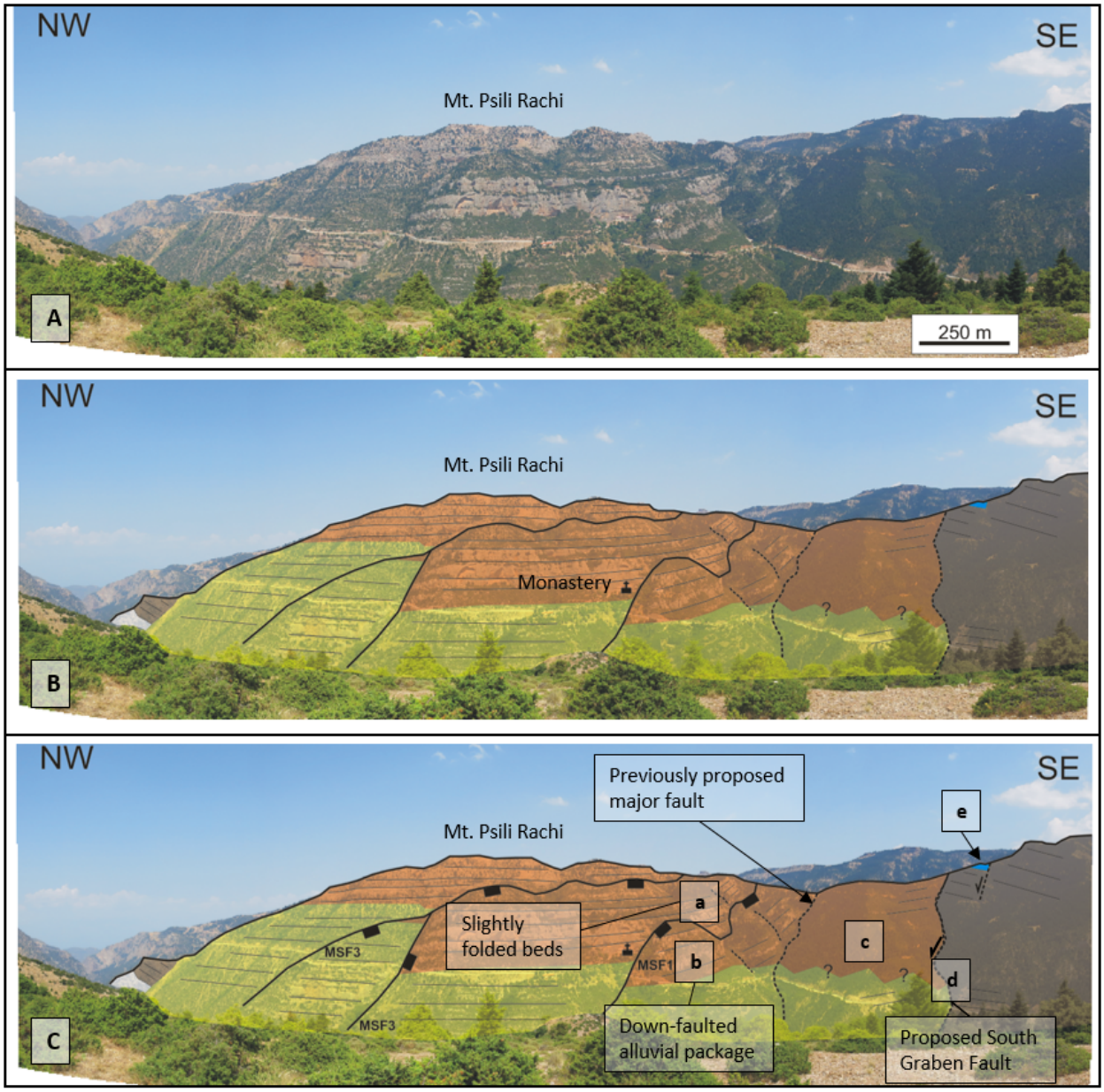

Figure 30: Section 1, View 3. A: original photo, B: observed lithological units and bedding, C: structural interpretation. The location of the photoed section is found in Figure 27.

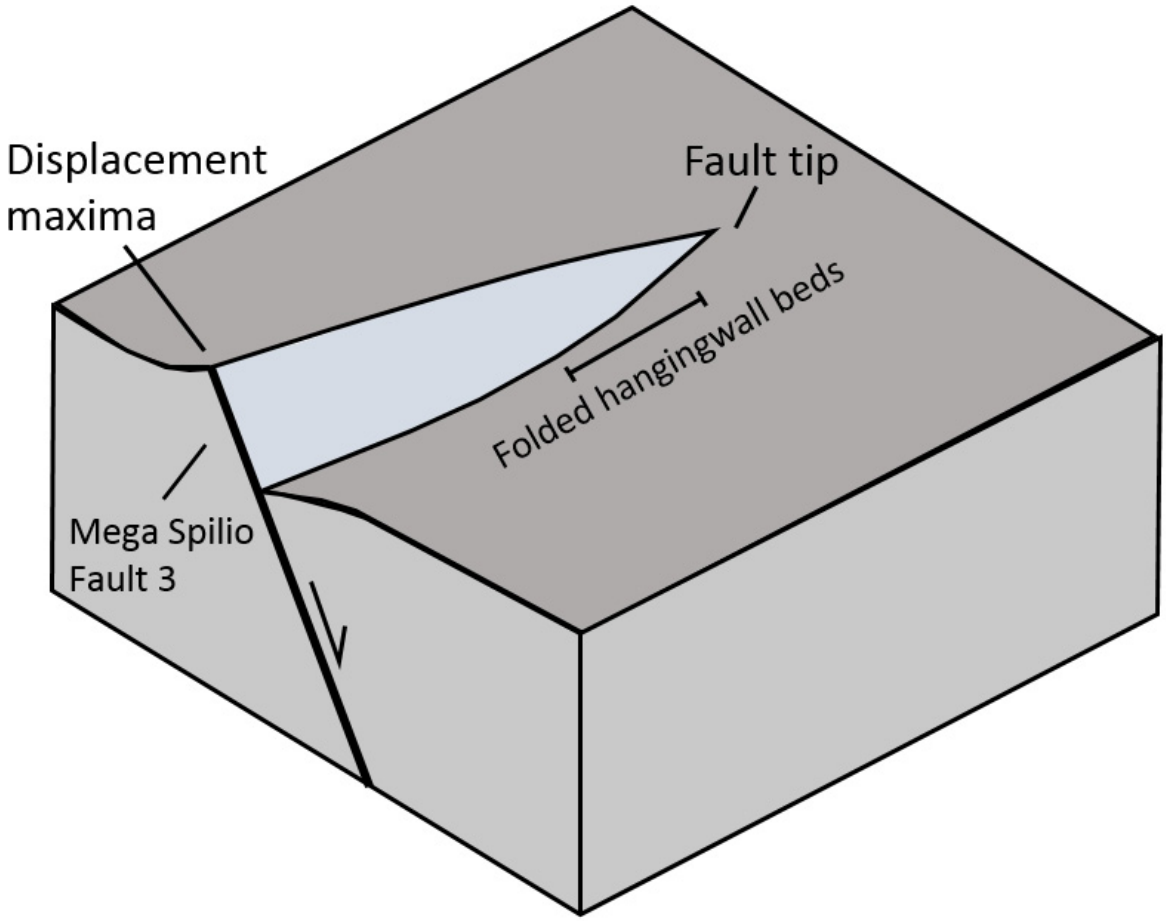

Figure 31: Conceptual model which can explain the folded Upper Alluvial Conglomerates in the hangingwall of MSF3. The bedding dip increases towards the fault tip.

3.3.4 View 4

View 4 (Figure 32), the southernmost studied part of Vouraikos River, exhibits a very thick succession of Basal Alluvial Conglomerates dipping 25-30°S towards the Kerpini-Tsivlos Fault. Its northern contact with the younger Fluvial and Upper Alluvial Conglomerates (the inferred South Graben Fault) is also shown here. At the base of the succession is a small rotated basement inlier (hidden behind the foreground in this photo). This inlier has previously been referred to as the Prinos Inlier (Ford *et al.,* 2013; Dahman, 2015).

Observations + interpretation:

a. The Prinos Inlier stretches for 300 metres and can be traced, from a fault contact (Figure 33a) in the north to an unconformity contact (Figure 33b) in the south, along the road in the bottom of the valley. The measured dip of the fault and unconformity is 20° and 48° respectively, indicating that the inlier is south-tilted. The unconformity exposure is rather poor, and its measured dip might not be reliable. If it is indeed dipping more than 40°, it would imply that the Basal Alluvial Conglomerates onlap the basement, as seen further north in View 1.
b. 150 metres south of the Prinos Inlier is another 30 metre small basement outcrop (Figure 33c), interpreted as being part of the footwall of the Toriza Fault identified by Dahman (2015).
c. The massive beds of Mt. Toriza abruptly terminate northwards against a north-dipping planar slope in the valley side, interpreted as a fault and its associated fault plane.
d. The beds of Mt. Toriza has previously been used as a prime example of syn-sedimentary tilting and progressive up-section dip decrease. However, the dip change observed here is very abrupt (from 27° to 10°), suggesting the presence of an unconformity separating two phases of alluvial conglomerate deposition. The unconformity is only visible in the upper 100 metres of the succession before being covered in vegetation, and so the thickness of the second-phase alluvial unit is uncertain. The overlying unit is here interpreted as the Upper Alluvial Conglomerates, which are overlying the Fluvial Conglomerates further north.

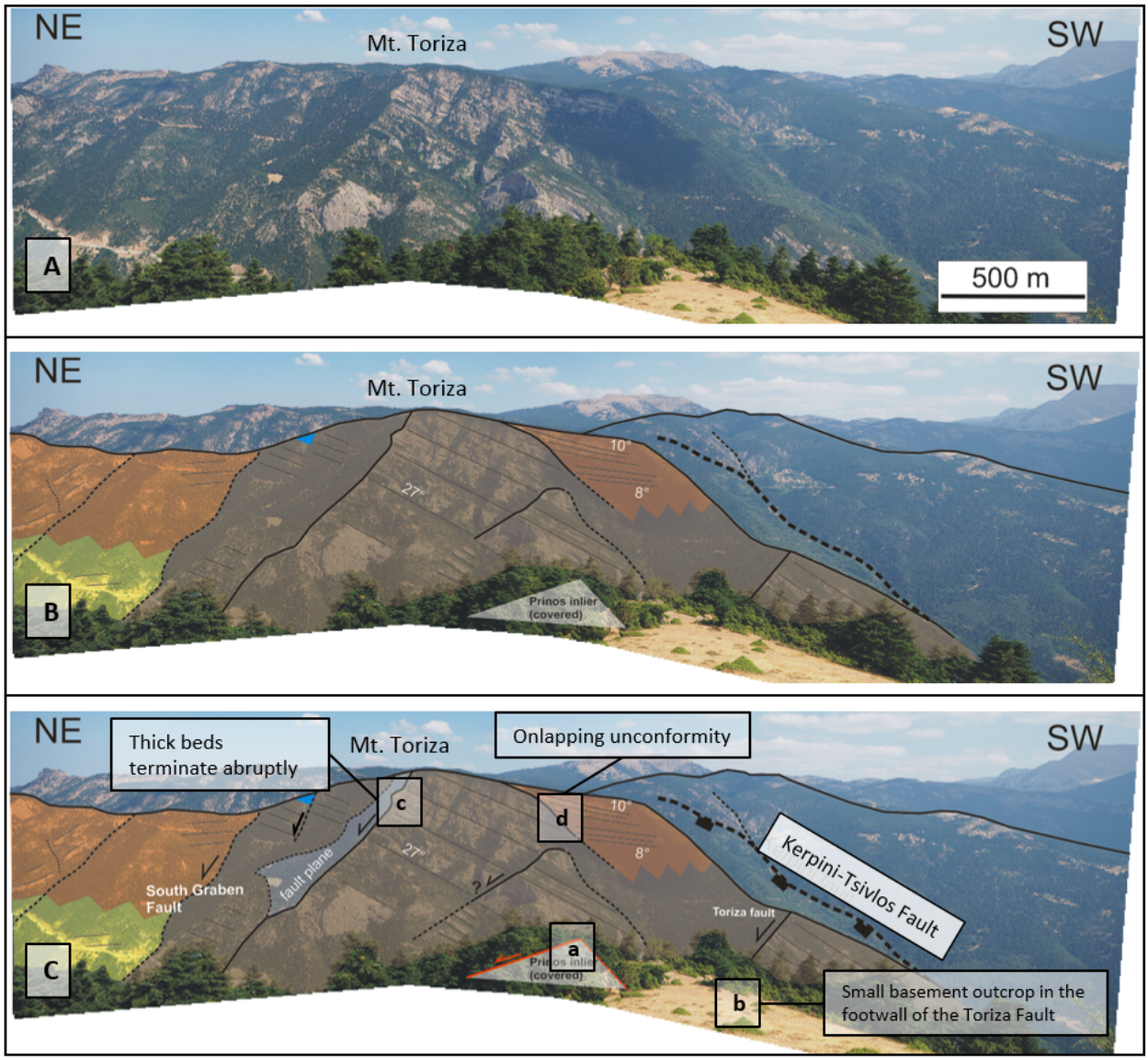

Figure 32: Section 1, View 4. A: Original photo, B: observed lithological units and bedding, C: Structural interpretation. The location of the photoed section is found in Figure 27.

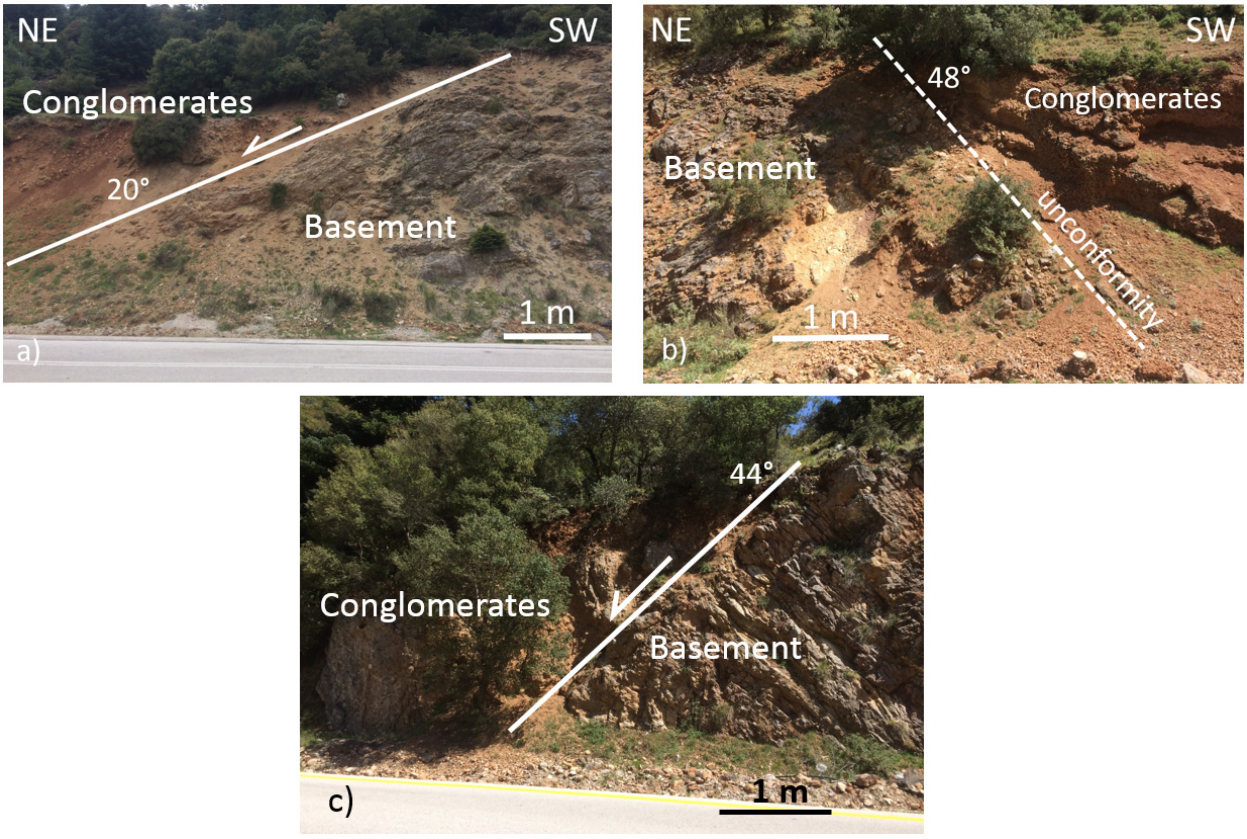

Figure 33: a) Prinos Fault. b) Poorly exposed Prinos unconformity. c) Toriza Fault.

3.3.5 Complete valley section

Figure 34 shows a simplified overview of the complete Section 1, highlighting the main interpretations from the above sub-chapters. All valley sections will be compared in Sub-chapter 3.8.

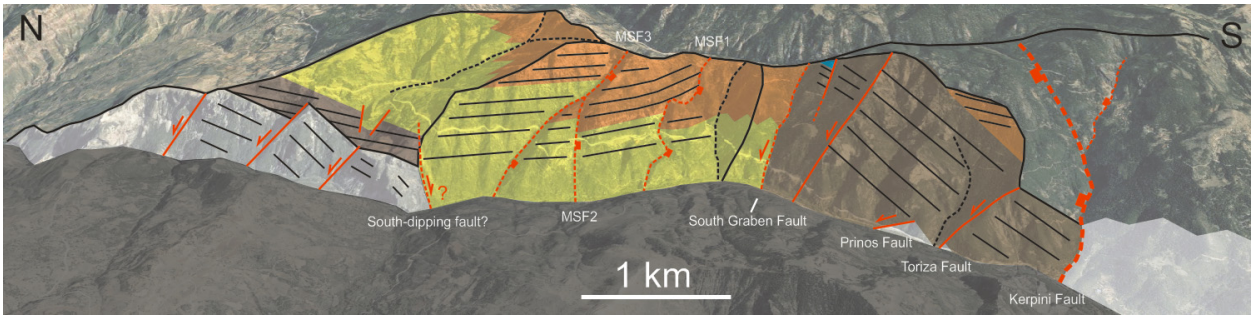

Figure 34: Complete interpretation of Section 1 on a satellite image from Google Earth. The horizontal and vertical scales are not proportional. The section is a compilation of the four views marked on Figure 27.

3.4 Valley section 2: Ladopotamos West

Section 2 is along the western side of Ladopotamos River, i.e. directly behind the mountain seen in Section 1. The state of exposure is good, and it is rather straightforward to correlate the features observed in Section 1. The Ladopotamos River has not incised as deep as the Vouraikos River, and some of the lower units are therefore not exposed. The features in Section 2 are captured by photos from three different viewpoints, all marked in Figure 35. They are here presented from south to north, starting where Section 1 was left (Mt. Toriza).

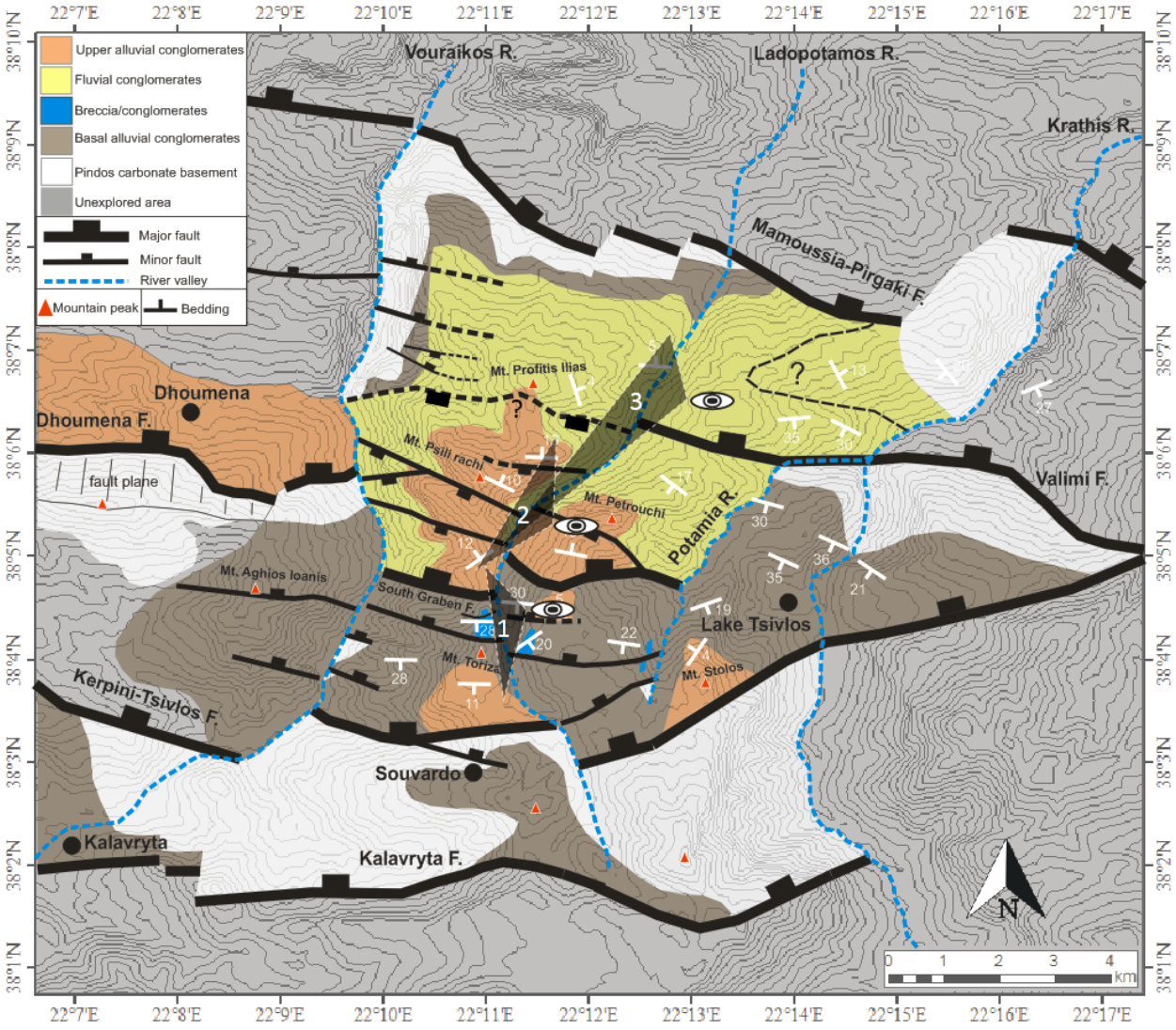

Figure 35: Structural map showing the three different viewpoints from which Section 2 is photoed.

3.4.1 View 1

From this view (Figure 36) one can see the south-dipping Basal Alluvial Conglomerates in the south, and the north-dipping Upper Alluvial Conglomerates in the north. The Basal Alluvial Conglomerates are overlain by a small package of Grey Breccia/conglomerates.

Observations + interpretation:

a. Whereas the northern boundary of the Basal Alluvial Conglomerates is poorly exposed in Section 1, it is here very clear. The south-tilted beds abruptly end along a linear feature, which is where the South Graben Fault is interpreted.
b. The Grey Conglomerate/breccia is offset 100 metres by a north-dipping fault. The fault plane is here covered in trees. The small down-faulted unit is also observed in Section 1.
c. The uppermost Grey Breccia/conglomerates terminate southwards against a third north-dipping fault which can be extrapolated from Section 1. The unit is not observed in the footwall of this fault.
d. The unconformity between the Basal and Upper Alluvial Conglomerates seen on the other side of Mt. Toriza (Section 1) is not observed here. It might be present, but covered by vegetation.

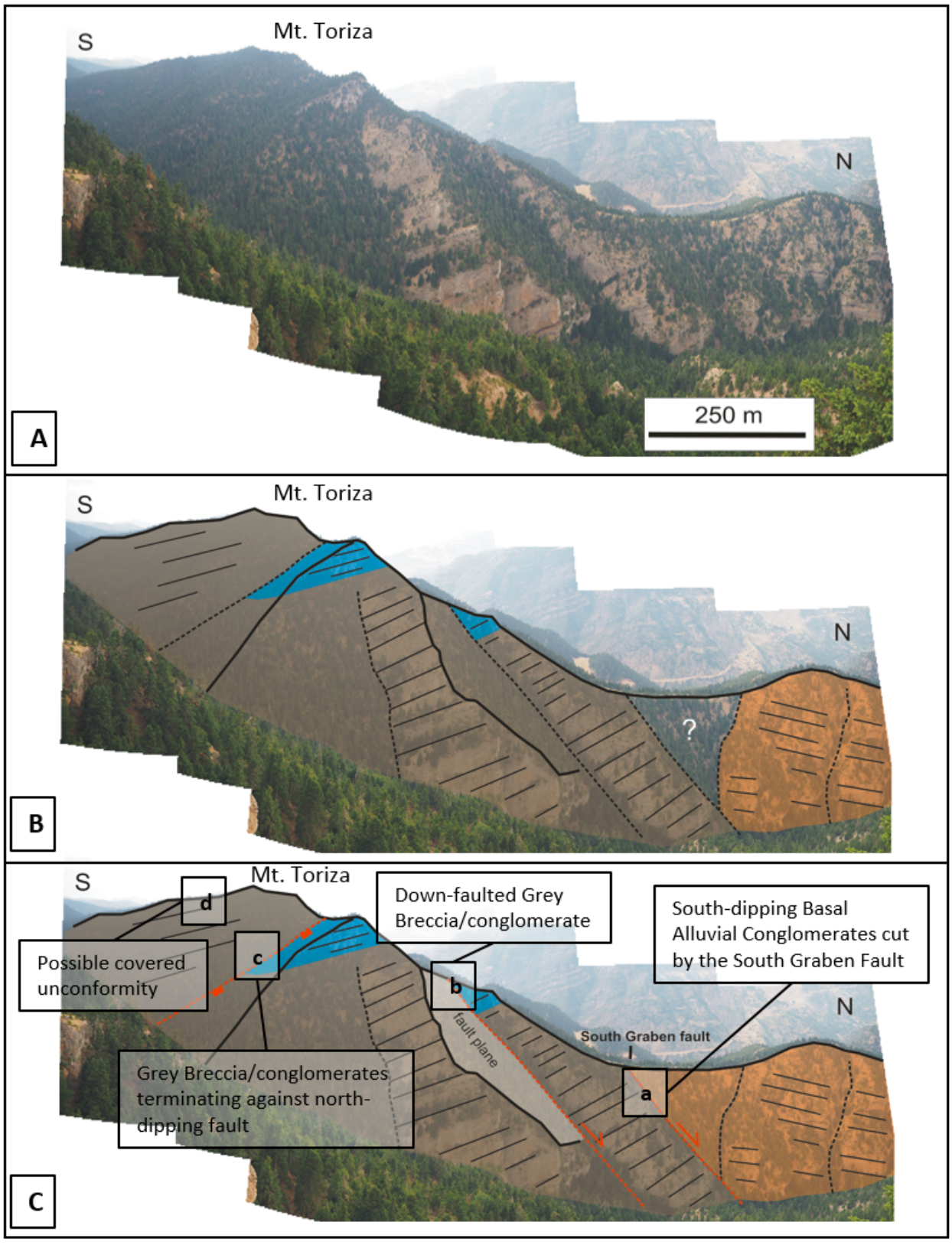

Figure 36: Section 2, View 1. A: original photo, B: observed lithological units and bedding, C: structural interpretation. The location of the photoed section is found in Figure 35.

3.4.2 View 2

From this view (Figure 37) one can observe the eastern side of Mt. Psili Rachi, and the massive Upper Alluvial Conglomerates overlying the Fluvial Conglomerates. Both units are here clearly approximately 10°N. As in Section 1, the Upper Alluvial Conglomerates climb northwards. This perspective is approximately along the strike of MSF1 and MSF3 observed in Section 1.

Observations + interpretation:

a. The fluvial/alluvial contact cannot be placed with the same level of confidence as in Section 1, as massive beds are observed almost all the way down to the base of the valley side. The valley side is too steep for close inspection of the units, and individual channels are not identified from distance. Based on the thickness of the Upper Alluvial Conglomerates in Section 1 (~200 m), the contact is here inferred at the base of the uppermost massive bed seen in the northern half of the photo. Given that the inferred fluvial/alluvial contact is correctly placed, the beds of the Fluvial Conglomerates are significantly thicker here compared to Section 1.
b. The half-synclinal shape of the Upper Alluvial Conglomerates in Section 1 is not seen on this side of Mt. Psili Rachi. It is thus believed that the shape is related to the displacement profile of MSF3 (increasing dip towards the fault tip), and not to fault-propagation folding or normal drag against a major north-dipping fault.

By extrapolating MSF1 and MSF3, their expected appearance in this section is at reasonable locations where there are evidence supporting faults.

c. MSF1 is marked by larger dips in its hangingwall compared to its footwall.
d. MSF3 is marked by an offset of the Upper Alluvial Conglomerates, and the unit appears thicker in the hangingwall.
e. To the north in the photo, the Upper Alluvial Conglomerates are displaced 100 metres by another south-dipping fault (hereby named Mega Spilio Fault 4 (MSF4)). This fault is not identified in Section 1.
f. The Fluvial Conglomerate beds are thinner in the footwall of MSF4 compared to the hangingwall. This is interpreted as distal thinning of the beds.

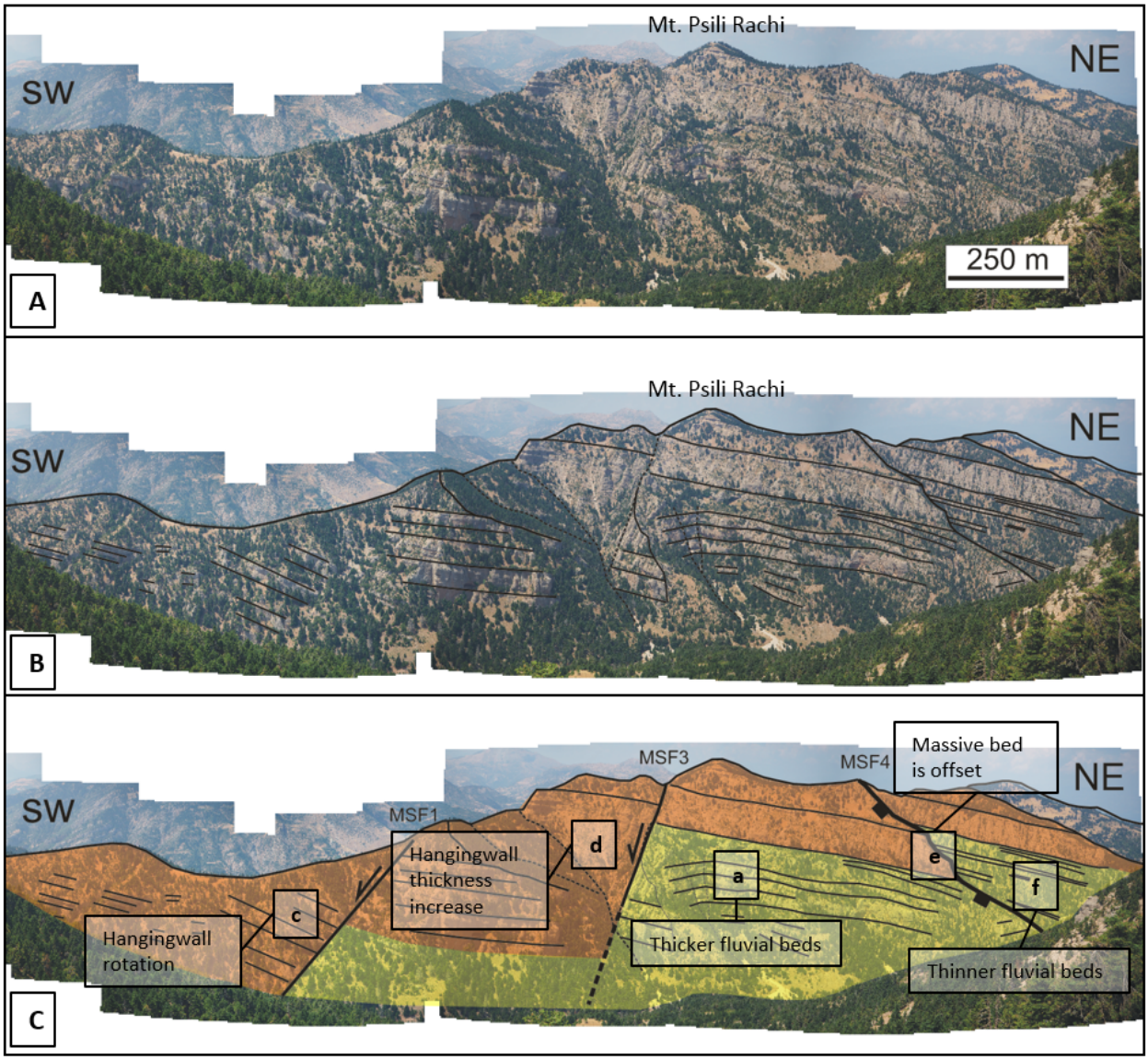

Figure 37: Section 2, View 2. A: original photo, B: bedding, C: structural and lithological interpretation. The location of the photoed section is found in Figure 35.

3.4.3 View 3

The northernmost part of Section 2 (Figure 38) displays the northern boundary of the Upper Alluvial Conglomerates. They are here laterally changing into a densely vegetated Fluvial Conglomerate succession. The Fluvial Conglomerates have few well-exposed beds observable from a distance, but from closer inspection they are generally thinner than those further south (in View 2). The succession is dominated by finer grained overbank deposits.

Observations + interpretation:

a. The massive Upper Alluvial Conglomerates terminate at an inlet in the valley side. Because of the planar nature of both the southern and northern inlet slope, it is reasonable to suspect the presence of a fault. A south-dipping fault here would explain why there are no Upper Alluvial Conglomerates north of the inlet. This will be further discussed in Chapter 4.
b. North of the valley side inlet only Fluvial Conglomerates are observed, consistently dipping ~5°N. This is slightly gentler than the beds south of the inlet, and could further indicate that there is a south-dipping fault in between.
c. There is another near-planar topographic surface in the very north of the photo, across which no beds could be traced. As tracing of beds might just be hindered by vegetation, the significance of the surface remain unknown.
d. An interesting observation when looking down the valley is the clear change of dip direction across the valley (a small part of the Upper Alluvial Conglomerates in Section 3 is visible to the very left in Figure 38). This will be discussed later in Chapter 4.

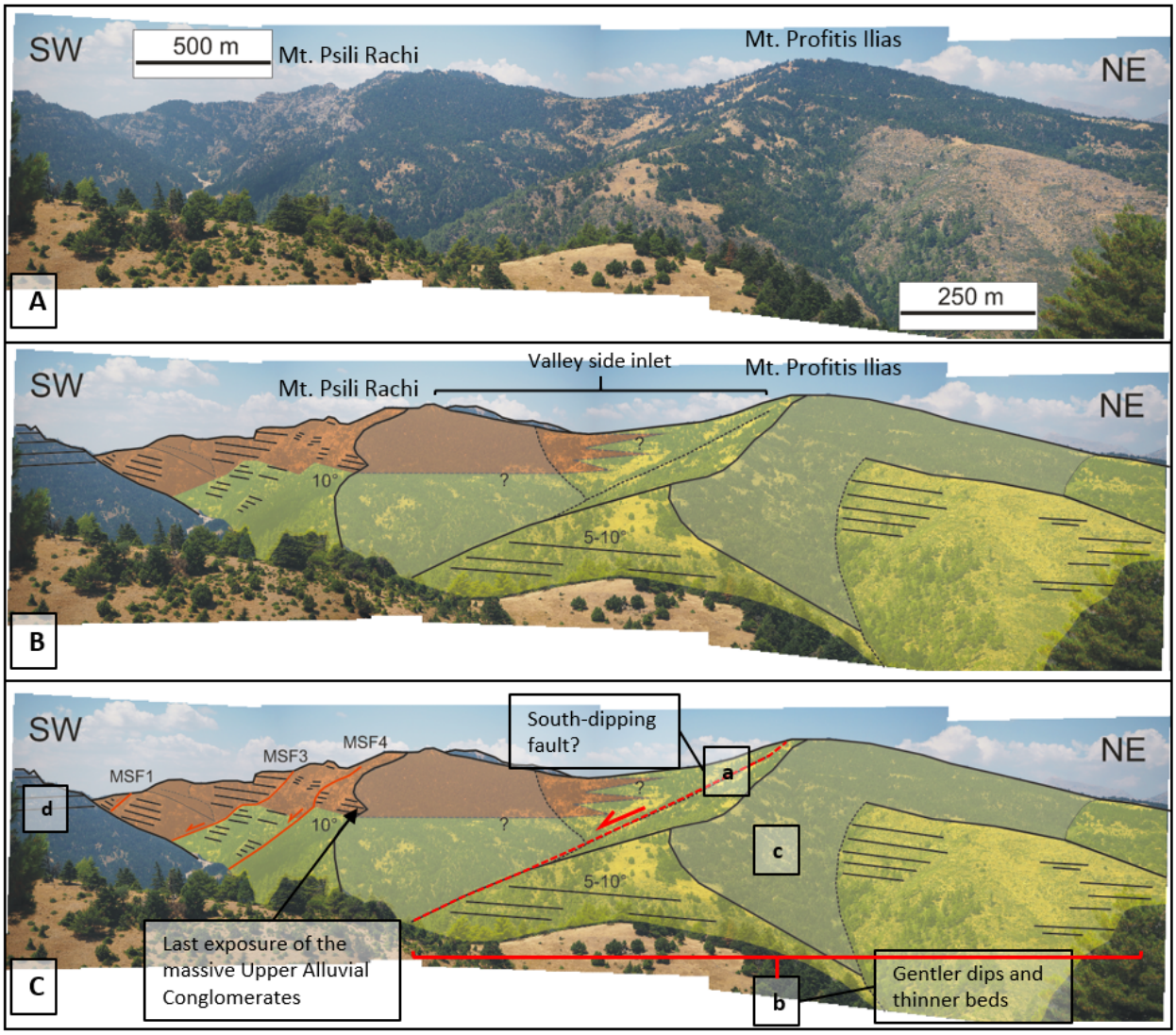

Figure 38: Section 2, View 3. A: original photo, B: observed lithological units and bedding, C: structural interpretation. The location of the photoed section is found in Figure 35.

3.4.4 Complete valley section

Figure 39 shows a simplified overview of the complete Section 2, highlighting the main interpretations from the previous sub-chapters. All valley sections will be compared in Sub-chapter 3.8.

Both the Fluvial and Upper Alluvial Conglomerates are north-dipping along the studied interval of Section 2, which is quite anomalous in a region dominated by south-tilted fault blocks. The major Mamoussia-Pirgaki Fault is located directly north of Section 2, and one would expect southward dips in its immediate uplifted footwall. The 10°N dip of the Upper Alluvial Conglomerates and underlying Fluvial Conglomerates might be justified by a south-dipping fault in the valley side inlet (described in the previous sub-chapter). The 5°N dip in the northernmost Fluvial Conglomerates can be interpreted either as a depositional dip (post rotation), or as rotation caused by an unidentified south-dipping fault north of Section 2.

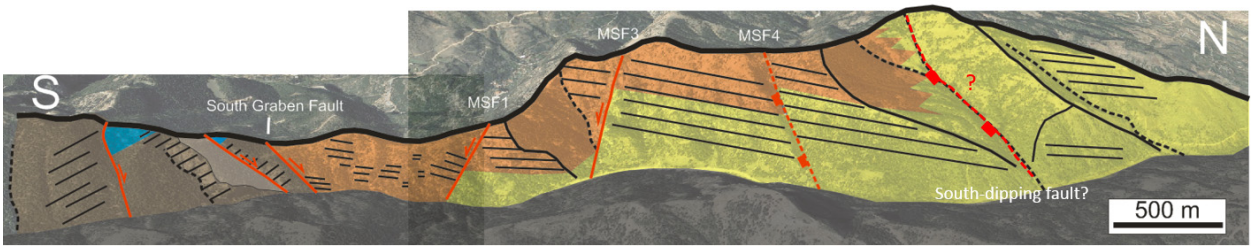

Figure 39: Full interpretation of Section 2 on photo from Google Earth. The horizontal and vertical scales are not proportional. The section is a compilation of the three views marked on Figure 35.

3.5 Valley section 3: Ladopotamos East

Section 3 is along the eastern side of Ladopotamos River Valley, and it exhibits some of the same structural and stratigraphic features as seen in Section 1 and 2. The Upper Alluvial Conglomerates are climbing northwards across possible south-dipping faults, and there is a major dip difference between the footwall and hangingwall sediments of the South Graben Fault (the Basal and Upper Alluvial Conglomerates respectively). In the footwall of the South Graben Fault the Basal Alluvial Conglomerates are unconformably overlain by the Upper Alluvial Conglomerates. The features in Section 3 are captured by photos from 4 viewpoints, all marked in Figure 40. They are presented from north to south. The state of exposure in this valley section is quite poor.

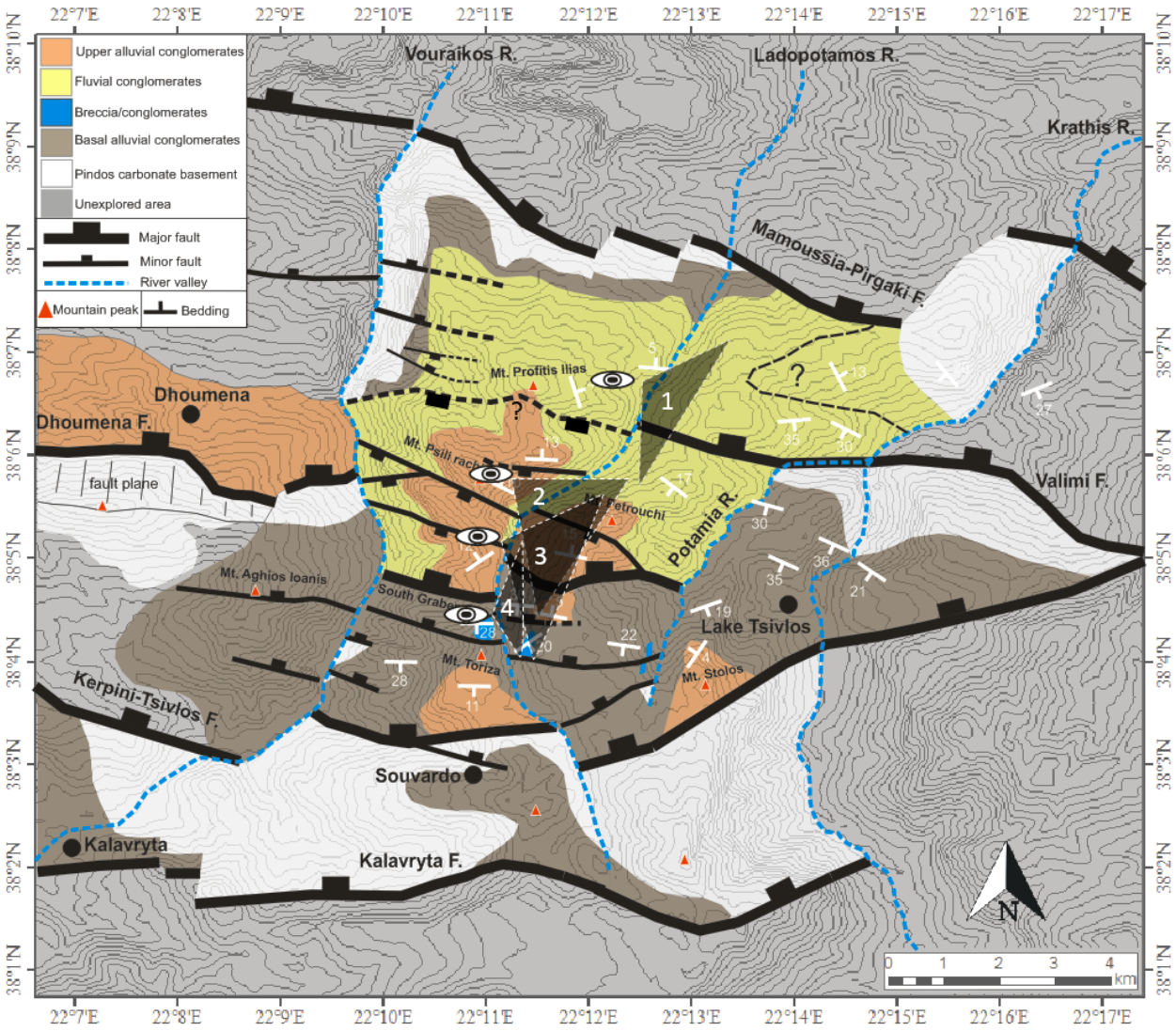

Figure 40: Structural map showing the four different viewpoints from which Section 3 is photoed.

3.5.1 View 1

In the northernmost part of Section 3 (Figure 41) only Fluvial Conglomerates are observed. The succession is overgrown by trees, and there are thus very little information to extract from this view. A near-linear feature amidst the vegetation is still worth mentioning, as it aligns with the strike of the Valimi Fault. It also aligns with the northern boundary of the Upper Alluvial Conglomerates in Section 2, where the potential presence of a fault was discussed.

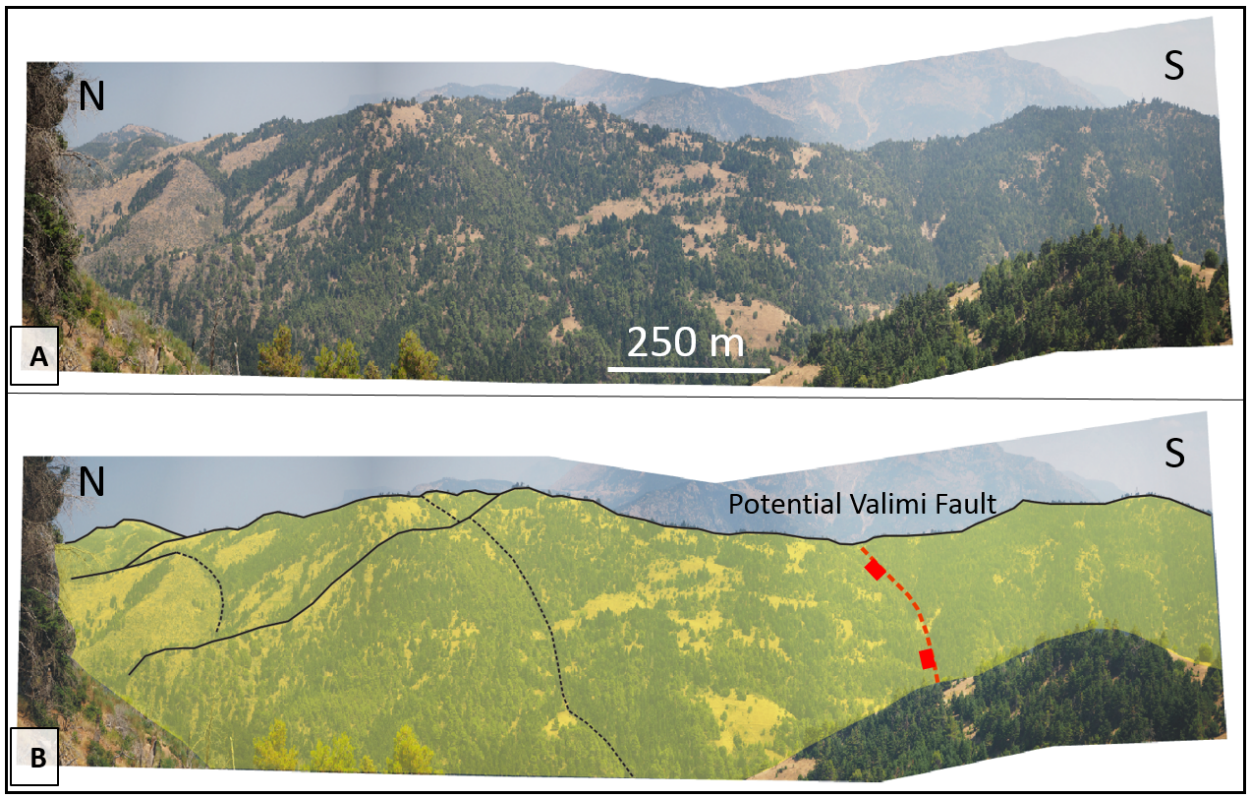

Figure 41: Section 3, View 1. A: original photo, B: lithology and structural interpretation. The location of the photoed section is found in Figure 40.

3.5.2 View 2

In View 2 (Figure 42) one can observe some massive Upper Alluvial Conglomerates at Mt. Petrouchi, overlying the Fluvial Conglomerates. One can also look south down the Ladopotamos River towards where the South Graben Fault is interpreted. This fault, along with the other southern features will be described in View 3 and 4.

Observations + interpretation:

a. The northern boundary of the Upper Alluvial Conglomerates is abrupt, and they appear to change laterally into Fluvial Conglomerates. Although not exposed, it is reasonable to suspect that this sharp contact is controlled by a south-dipping fault. The south-dipping MSF4 is observed directly across the valley in Section 2, and could potentially correlate across. The possible presence of a fault here will be further discussed in Sub-chapter 3.6, where a photo of the other side of Mt. Petrouchi is provided.
b. The Upper Alluvial Conglomerates at Mt. Petrouchi are sub-horizontal, while the ones directly south of it are dipping 10°N. This dip change is very sudden, and it is interpreted to be caused by a south-dipping fault, hereby referred to as the Petrouchi Fault. Whereas the base of the Upper Alluvial Conglomerates is well exposed in the footwall of the Petrouchi Fault, it is not identified in the hangingwall because of dense vegetation. The displacement of this fault is thus unclear, but it would have to be several tens of metres in order to rotate the beds ~10°.
c. The Petrouchi Fault and South Graben Fault forms a graben. As the graben beds dip towards the north, the Petrouchi Fault is likely younger than the South Graben Fault.

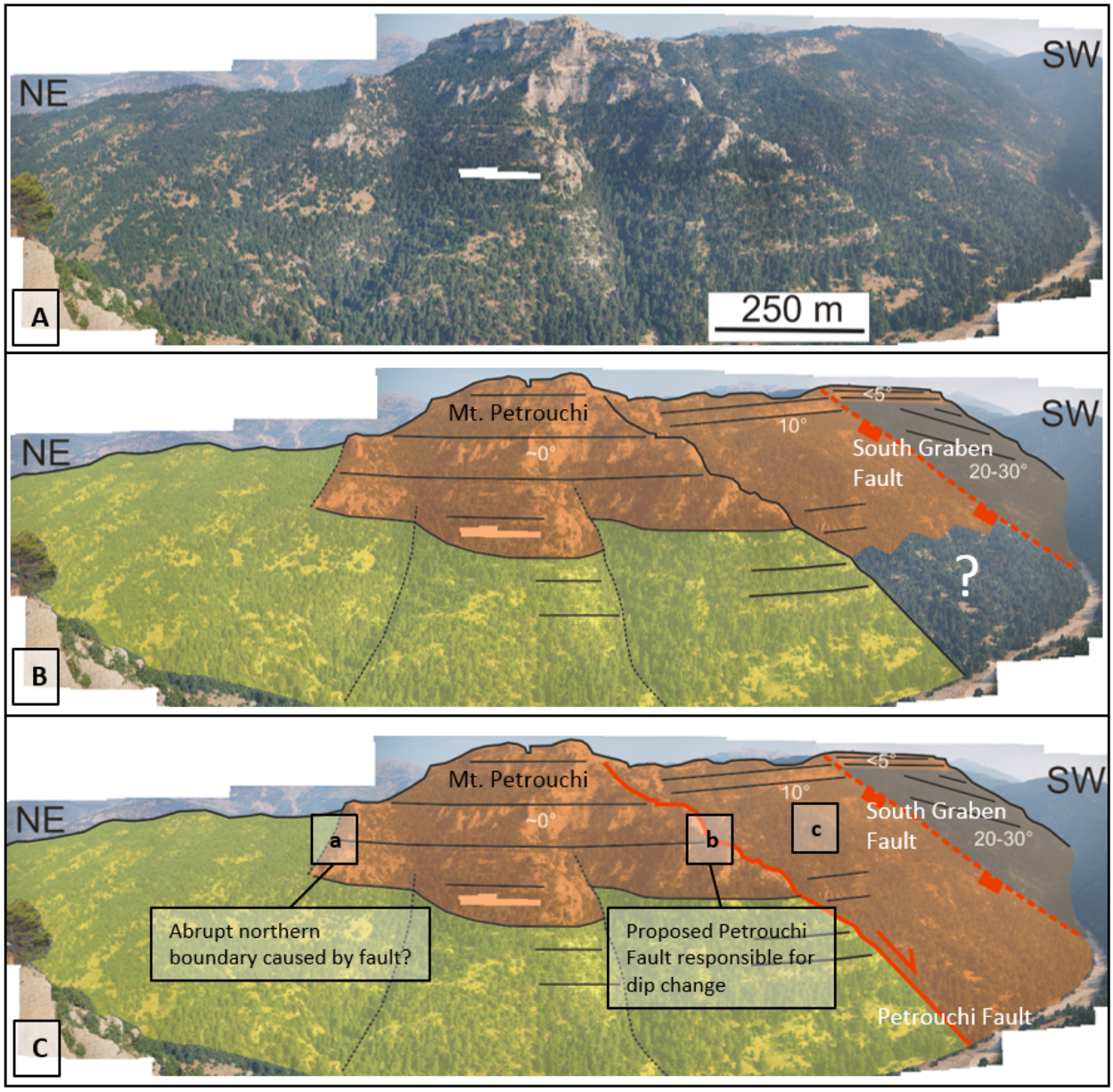

Figure 42: Section 3, View 2. A: original photo, B: observed lithological units and bedding (plus the South Graben Fault in the distance), C: structural interpretation. The location of the photoed section is found in Figure 40.

3.5.3 View 3

View 3 (Figure 43) is centred on the contact between the south-dipping Basal Alluvial Conglomerates and the north-dipping Upper Alluvial Conglomerates, where the South Graben Fault is interpreted.

Observations + interpretation:

a. Between the south and north-dipping conglomerates there is a pronounced linear feature in the valley side. This is interpreted as the continuation of the South Graben Fault from Section 2, after a 600 metre step northwards.
b. There is a 20° angular unconformity in the footwall of the inferred South Graben Fault, as south-dipping Basal Alluvial Conglomerates truncate into an overlying 80 metre package of sub-horizontal alluvial conglomerates. Whereas the unconformity observed in Section 1 is not that clear, it is from this observation evident that there were in fact two stages of alluvial deposition with a significant time gap in between. The older unit has been rotated before deposition of the second unit.
c. The second-phase alluvial unit (Figure 23) is similar to the ones in the hangingwall of the South Graben Fault and at Mt. Petrouchi (Figure 22) in terms of colour, bed thickness and clast size, and it is thus believed to belong to the Upper Alluvial Conglomerates.
d. In the immediate footwall of the South Graben Fault, near the bottom of the valley, is a thick package with horizontal beds that does not seem to fit in with the steeply south-dipping conglomerates. This will be discussed in View 4, as more beds are exposed from that perspective.

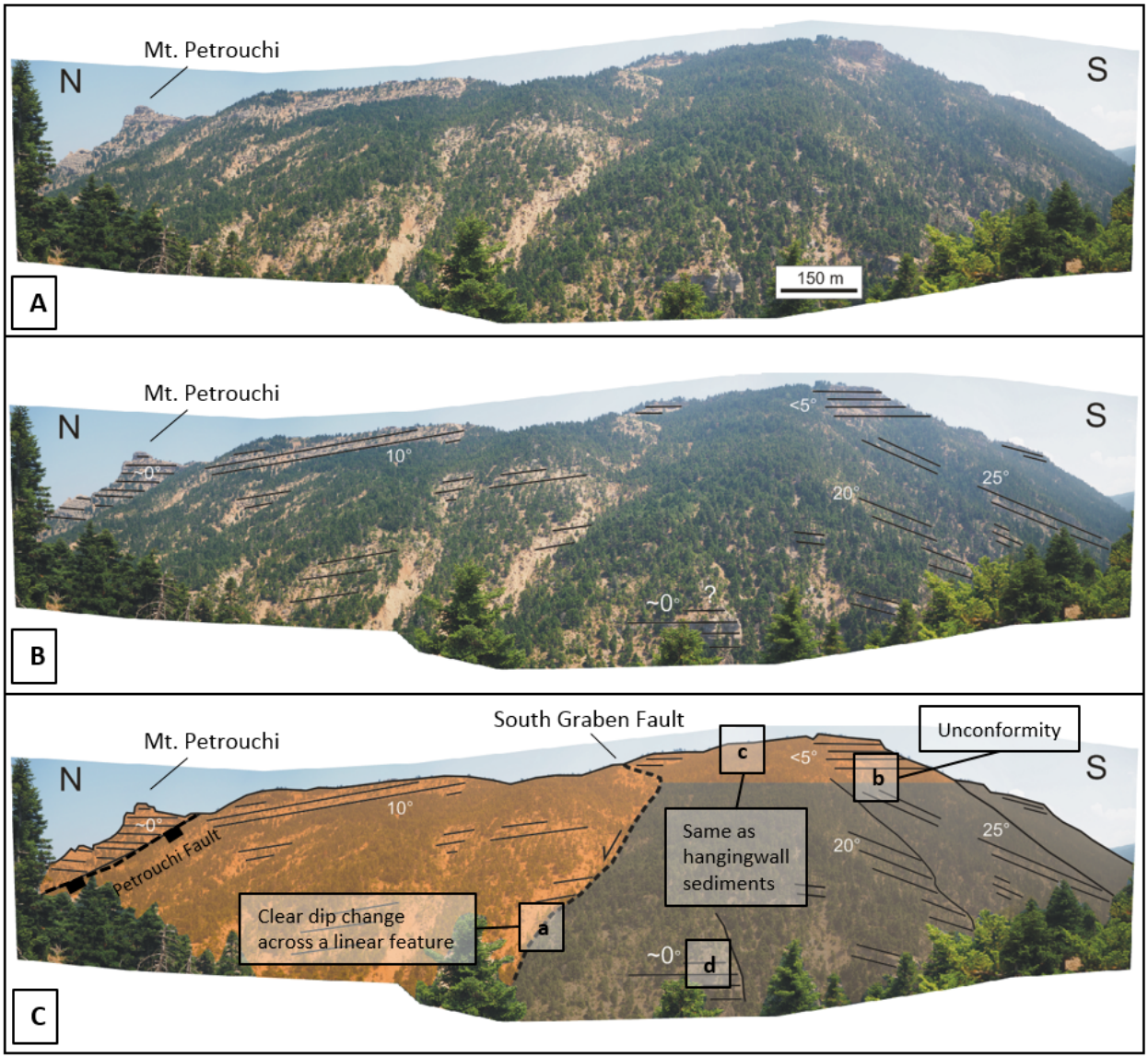

Figure 43: Section 3, View 3. A: original photo, B: bedding, C: lithological and structural interpretation. The location of the photoed section is found in Figure 40.

3.5.4 View 4

View 4 (Figure 44) allows for a closer look at the unconformity in the footwall of the South Graben Fault, as well as a better perspective on the Basal Alluvial Conglomerate beds. To the very south, the Basal Alluvial Conglomerates are overlain by Grey Breccia/conglomerates.

Observations + interpretation:

a. Although it is difficult to see in this photo, the Basal Alluvial Conglomerates in the immediate footwall of the South Graben Fault are horizontal. Whereas the horizontal beds are only visible at the base of the valley side in View 3, they are here seen at even higher elevations. The dip angles of the Basal Alluvial Conglomerates are progressively increasing southwards, from a horizontal dip to 33° over a distance of 800 metres. However, the dip does not increase smoothly and the beds are not folded. It increases in stages (from block to block) across discontinuities in the valley side. This is interpreted as minor faulting related to normal drag along the South Graben Fault.
b. The package of Upper Alluvial Conglomerates on top is not affected by the faulting, and is thus believed to post-date the initiation of the South Graben Fault.
c. The southern extent of the Upper Alluvial Conglomerates is limited by a proposed north-dipping fault. The presence of a fault here is supported by a 10° hangingwall dip increase and by juxtaposition of the Upper Alluvial Conglomerates against the Basal Alluvial Conglomerates.
d. To the very south, a 30 metre thick package of Grey Breccia/conglomerate overlies the Basal Alluvial Conglomerates. Its dip angle is similar to the Basal Alluvial Conglomerates in the immediate hangingwall of the fault inferred in “c” (23°S). Some thin beds below have steep anomalous dips of 60°S, and is interpreted as slump deposits covering the Basal Alluvial Conglomerates. The contact between the Grey Breccia/conglomerates and Basal Alluvial Conglomerates is believed to be parallel, as observed in Section 2.

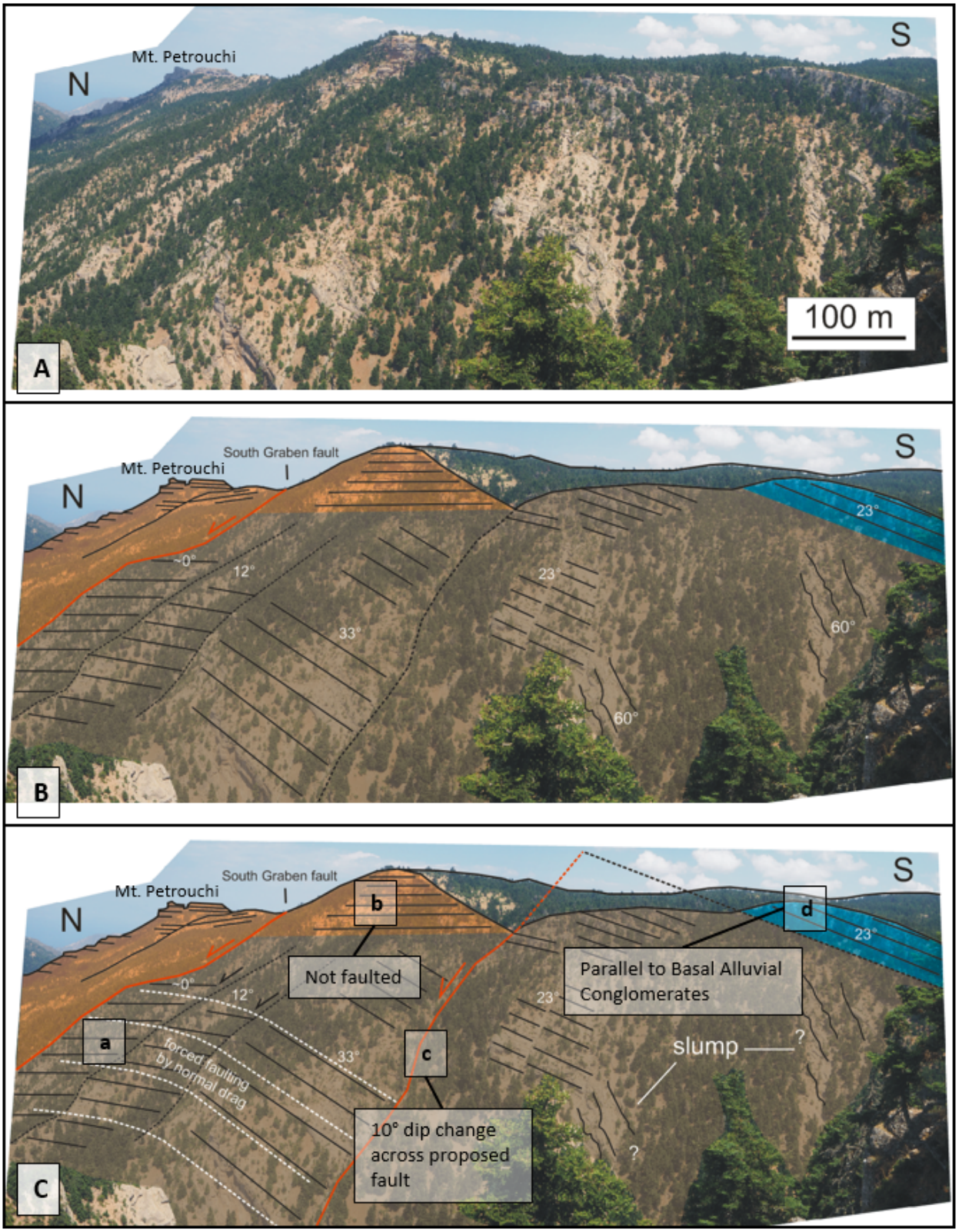

Figure 44: Section 3, View 4. A: original photo, B: observed lithological units and bedding (plus the South Graben Fault), C: structural interpretation. The location of the photoed section is found in Figure 40.

3.5.5 Complete valley section

Figure 45 shows a simplified overview of the complete Section 3, highlighting the main interpretations from the previous sub-chapters. All valley sections will be compared in Sub-chapter 3.8.

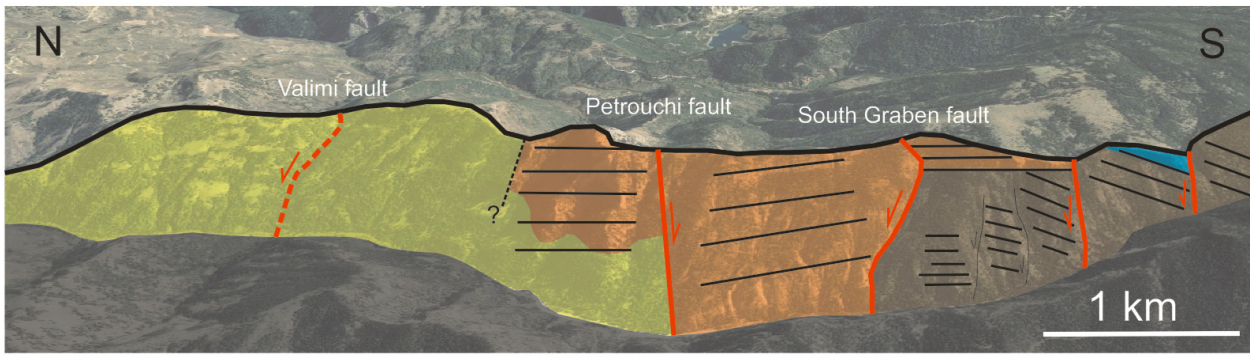

Figure 45: Full interpretation of Section 3 on photo from Google Earth. The horizontal and vertical scales are not proportional. The section is a compilation of the four views in this sub-chapter.

3.6 Valley section 4: Potamia/Krathis West

Section 4 is along the western valley side of Krathis and Potamia Rivers, i.e. the eastern side of the mountain in Section 3. Most of the features in Section 3 are also observed here. They are captured by photos from three different viewpoints, all marked in Figure 46. They are here presented from south to north. The state of exposure in this section is generally better than in Section 3.

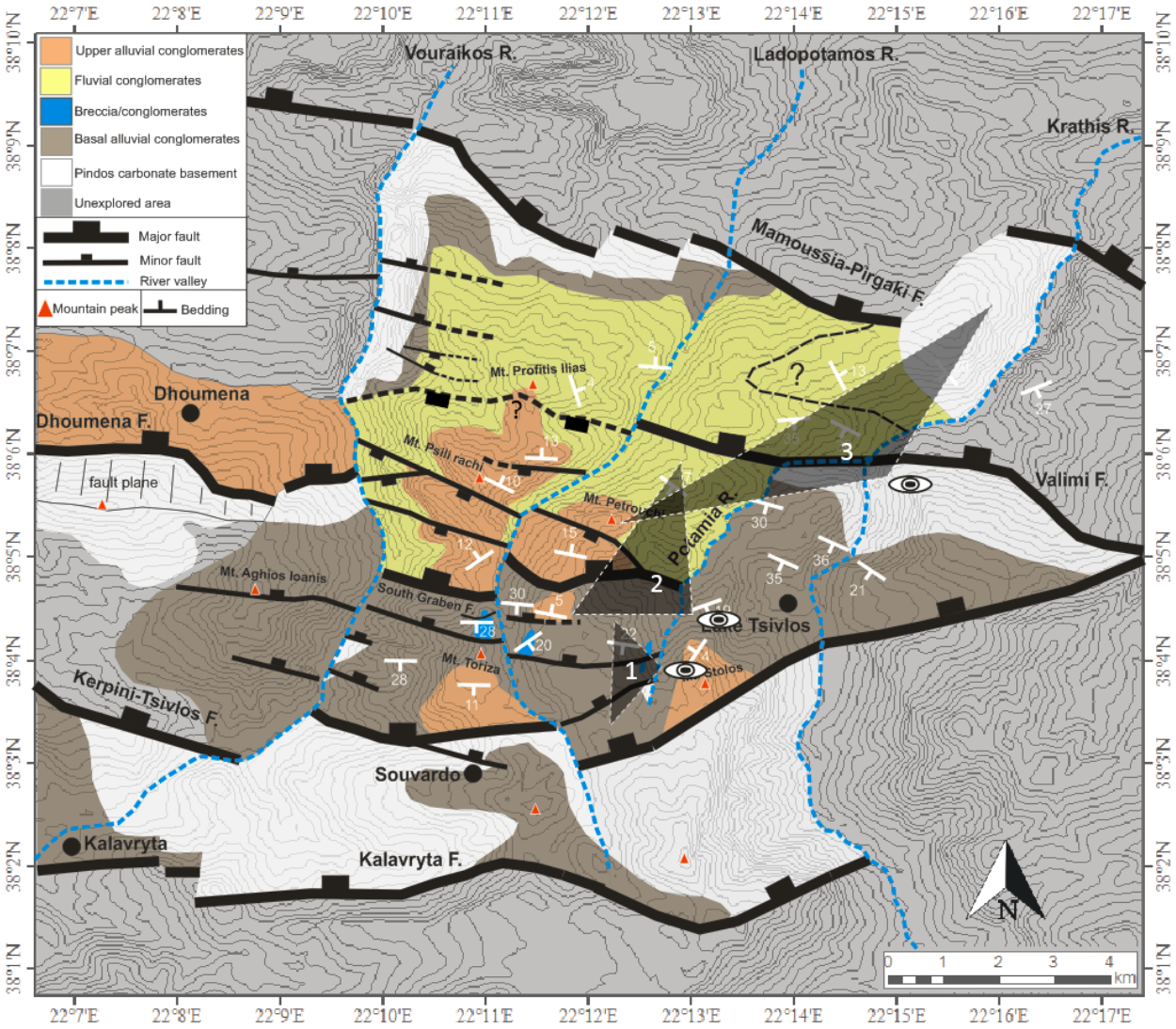

Figure 46: Structural map showing the three viewpoints from which Section 4 is photoed.

3.6.1 View 1

The southernmost part of Section 4 (Figure 47) is in the immediate hangingwall of the Kerpini-Tsivlos Fault. The valley side is densely vegetated, and there are few features visible on the photo.

Observations + interpretation:

a. A few hundred metres north of the Kerpini-Tsivlos Fault is a small basement inlier (Figure 47) passing into south-tilted Basal Alluvial Conglomerates northwards, suggesting the presence of a north-dipping fault. Its displacement is estimated to be ~500 metres. The exact contacts between the basement and Basal Alluvial Conglomerates are not identified, and so the dip of the fault and unconformity surface is unknown.
b. Within the Basal Alluvial Conglomerates is a 10 metre thick package of Grey Breccia/conglomerate (Figure 26). Its extent is not determined as the valley side is mostly covered by soil and vegetation.
c. This Grey Breccia/conglomerate package is displaced ~30 metres by another smaller north-dipping fault. The beds are dipping slightly steeper in the hangingwall.

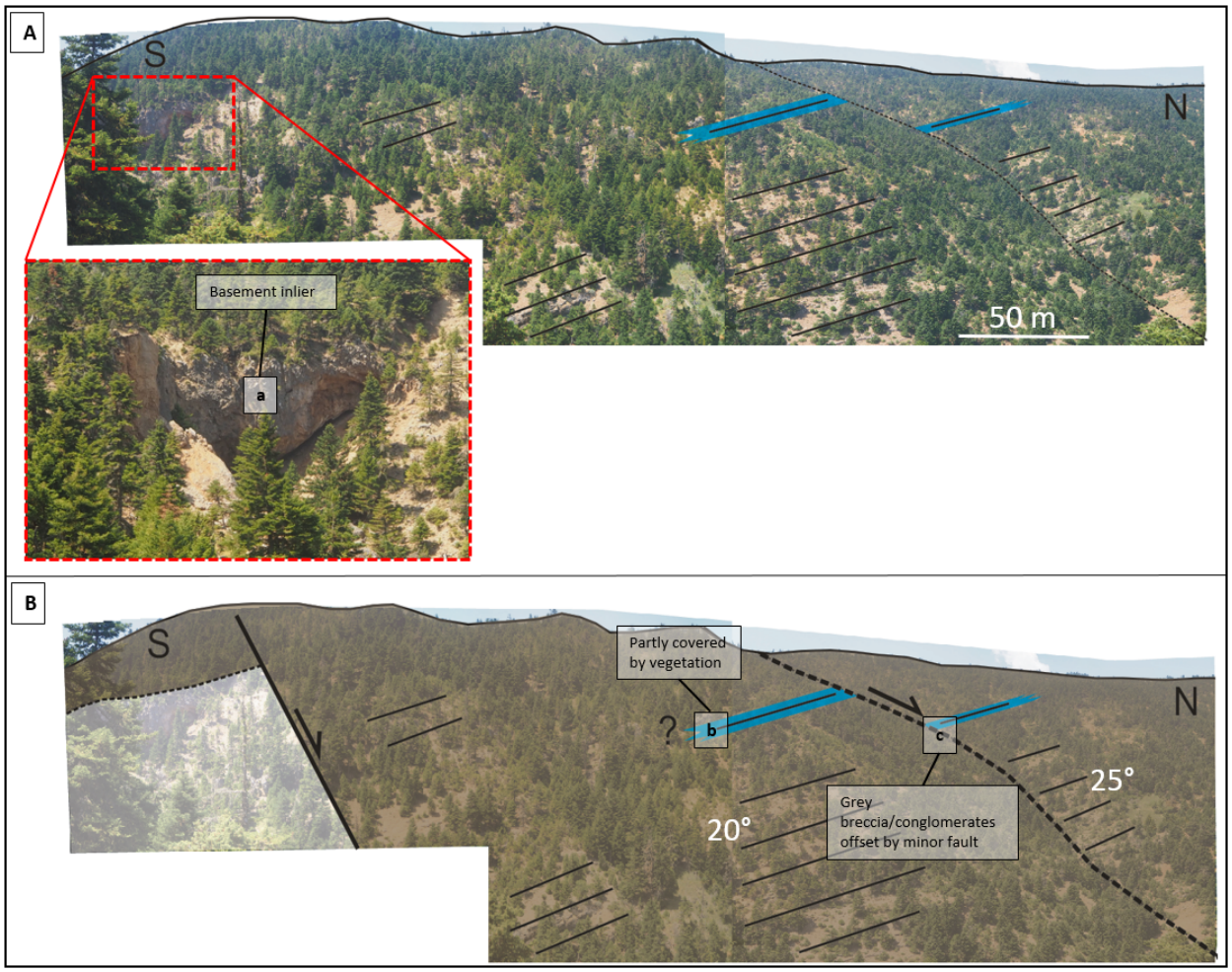

Figure 47: Section 4, View 1. A: bedding and lithological units, B: structural interpretation. The location of the photoed section is found in Figure 46.

3.6.2 View 2

From View 2 (Figure 48) one can observe the northern boundary of the Basal Alluvial Conglomerates, and the Fluvial and Upper Alluvial Conglomerates at Mt. Petrouchi. In contrast to Section 3, the fluvial beds here are well exposed.

Observations + interpretation:

a. The Basal Alluvial Conglomerates consistently dip 20-25°S until they reach the South Graben Fault which is extrapolated from Section 3.
b. As in Section 3, the Upper Alluvial Conglomerates in the hangingwall of the South Graben Fault are dipping north towards Mt. Petrouchi, where there is a sudden change into massive horizontal beds. The Petrouchi Fault, inferred in Section 3, is thus evidenced here as well.
c. The horizontal Upper Alluvial Conglomerates at the peak of Mt. Petrouchi (i.e. the footwall of the Petrouchi Fault) are progressively increasing in dip down-section, reaching dips of approximately 20°S in the underlying Fluvial Conglomerates. Such bedding geometries are typical for syn-rift deposition, and it seems evident that these sediments were growing towards the South Graben Fault which was active at the time of deposition. The Petrouchi Fault then post-dates the South Graben Fault, causing a later northward rotation of the graben sediments.
d. The contact between the Fluvial and Upper Alluvial Conglomerates is not identified in the graben, and consequently the displacement on the Petrouchi Fault remains uncertain.
e. Some sub-horizontal beds are observed on the very top of the footwall of the South Graben Fault, which most likely belong to the unconformable Upper Alluvial Conglomerate package seen in Section 3 (although the unconformity is not visible here).
f. An abrupt northward termination of the Upper Alluvial Conglomerates was observed in Section 3, suggesting it might be limited by a south-dipping fault. In Section 4 it seems more like its extent is controlled by erosion, as the contact between the Fluvial and Upper Alluvial Conglomerates extrapolates into mid-air immediately north of Mt. Petrouchi. If a south-dipping fault is present north of Mt. Petrouchi, the displacement would in that case be very small.

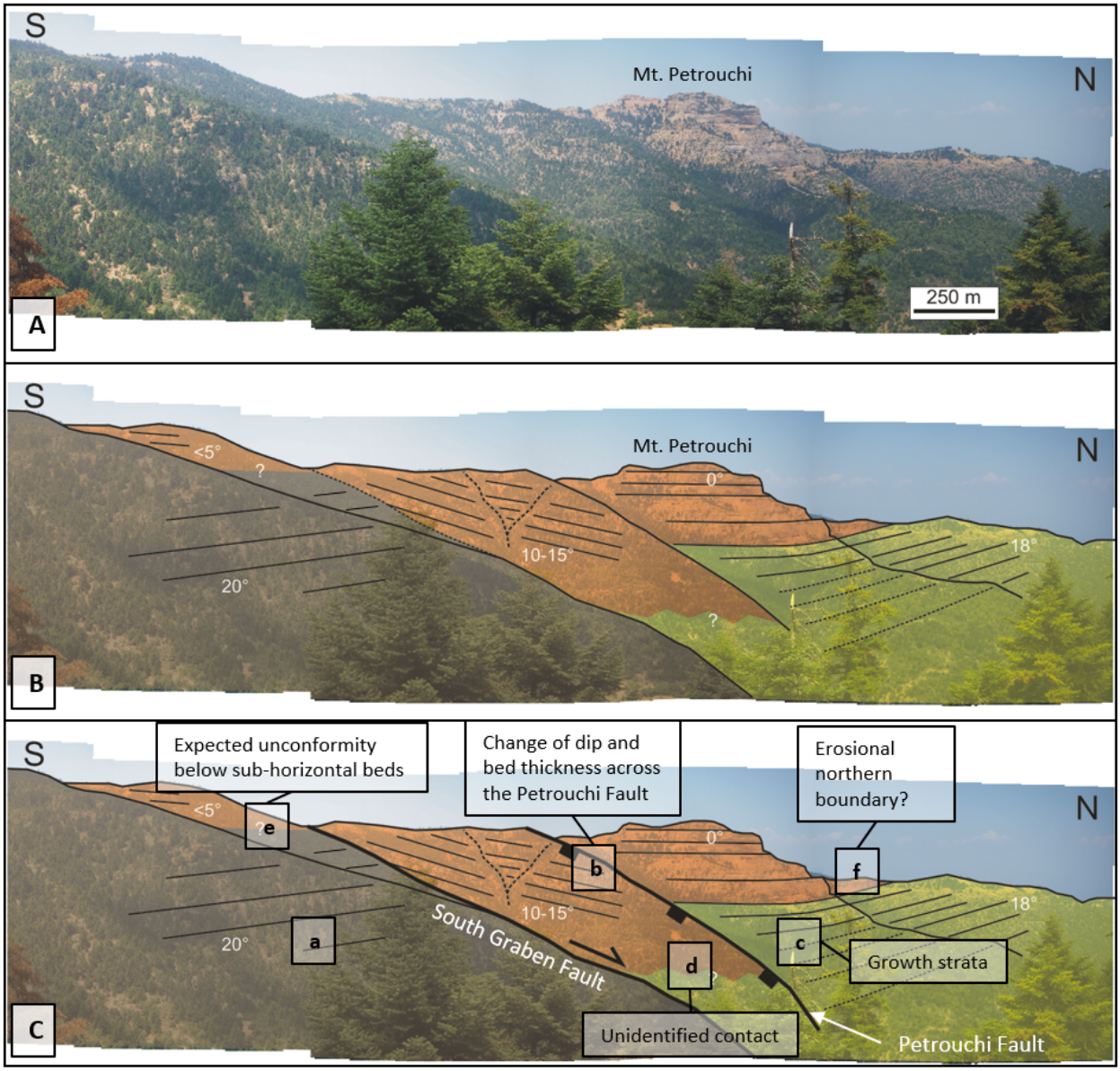

Figure 48: Section 4, View 2. A: original photo, B: observed lithological units and bedding, C: structural interpretation. The location of the photoed section is found in Figure 46.

3.6.3 View 3

Figure 49 displays the northernmost (fluvial dominated) part of Section 4, from Mt. Petrouchi in the south to the uplifted basement footwall of the Mamoussia-Pirgaki Fault in the north.

Observations + interpretation:

a. North of Mt. Petrouchi there is a sudden and drastic change in dip angle within the Fluvial Conglomerates, from 20°S below Mt. Petrouchi, to steeply dipping beds of 35-40°S. This is interpreted as hangingwall rotation related to the Valimi Fault. This is a major basement involved fault (displacement of 1-1.5 km) which is traceable from the east along a clear basement/conglomerate contact. The strike of the Valimi Fault aligns well with the observed dip change in Section 4.
b. Another drastic dip change is observed approximately two kilometres north of the Valimi Fault, as conglomerates are dipping 13°N towards a south-tilted basement block (the uplifted footwall crest of the Maomoussia-Pirgaki Fault). These conglomerates are not studied in detail, but were mapped as Fluvial Conglomerates in the field based on bed thickness (~1 m), clast imbrication (indicates NE flow, Figure 50) and interlayers of sand/silt. However, no clear channel geometries are identified. It is problematic to correlate this unit to the Fluvial Conglomerates in the immediate hangingwall of the Valimi Fault, as its relationship with the steeply south-dipping beds cannot really be explained with a fault. It might be a late progradational unit with a depositional dip of 13°, unconformably overlying the south-dipping Fluvial Conglomerates.

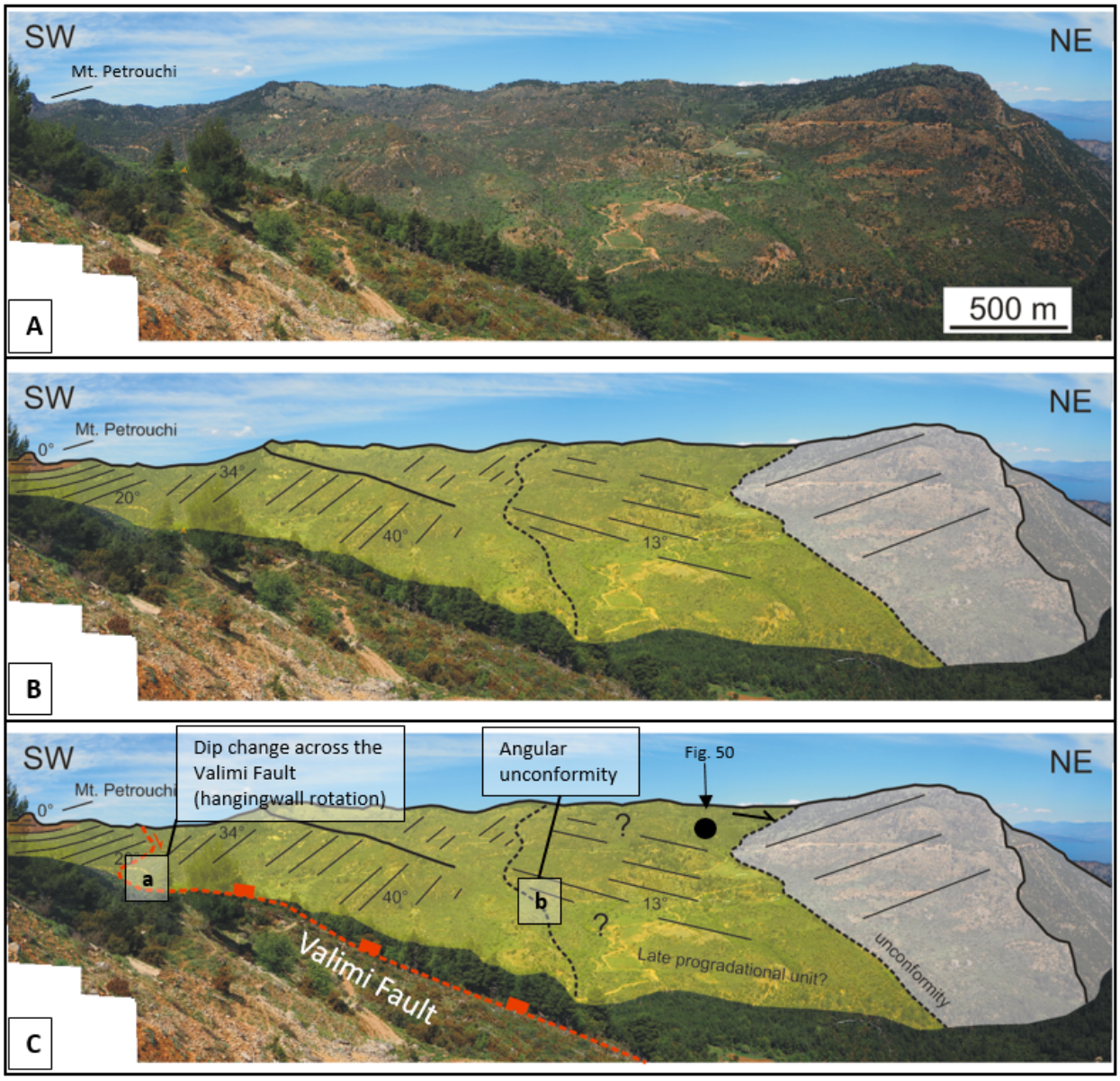

Figure 49: Section 4, View 3. A: original photo, B: observed lithological units and bedding, C: structural interpretation. The location of the photoed section is found in Figure 46.

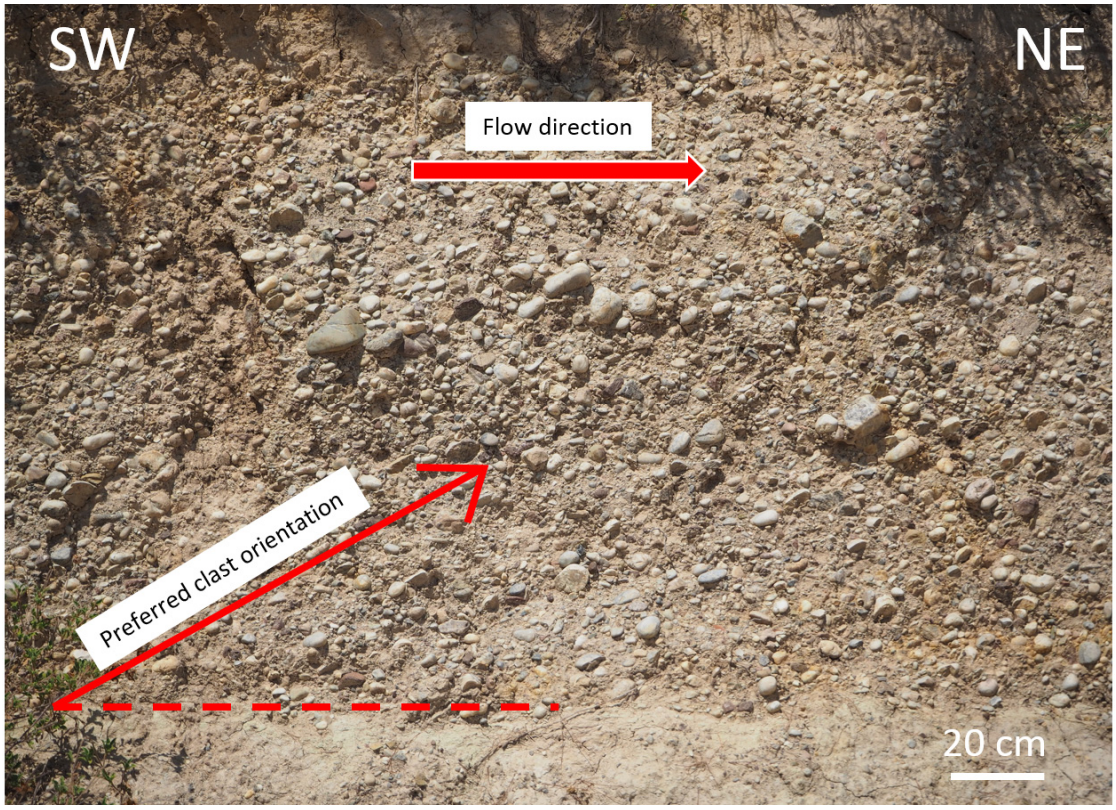

Figure 50: Outcrop of the northernmost north-dipping conglomerates in Section 4, which might be a late NE-prograding unit. The outcrop location is marked on Figure 49

3.6.4 Complete valley section

Figure 51 shows a simplified overview of the complete Section 4, highlighting the main interpretations from the above sub-chapters. All valley sections will be compared in Sub-chapter 3.8.

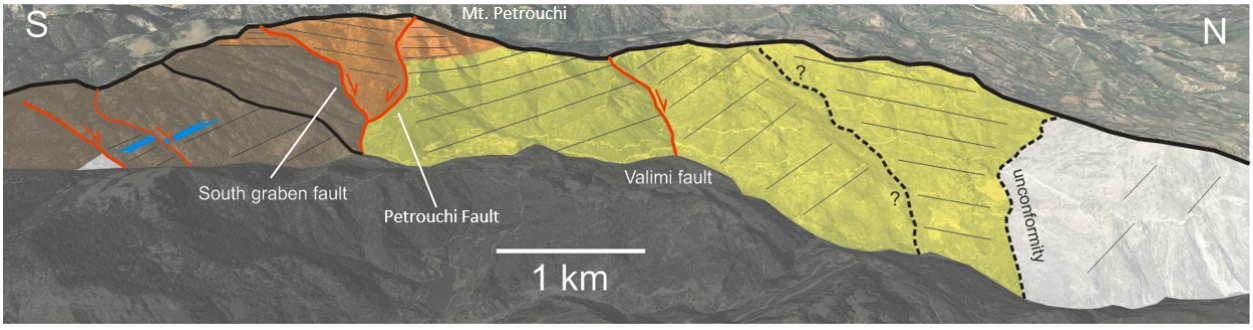

Figure 51: Google Earth photo with interpretation of Section 4. The horizontal and vertical scales are not proportional. The section is a compilation of the three views in the previous sub-chapter.

3.7 Valley section 5: Krathis West – Tsivlos

Section 5 (location marked on Figure 52) is located in the western valley side of Krathis River, limited by the Kerpini-Tsivlos Fault in the south and the Valimi Fault in the north. The section is only 3.5 kilometres long, and its main features are captured by one single composite photo (Figure 53). It displays a thick succession of Basal Alluvial Conglomerates on top of an exposed basement unconformity.

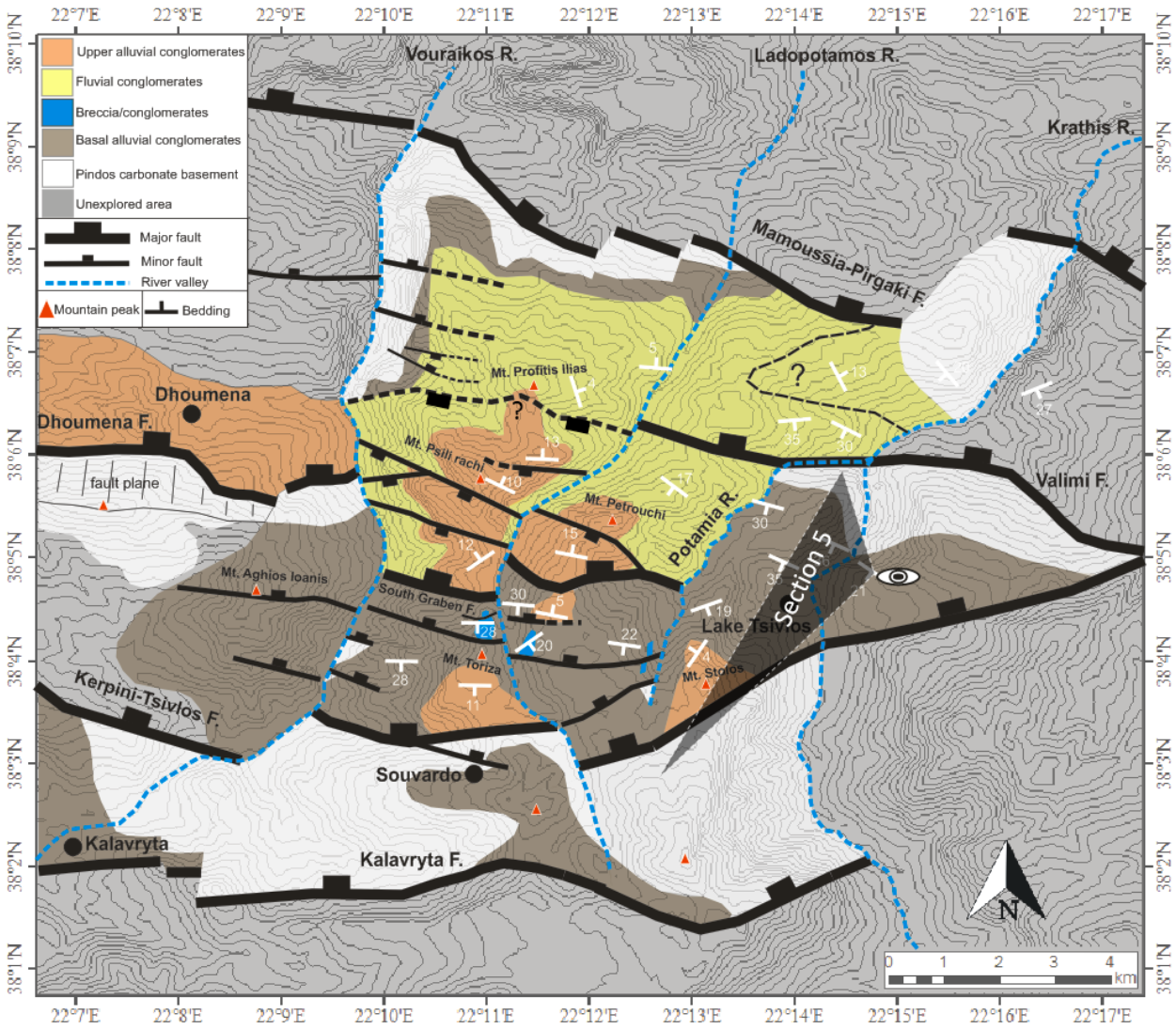

Figure 52: Structural map showing the viewpoint from which Section 5 is photoed.

Observations + interpretation:

a. The Kerpini-Tsivlos Fault is here very evident, as a massive basement unit is down-thrown more than two kilometres and buried below a thick succession of Basal Alluvial Conglomerates. A part of its fault plane is also exposed.
b. The basement crops out again in the immediate footwall of the Valimi Fault. It is strongly south-tilted, and the unconformity surface is overlain (seemingly parallel) by Basal Alluvial Conglomerates.
c. Whereas none of the other studied valley sections reveal syn-rift geometries within the Basal Alluvial Conglomerates, it is here evidence of sedimentation while faulting. At the base of the valley side is a package of massive beds dipping 35°S. This package is onlapped by thinner beds dipping 24°S, apparently decreasing up-section gradually to 13°S. The onlap indicates that the whole unit was not deposited continuously while the Kerpini-Tsivlos Fault was moving. It was deposited in two or several pulses. The time gap between the first and second pulse was significant, allowing the fault block to rotate 11° at the time of non-deposition.
d. At the peak of Mt. Stolos is a more solid-looking package of onlapping sub-horizontal beds (Figure 54). From a distance this package is similar in appearance to the Upper Alluvial Conglomerates seen unconformably overlying the Basal Alluvial Conglomerates in Section 1 and 3. It is here interpreted as the same Upper Alluvial Conglomerate unit, although it could also be considered as the uppermost part of the syn-rift sequence of Basal Alluvial Conglomerates.

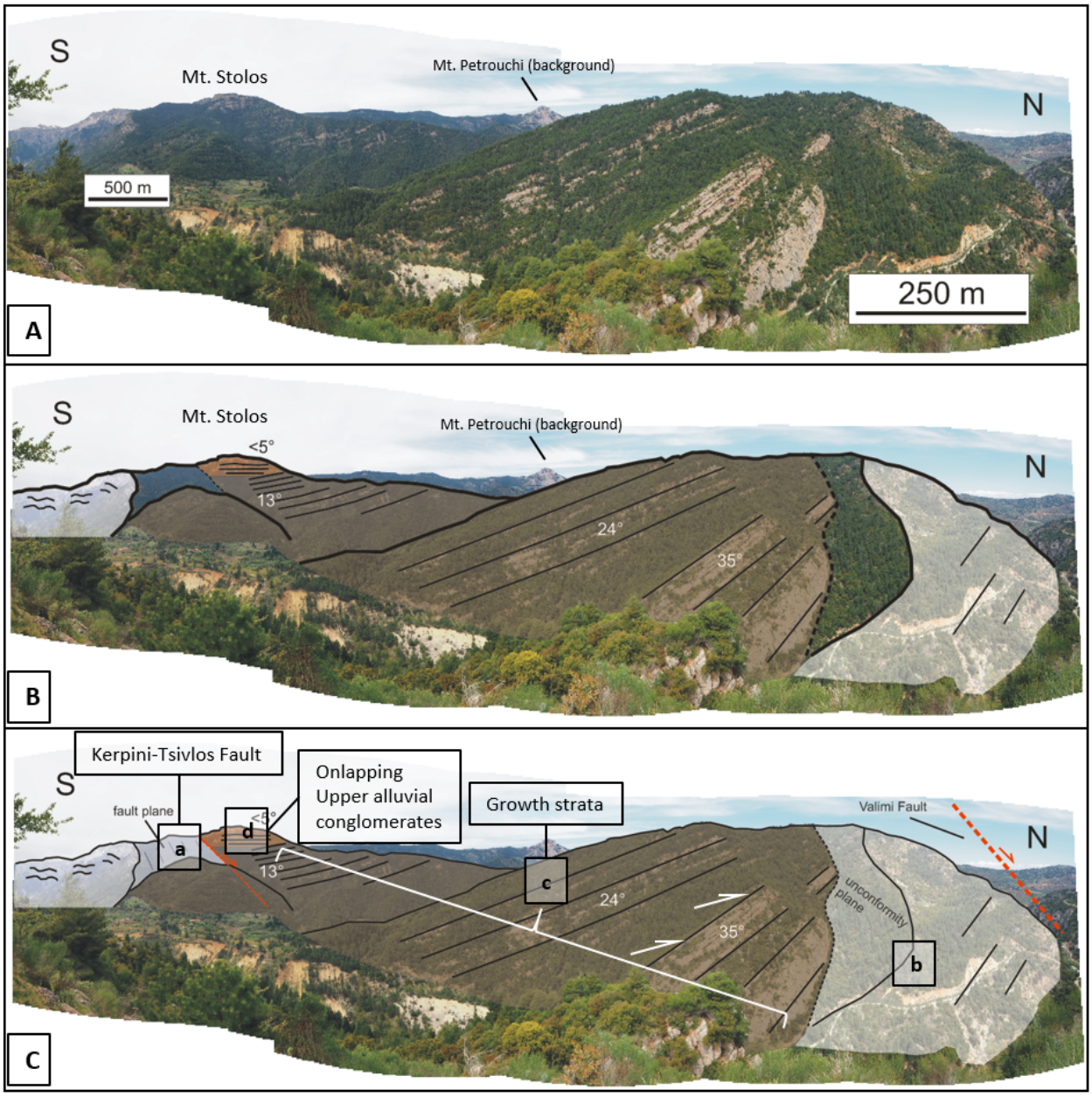

Figure 53: Section 5. A: original photo, B: observed lithological units and bedding, C: structural interpretation. The location of the photoed section is found in Figure 52.

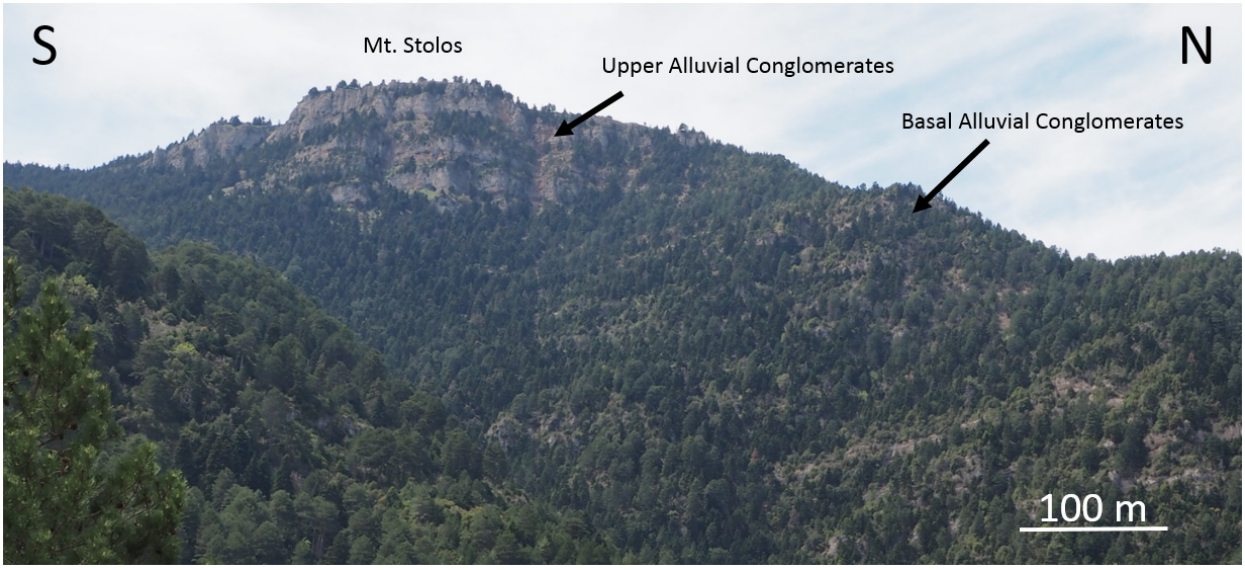

Figure 54: Zoomed-in photo of the uppermost conglomerate beds in Section 5, interpreted as the Upper Alluvial Conglomerates and differentiated from the Basal Alluvial Conglomerates.

3.8 East-west correlation

In this sub-chapter the similarities and differences between the studied valley sections will be addressed, as well as the critical changes observed across the river valleys. All five interpreted valley sections are shown in Figure 55 for comparison. The location of each section is marked on Figure 55.

Section 1 to Section 4 share some of the main features:

- There is a sharp lithological and dip change across the South Graben Fault.
- The measured dips in the footwall (20-30°S) and immediate hangingwall of the South Graben Fault (10-15°N) are similar in all four sections.
- The Upper Alluvial Conglomerates are climbing northwards across south-dipping faults.
- An unconformity between the Upper and Basal Alluvial Conglomerates are observed in all sections except Section 2 (where it might just be covered by vegetation).

Lithologies and several faults are traceable from one river valley to the next. In other words, there seems to be a general correlation between Section 1 and 2 and between Section 3 and 4 (correlated faults are marked on Figure 55). However, with the exception of the Mamoussia-Pirgaki Fault, not a single fault is directly traced across the Ladopotamos and Potamia Rivers. Both the Valimi and

Kerpini-Tsivlos Faults are correlated across Krathis River, and so is the basement unconformity in Section 5 (Kerpini-Tsivlos Fault Block). However, in the northern part of Krathis River (hangingwall of the Valimi Fault) there is a significant change across the river valley, described below.

Critical observations in Ladopotamos River:

- The Kerpini-Tsivlos Fault steps one kilometre to the right.
- The South Graben Fault steps 600 metres to the left.
- The Fluvial and Upper Alluvial Conglomerates north of the South Graben Fault are on the western side dipping northwards all the way towards the Mamoussia-Pirgaki Fault. On the eastern side they are dominantly dipping to the south.
- There is a down-section dip increase (growth strata) within the Fluvial and Upper Alluvial Conglomerate succession on the eastern side. This is not observed in the west, where the beds are parallel.

Critical observations in Potamia River:

- The basement in the immediate footwall of the Valimi Fault is more elevated on the eastern side.
- The basement in the immediate hangingwall of the Kerpini-Tsivlos Fault is more elevated on the western side.
- There are Fluvial Conglomerates only on the western side.
- In the immediate footwall of the Valimi Fault, the south-dipping beds are significantly steeper (10-15°) in the east compared to the west.
- No evidence of faulting is observed in the east, whereas four faults are identified in the west.

Critical observations in Krathis River, Valimi Fault Block (Figure 57):

- The basement is approximately 600 metres higher elevated on the western side compared to the eastern side.

- On the eastern side is a thick succession of non-basement sediments (which has not been studied in this project), dipping in the opposite direction compared to the basement on the western side.

The presence of a NNE-SSW striking fault in Krathis River seems evident, be it a transfer fault or an east-dipping normal fault.

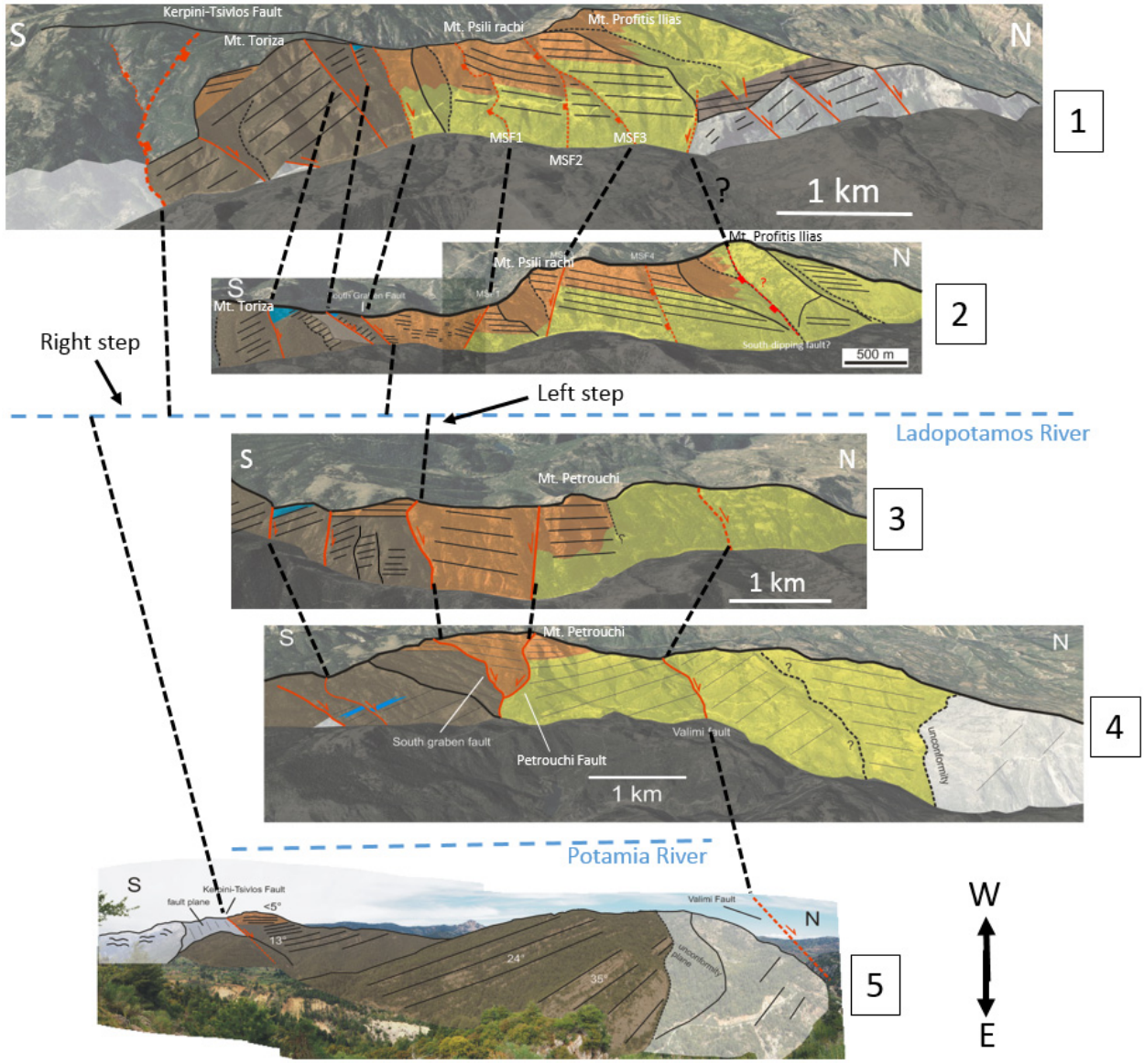

Figure 55: Comparison of all five studied valley sections (approximately to scale) and correlation of faults (dashed black lines). The location of each section is marked on Figure 56.

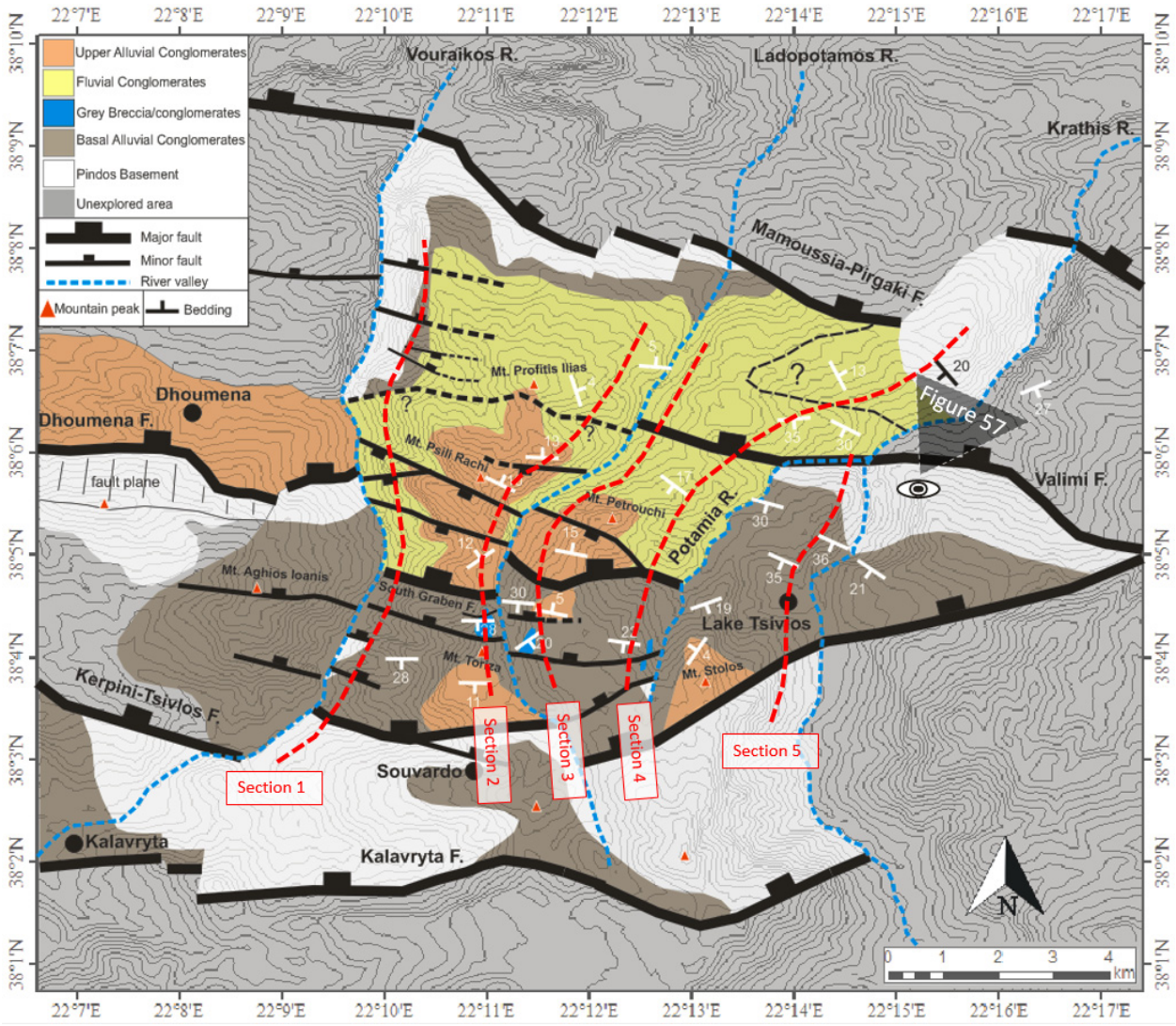

Figure 56: Structural map showing the location of the five studied valley sections and Figure 57.

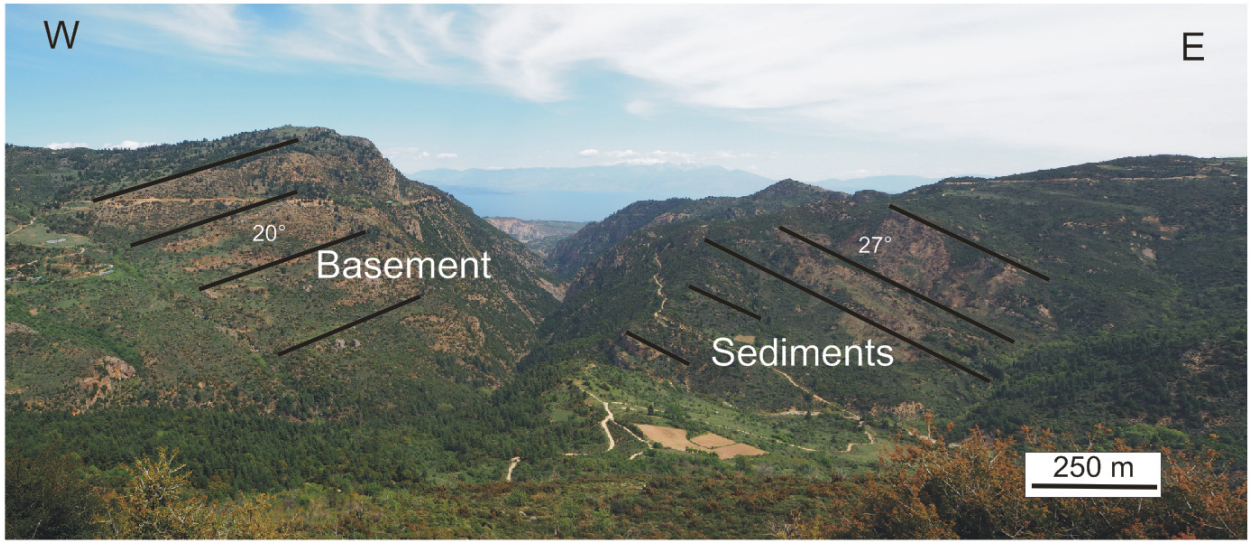

Figure 57: View down Krathis River. The eastern side is downthrown approximately 600 metres by a NNE-SSW striking fault. The location of the photo is marked on Figure 56.

Chapter 4 – Structural validation

The structural observations and interpretations are validated by combining Google Earth and 3D modelling in Petrel. The image resolution of the study area in Google Earth is very good, and topographic features observed there are used for preliminary extrapolation of faults. As these features might be misleading in the process of fault correlation, the faults are also modelled in Petrel. The DEM used in Petrel has a grid size of 90 x 90 m, which is small enough to resolve the main topographic features of the study area. Artificial planar surfaces are put in their correct locations on the DEM (where faults/unconformities are observed in the field). This is essentially to check that the present day topography does not yield misleading indications regarding correlation of faults between the valley sections. Figure 58 presents an overview of the faults which are physically observed in the field, and how they are later extrapolated subsequent to the structural validation.

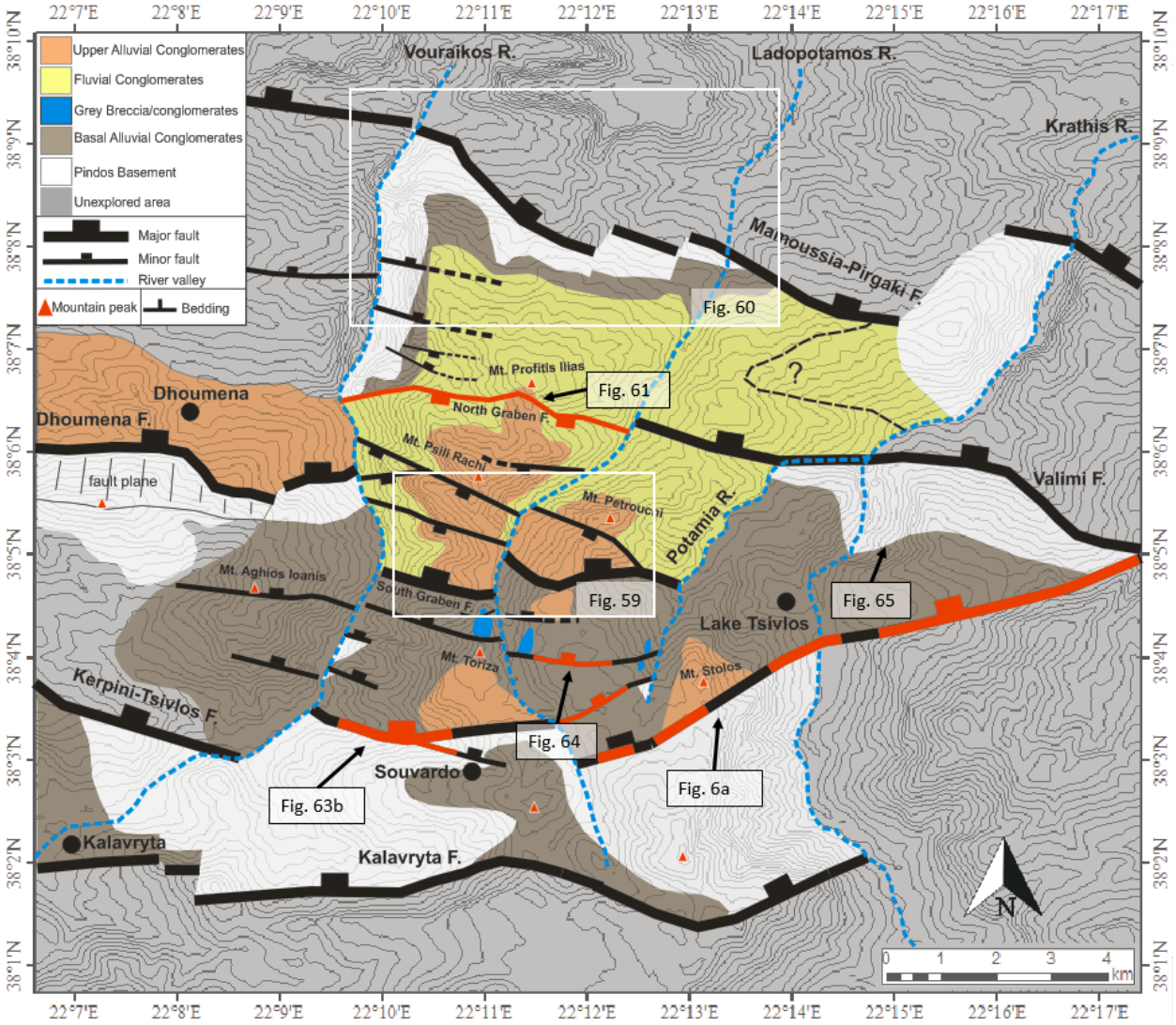

Figure 58: Illustration of how the faults are extrapolated. Black fault line = observed fault. Red fault line = inferred fault.

The central part of Ladopotamos River (Figure 59) is a good example of where modelling sheds light on whether faults correlate or not. The topographic traces of the south-dipping MSF1 and MSF3 are prominent (clear offsets both in the field and on the DEM), and their fault planes can be modelled with great accuracy on the western side of the river valley. The South Graben and Petrouchi Faults (eastern side of the river valley) are not as prominent, but their fault planes are modelled such that they intersect an observed fault on both sides of Mt. Petrouchi. The south-dipping MSF3 and Petrouchi Fault was initially suspected to correlate, but after modelling them, they are clearly not aligned. The same goes for the South Graben Fault, as it is not possible to join

the points at which the fault is observed with a single fault plane. These miscorrelations might be caused by an underlying N-S fault in the river valley.

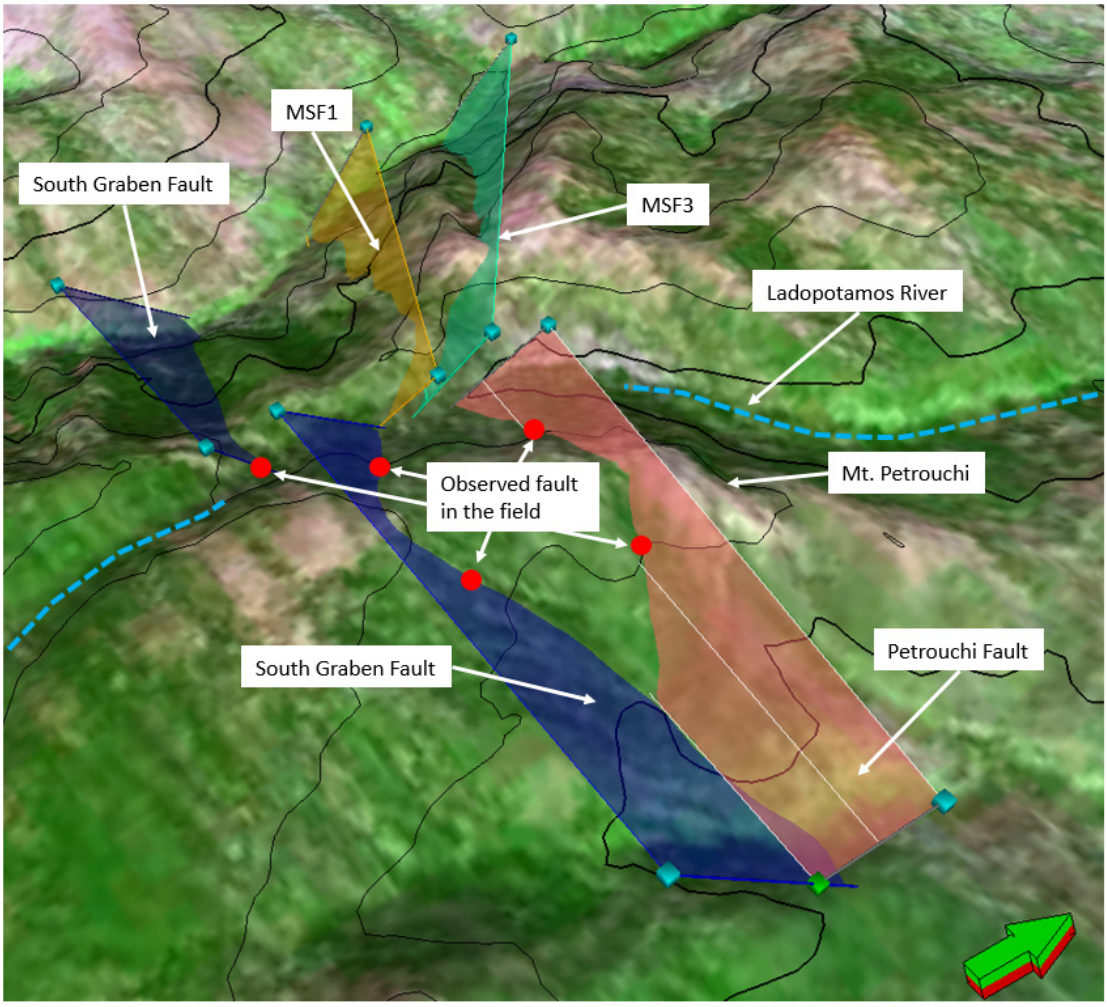

Figure 59: Image from Petrel where faults are not correlatable across Ladopotamos River. The location of the modelled faults is found in Figure 58.

The two left-steps in the Mamoussia-Pirgaki Fault between Vouraikos and Ladopotamos River is interpreted based on the fault trace in Google Earth (Figure 60). The trace is not very clear, and based on satellite images alone, these steps are yet to be confirmed.

Figure 60: Mamoussia-Pirgaki Fault trace (marked with arrows) in Google Earth. The location of the photo is found in Figure 58.

The sharp lateral contact between Fluvial and Basal Alluvial Conglomerates observed north in the Vouraikos River (Figure 28) was suspected to be a south-dipping fault or an unconformity made by incised rivers. Directly east from this contact, in Section 2, is the inlet in the valley side (Figure 38) where a south-dipping fault was also suspected. In Google Earth one can trace an E-W feature directly from the inlet to the contact in the Vouraikos River. By modelling a south-dipping plane in Petrel, its intersection with the topographic surface reproduces a trace similar to this feature (Figure 61). A south-dipping fault is thus favoured over a river incision, and it is interpreted as a major graben bounding fault responsible for the observed north-tilt of the Fluvial and Upper Alluvial Conglomerates. It is hereby referred to as the North Graben Fault.

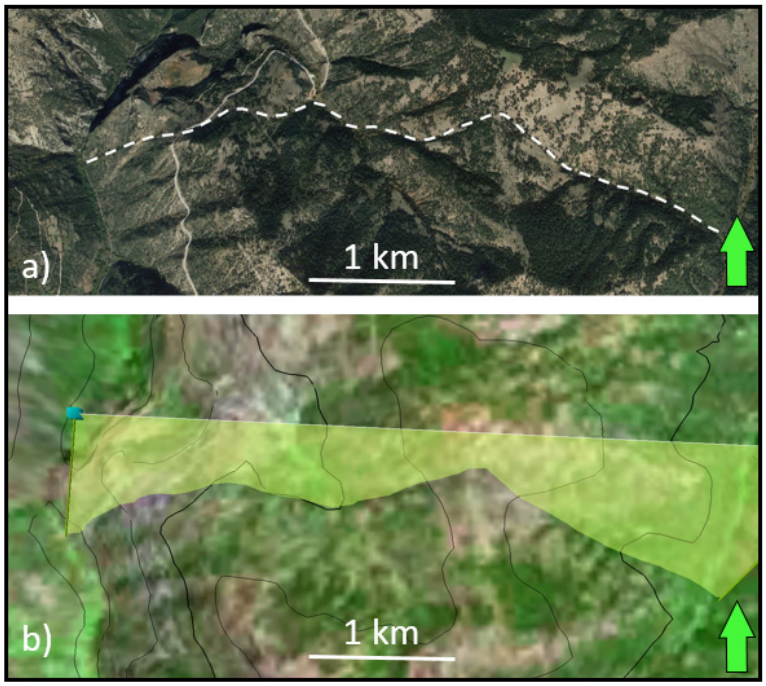

Figure 61: Comparison of the suspected North Graben Fault trace in Google Earth (a) with model fault trace in Petrel (b). The modelled plane dips 45°S.

The South Graben Fault is also validated using this method. Its trace can be accurately reproduced by modelling two separate planar surfaces (Figure 62), and it is evident that the fault steps in Ladopotamos River.

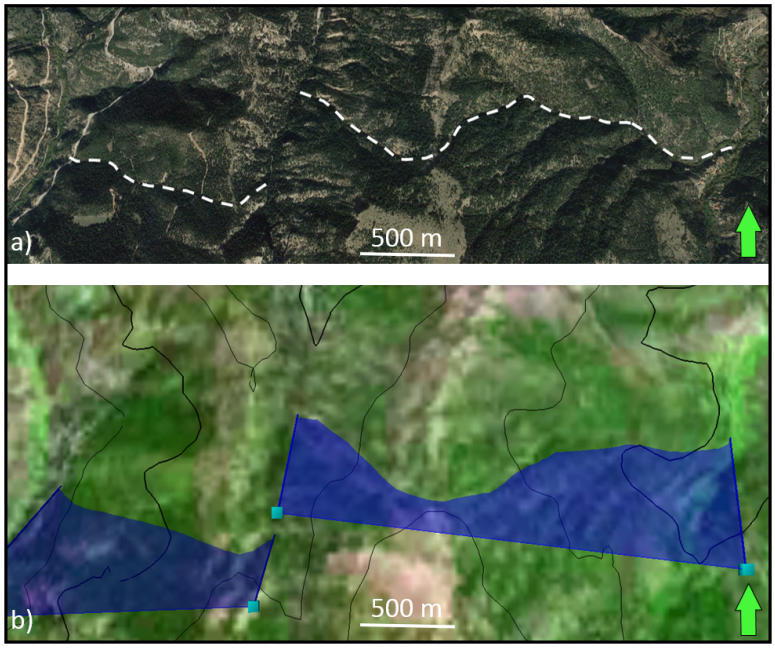

Figure 62: Comparison of suspected South Graben Fault trace in Google Earth (a) with model fault trace in Petrel (b). The modelled planes dip 40°N.

Four basement/conglomerate contacts along the eastern Kerpini-Tsivlos Fault are observed in the field, and they are nearly perfectly aligned with the modelled plane (Figure 63a). The fault is thus correlated from Krathis River to Ladopotamos River, where it right-steps one kilometre in the latter river valley. The central Kerpini-Tsivlos Fault (north of the town of Souvardo) cannot be modelled unless the fault plane is significantly curved (Figure 63b), casting doubt over the initial fault interpretation. It should possibly be considered as two individual faults; one striking WNW-ESE and tipping out east of Souvardo, and the other striking WSW-ENE and stepping in the Ladopotamos River.

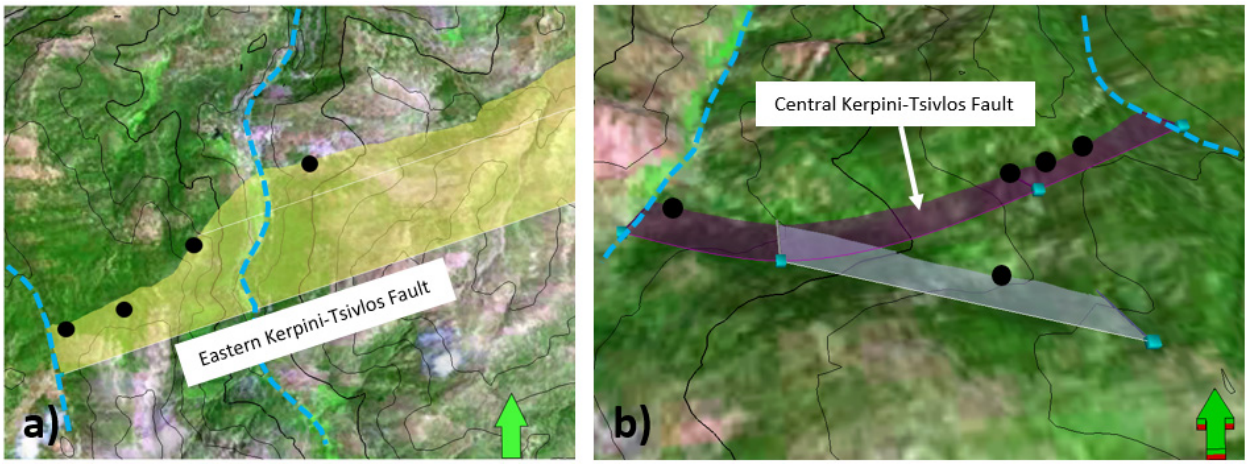

Figure 63: a) Trace of the modelled eastern Kerpini-Tsivlos Fault, with plane dipping 42°NNW. b) Modelled central Kerpini-Tsivlos Fault and branched fault by the town of Souvardo. Black dots show the locations of observed fault contacts in the field. The locations of a) and b) are seen in Figure 58.

A minor north-dipping fault which displace the Grey Breccia/conglomerates (~30 m) in Section 4 (Figure 47) has a prominent trace in Google Earth, and it is also visible on the DEM in Petrel (Figure 64). By aligning a plane along this trace, it correlates to the southern boundary of the Grey Breccia/conglomerates in Section 3 where a fault was suspected (although poorly exposed).

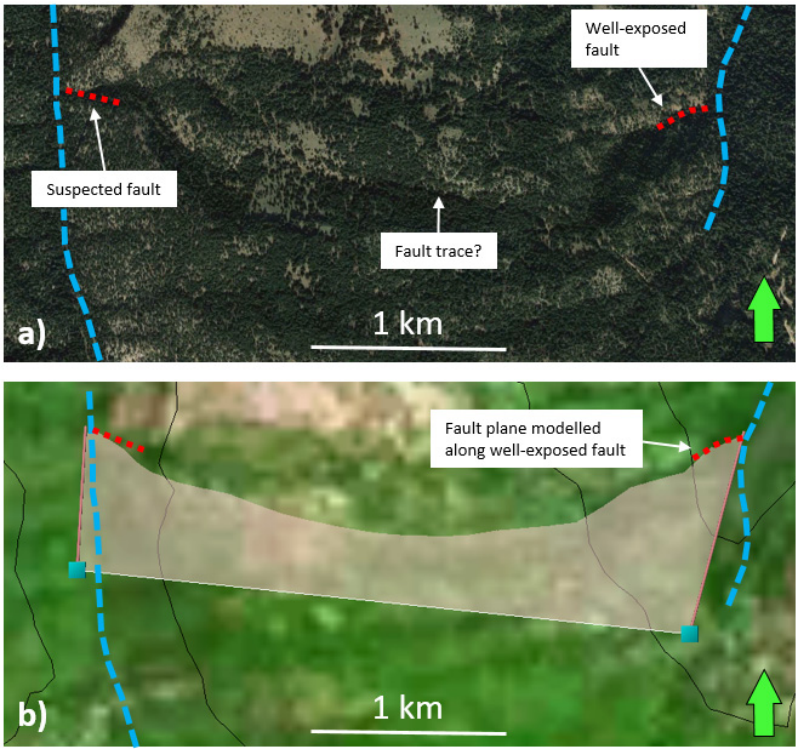

*Figure 64: **a)** Suspected fault trace in Google Earth. **b)** Modelled fault plane in Petrel. The location of the figures are marked on Figure 58*

In the field, the basement unconformity in the easternmost Kerpini-Tsivlos Fault Block appear to correlate across Krathis River. This is validated in Petrel (Figure 65), as a plane dipping 35°SSW is successfully aligned along the unconformity on both sides of the river valley. In the Potamia River the unconformity plane terminates, as the basement is downthrown at least 250 metres to the west.

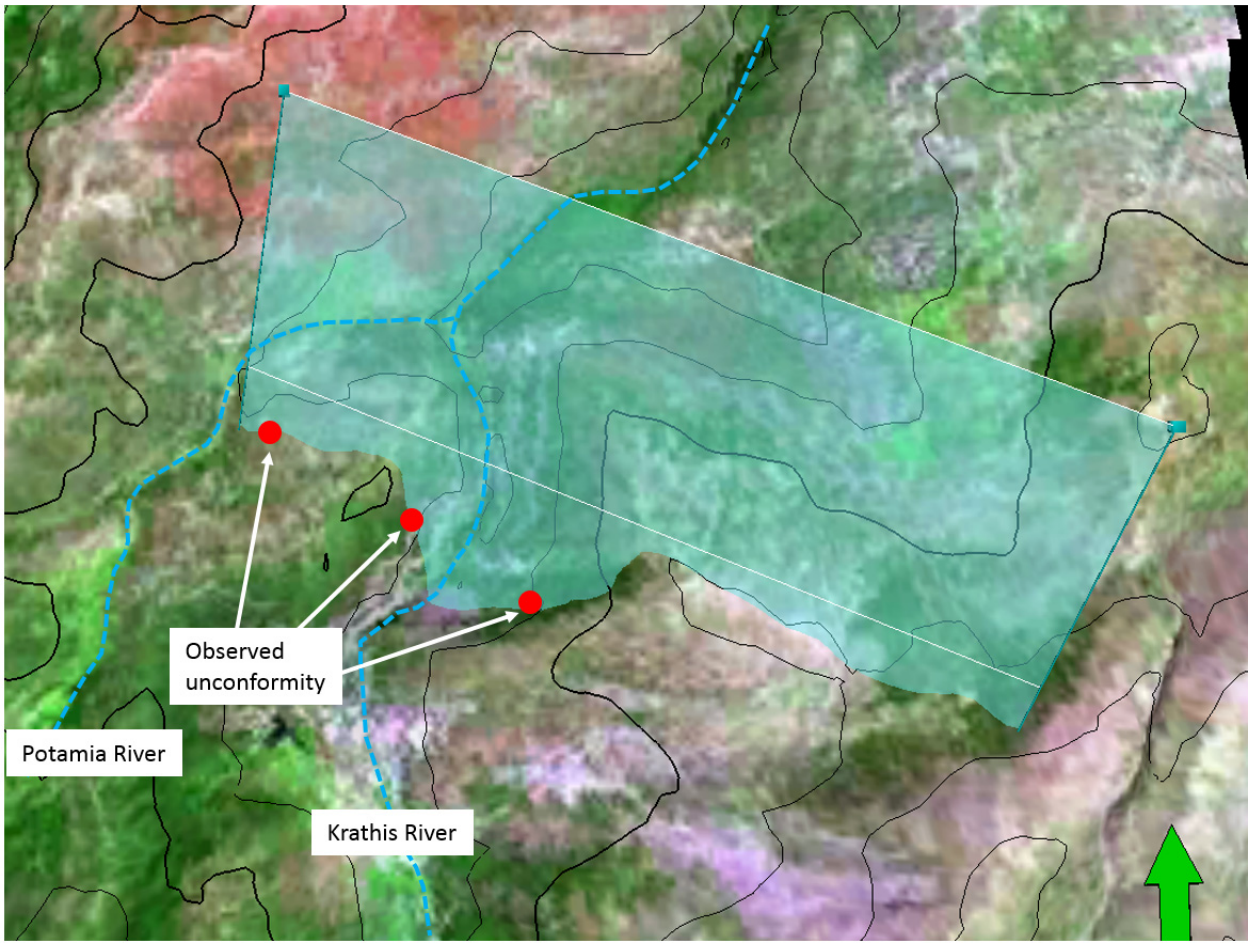

Figure 65: Modelled basement unconformity (dipping 35°SSW) in the easternmost Kerpini-Tsivlos Fault Block. The location of this figure can be seen in Figure 58.

Chapter 5 – Discussion

5.1 Structural interpretation

This sub-chapter will discuss the present structural configuration of the study area along both N-S and E-W cross sections, as well as the miscorrelations observed across Ladopotamos, Potamia and Krathis River Valleys.

5.1.1 N-S cross sections

Three approximately N-S oriented cross sections (locations marked on Figure 66) are constructed in order to visualize the structural changes across the river valleys. The elevation of the basement is mostly speculative as there are few exposures of it in the study area, especially in the central part. Wherever it is exposed, the dip of its unconformity surface is projected lineary.

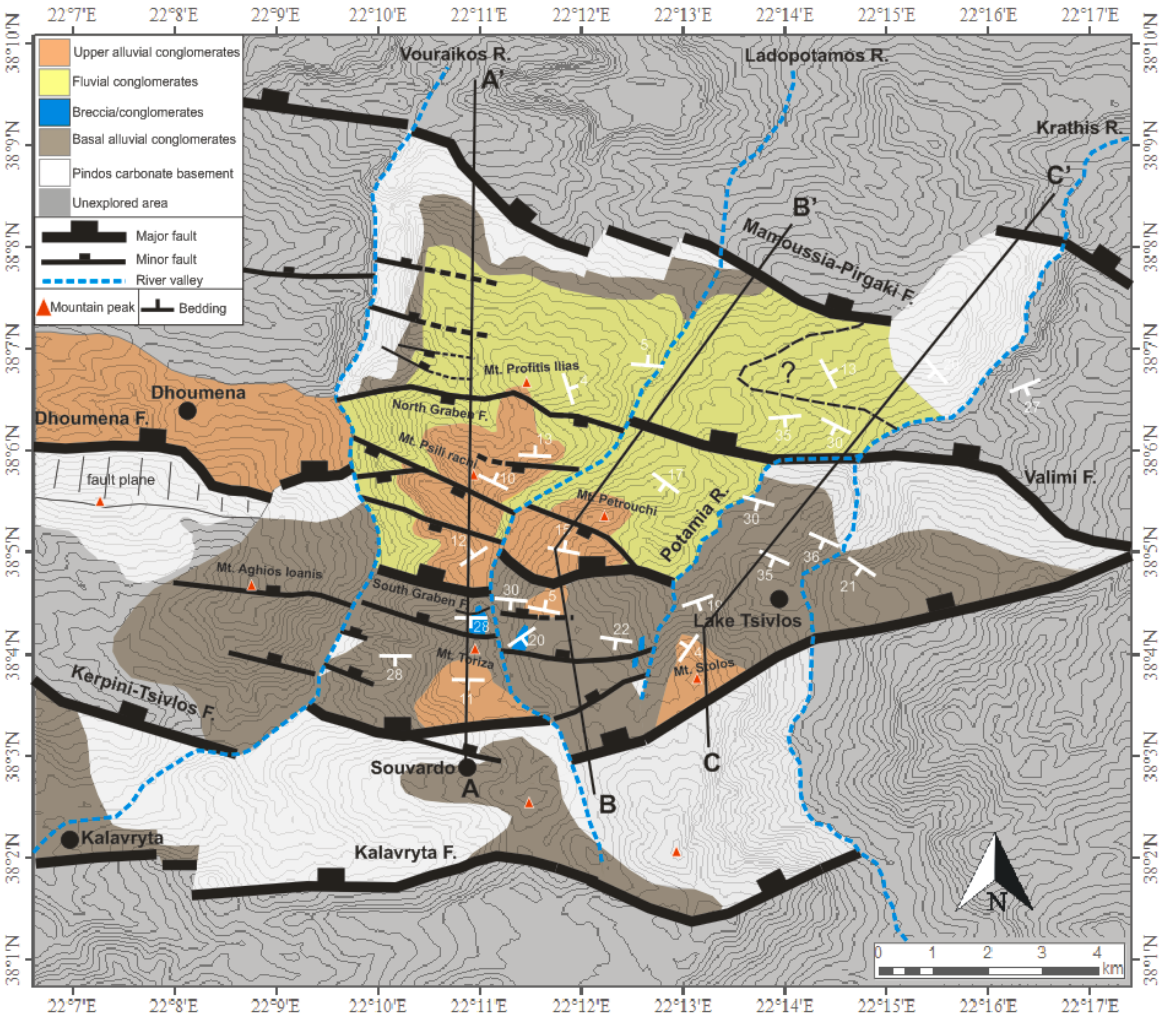

Figure 66: Structural map showing the locations of the three interpreted N-S cross sections.

The western cross section (Figure 67) displays the wide graben bounded by the South Graben Fault and North Graben Fault, dominantly filled with Fluvial Conglomerates. Although the base of these Fluvial Conglomerates are not exposed in the field, they are believed to overlie Basal Alluvial Conglomerates as observed in the northern part. The Prinos Inlier is interpreted as a pre-sedimentary basement feature which has later been south-tilted towards the Kerpini-Tsivlos Fault along with the massive succession of Basal Alluvial Conglomerates.

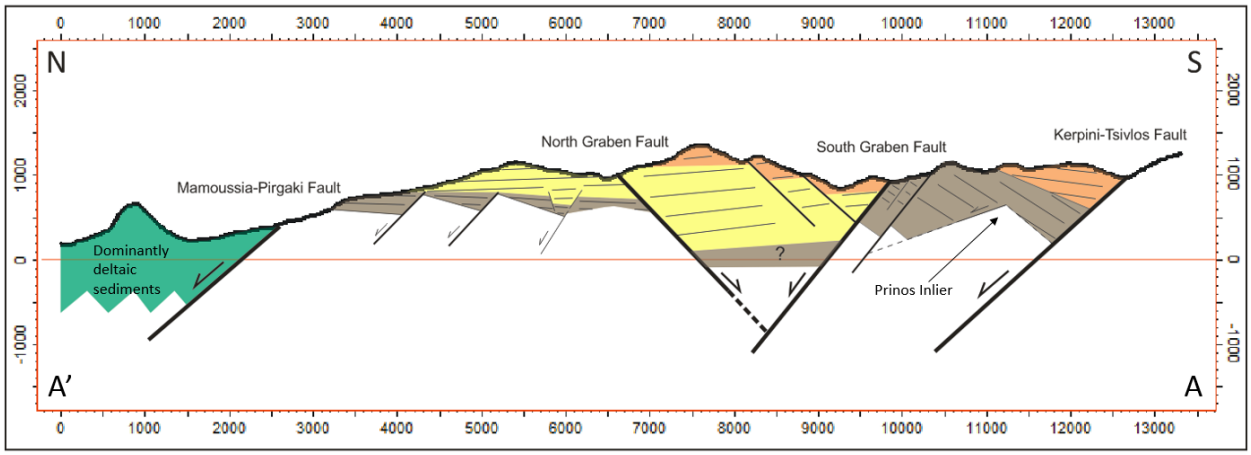

Figure 67: Western cross section (A-A'). The location of the cross section is marked on Figure 66.

The central cross section (Figure 68) is dominated by south-tilted beds within three pronounced rotated fault blocks. In contrast to the western cross section (Figure 67), north-dips are only present in the small graben limited by the South Graben Fault and Petrouchi Fault. Basal Alluvial Conglomerates are inferred in the hangingwall of the South Graben Fault, although the base of the Fluvial Conglomerates is unexposed. The exposed Basal Alluvial Conglomerates in the immediate footwall of the Mamoussia-Pirgaki Fault is extracted from the structural map by Ford *et al.* (2013), but not personally identified in the field.

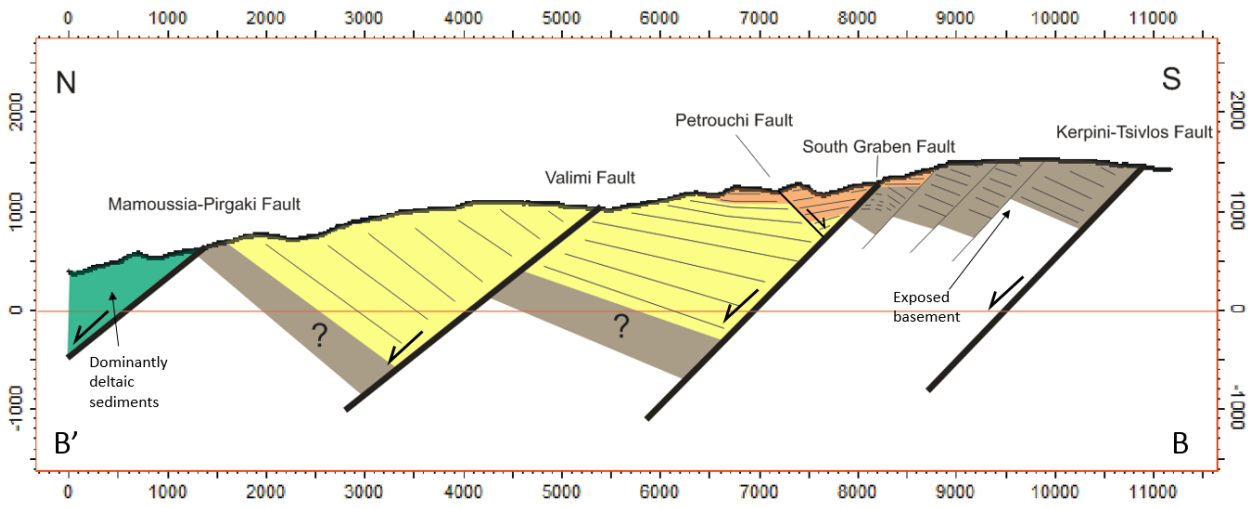

Figure 68: Central cross section (B-B'). The location of the cross section is marked on Figure 66.

The eastern cross section (Figure 69) consists solely of the major Kerpini-Tsivlos, Valimi and Mamoussia-Pirgaki Faults, constituting two massive rotated fault blocks. The throw of the Kerpini-Tsivlos Fault is significantly greater here (~2.2 km) compared to the central cross section (~800 m, Figure 68). Such a rapid change, over a lateral distance of roughly 2 kilometres, is in severe disagreement with any previously observed displacement profiles (Anders *et al.* (1993) and references therein). Although the Kerpini-Tsivlos Fault in both cross sections align along the same strike (Figure 63a), it seems evident that the fault is not continuous between the two cross sections.

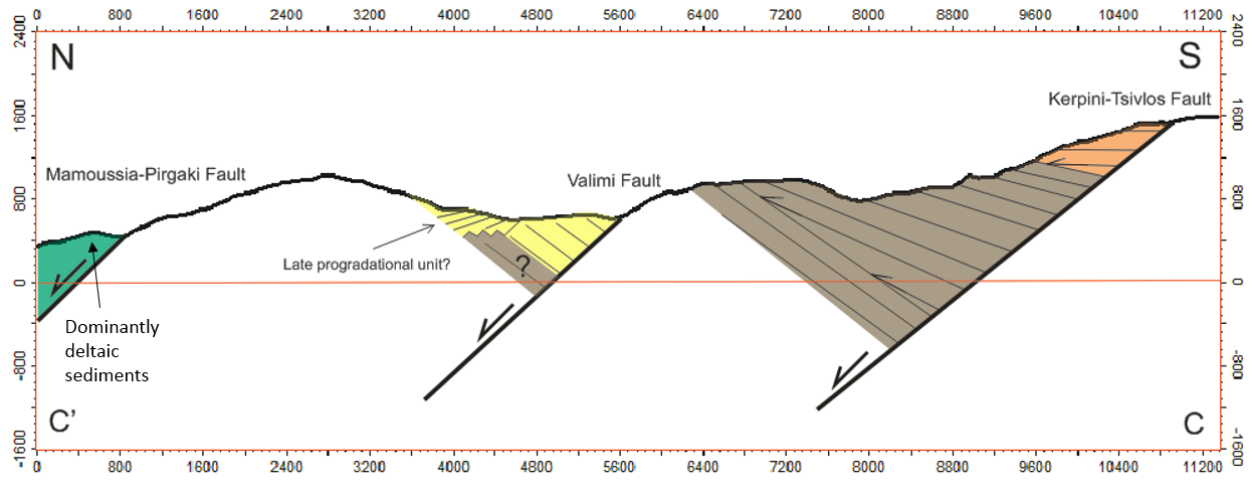

Figure 69: Eastern cross section (C-C'). The location of the cross section is marked on Figure 66.

Although there are major structural changes between the three cross sections, and the number of faults varies, the cumulative displacement is approximately the same (~5 km) for all of them (Figure 70). Such a good correlation is not necessarily expected, as only a part of the southern rift margin is studied. The cumulative displacement is calculated by summing the roughly estimated throws of all the basement-involved faults.

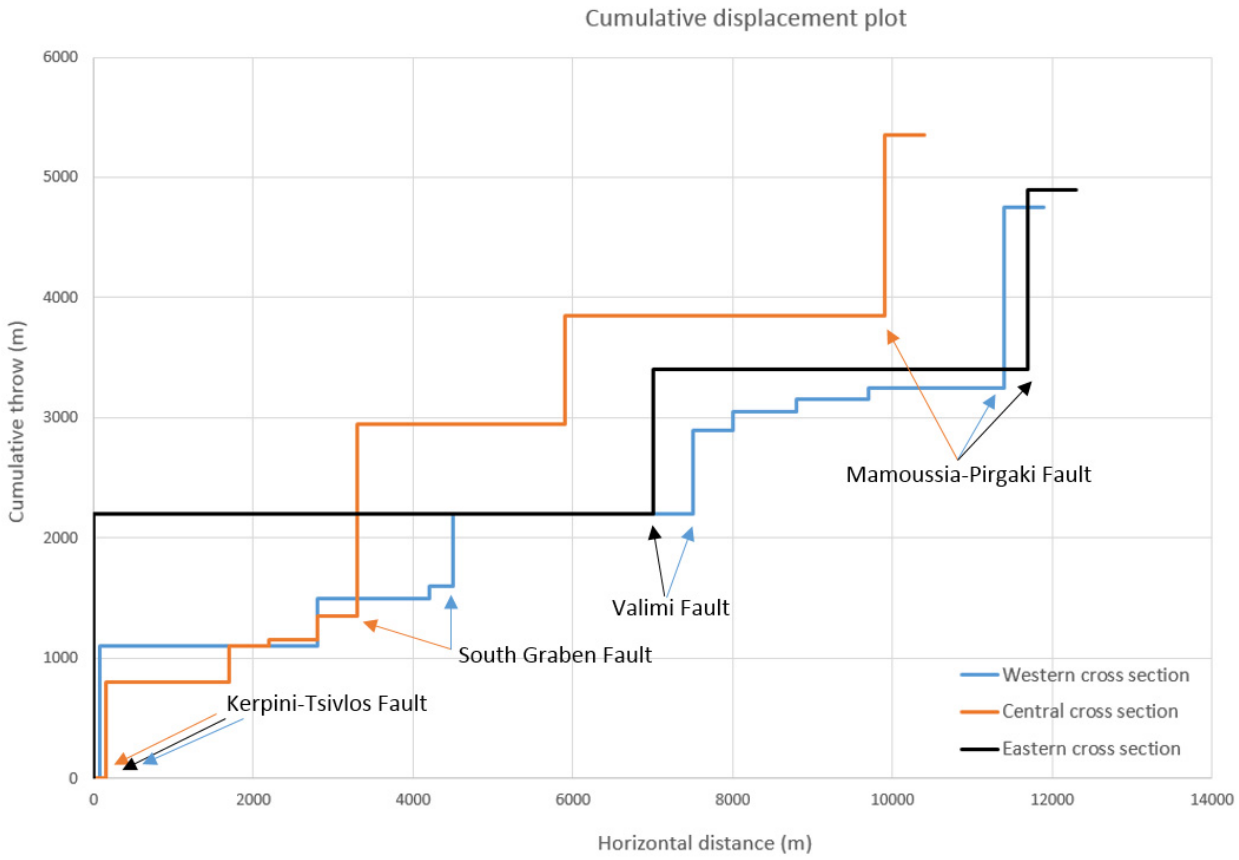

Figure 70: Cumulative displacement plot of the western (Figure 67), central (Figure 68) and eastern (Figure 69) cross sections. The Kerpini-Tsivlos Fault is located by the zero-point for all three sections.

5.1.2 Rift segmentation

The evidences of rift segmentation in the study area are substantial. The Ladopotamos, Potamia and Krathis River Valleys comprise extensive NNE-SSW intervals across which faults, the basement unconformity and/or lithologies do not correlate, concurrent to the observations by Dahman (2015) in the Vouraikos River. The river valleys seem to have an underlying fault control, and the intervals of miscorrelation are interpreted as high-angle transfer faults enclosing individual segments. Each segment has likely evolved independently of the others, supported by the variety in bedding geometries, number of faults, basement elevation and degree of rotation across the transfer faults. The idea of relay structures is not favoured due to the sheer amount of miscorrelations along relatively straight intervals.

By including the observations by Dahman (2015), five transfer faults in the scale of 3-15 kilometres are here inferred (Figure 71):

1. The Roghi Transfer Fault, along which the Dhoumena Fault left-steps and the basement is downthrown in the east. This fault was proposed by Dahman (2015), and it is believed to control the accommodation space in which the thick alluvial succession of Mt. Aghios Ioanis was deposited.
2. The Vouraikos Transfer Fault which partly follows the trend of Vouraikos River until it eventually links with the Roghi Transfer Fault northwards, and encloses Mt. Aghios Ioanis into an individual segment. The fault is evidenced by the termination of the Dhoumena Fault and South Graben Fault, a left-step in the Kerpini-Tsivlos Fault, and a significant basement offset (>500 m across its northernmost part). Southwards it is believed to correlate to one of the two steps in the Kalavryta Fault.
3. The Ladopotamos Transfer Fault which follows the trend of Ladopotamos River where no faults are correlated across. It is further evidenced by steps in the Kerpini-Tsivlos Fault and South Graben Fault, as well as opposite dip directions on its eastern and western side (north of the South Graben Fault). It is interpreted to deviate from the river valley in the north, to correlate to one of the steps in the Mamoussia-Pirgaki Fault.
4. The Potamia Transfer Fault which is located in the Potamia River where the South Graben Fault terminates eastwards. It separates two completely different segments; a western segment consisting of two rotated fault blocks cut by smaller faults, and an eastern segment

consisting of a single massive rotated fault block. The displacement of the Kerpini-Tsivlos Fault is significantly greater in the eastern segment, where the footwall of the Valimi Fault is also more uplifted. The Potamia Transfer Fault may link to a step in the Mamoussia-Pirgaki Fault to the NNE, but there is no observed discontinuity along the Valimi Fault to support this.

5. The Krathis Transfer Fault which is located in the very north-eastern part of the study area. It is evidenced by a 600 metre basement offset (eastern side is downthrown) and a change of dip direction across the Krathis River.

This interpretation involves rather significant curves along the Roghi and Ladopotamos Transfer Faults. An alternative (and more conventional) model involving straight transfer faults is presented in Figure 72. In this model the Roghi and Ladopotamos Transfer Faults are split into two and three faults respectively. However, E-W structural changes seem to almost obsequiously take place in Ladopotamos River, and three individual straight transfer faults fail to resolve all of them. One would have to further split them into four or five straight transfer faults in order to do so. The original model involving extensive (and some places curved) transfer faults is thus preferred.

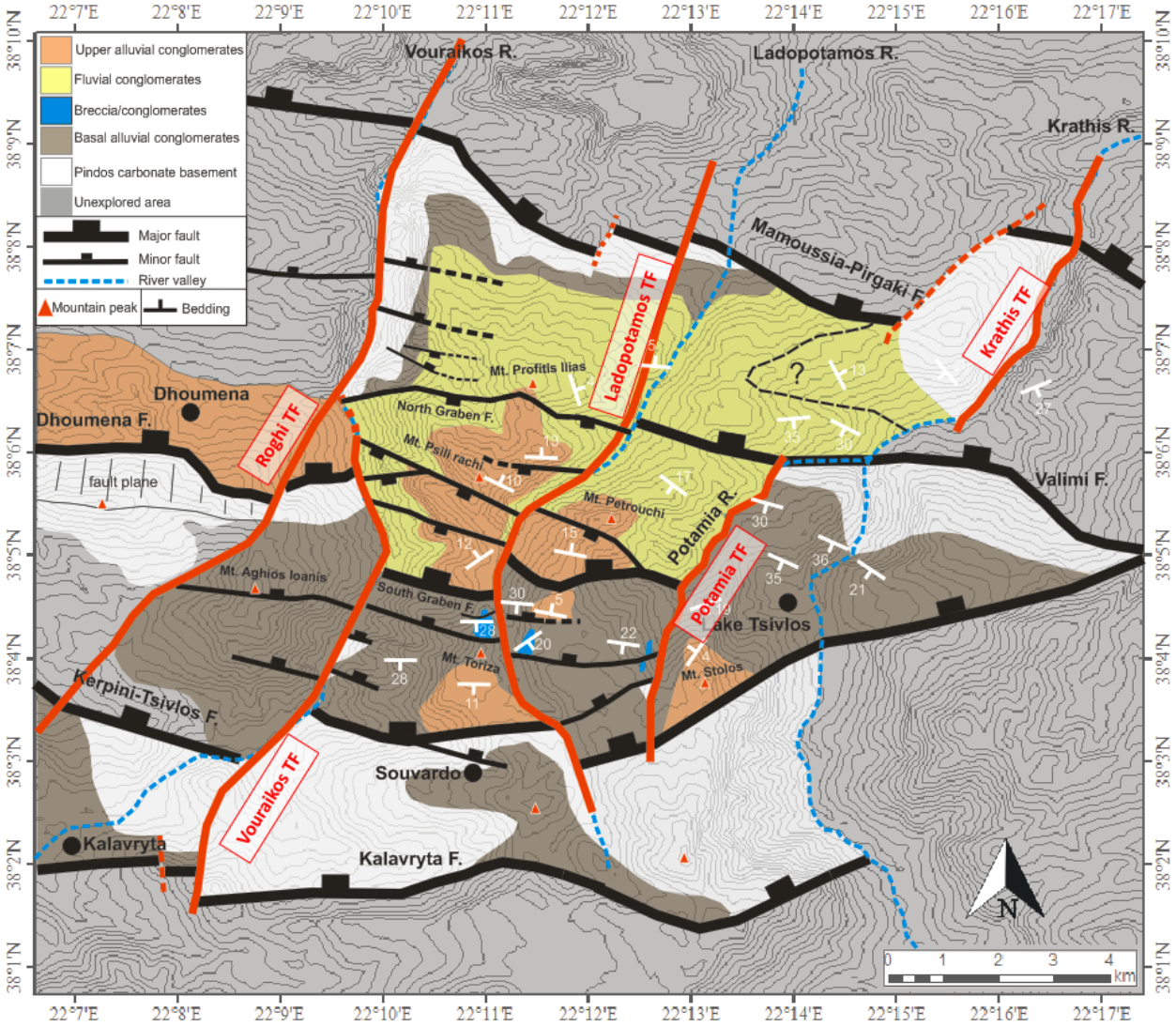

Figure 71: Structural map with proposed transfer faults (solid red lines) and other identified fault steps (dashed red lines).

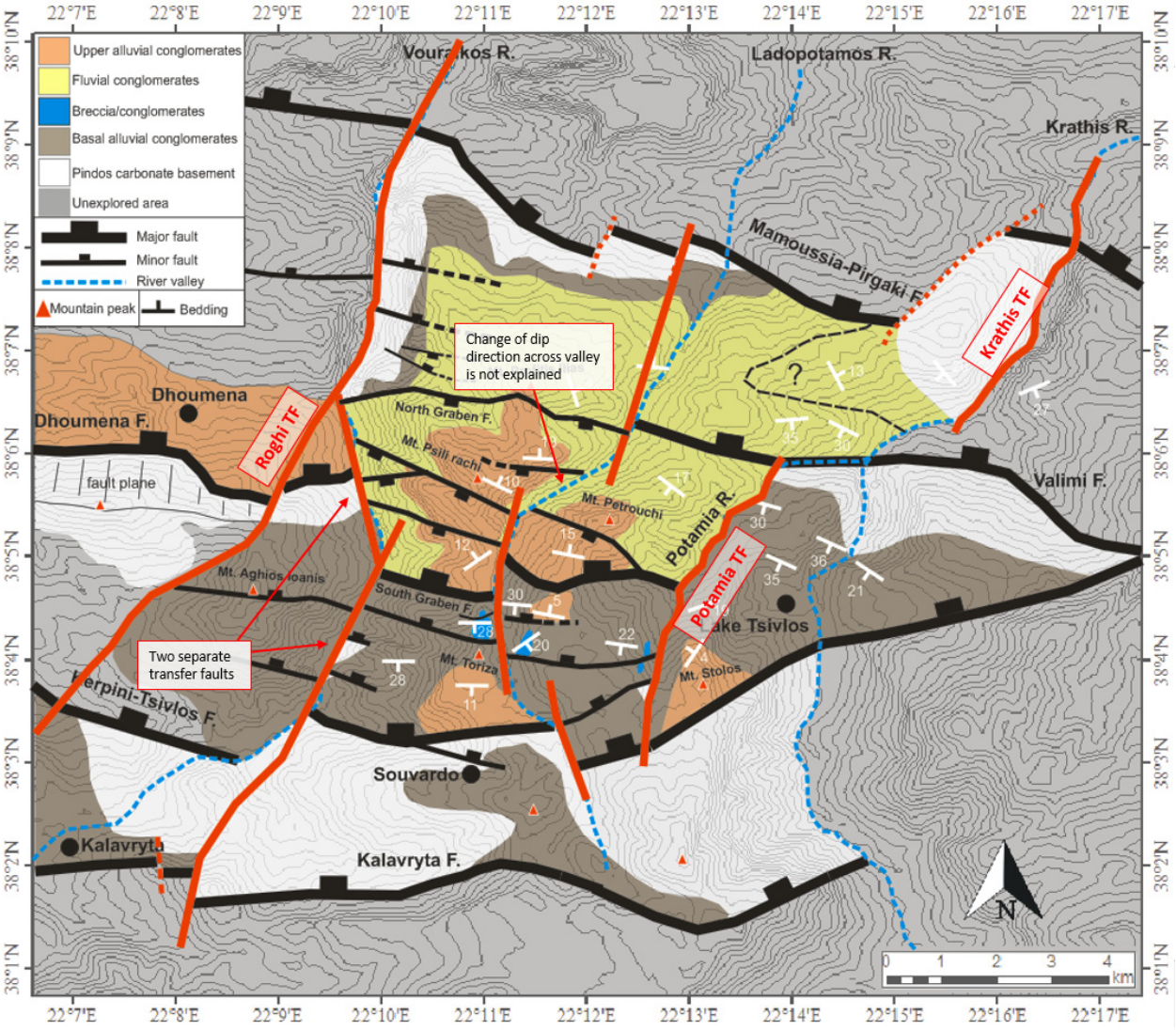

Figure 72: Structural map with alternative interpretation involving straight transfer faults (red lines). In this model the transfer faults themselves are stepping in the Ladopotamos River.

The interpreted segmentation of the study area is shown in Figure 73, further illustrated by three E-W cross sections (Figure 74, Figure 75 and Figure 76).

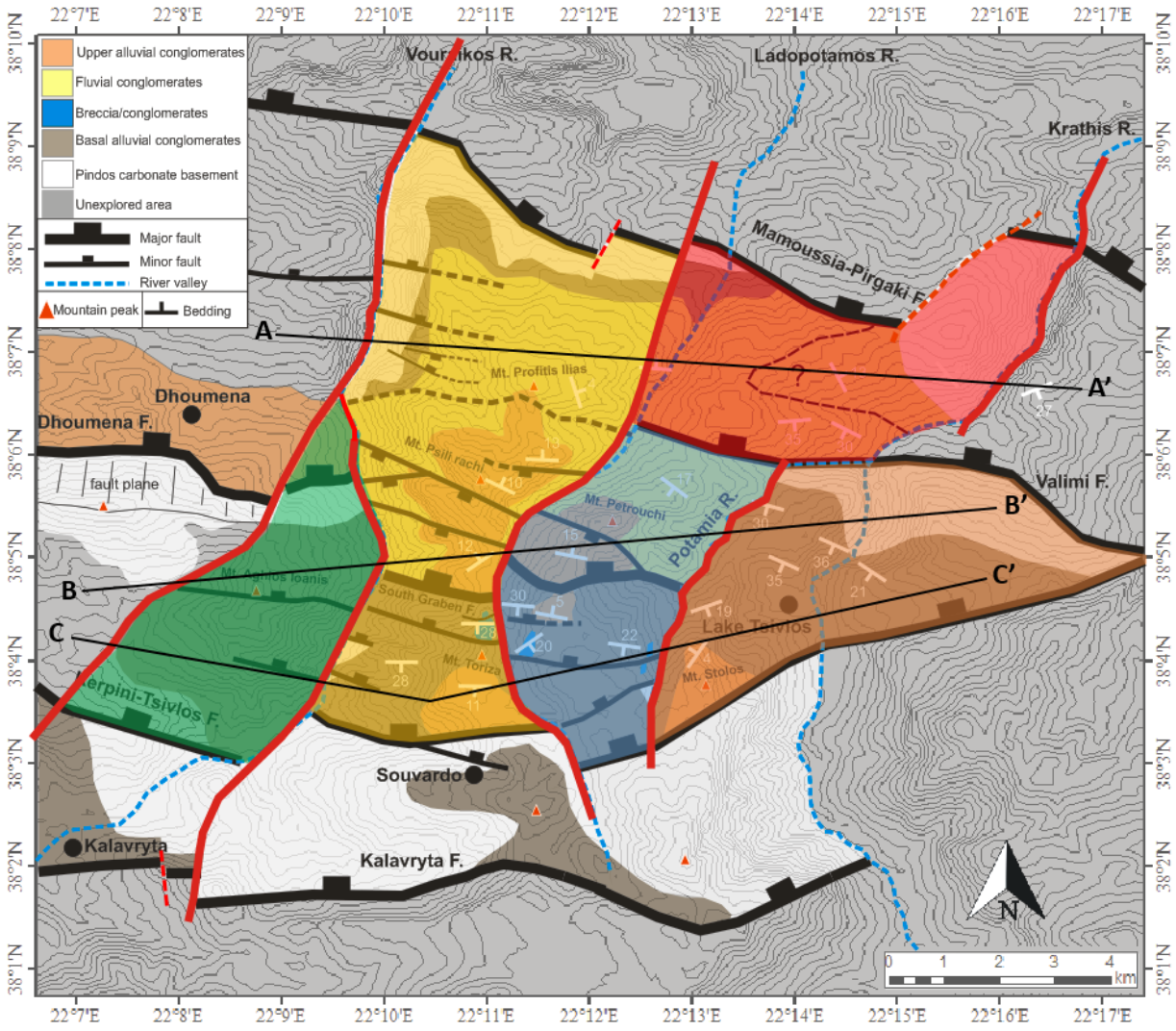

Figure 73: Proposed segmentation of the study area. The individual segments are separated by the inferred transfer faults (solid red lines).

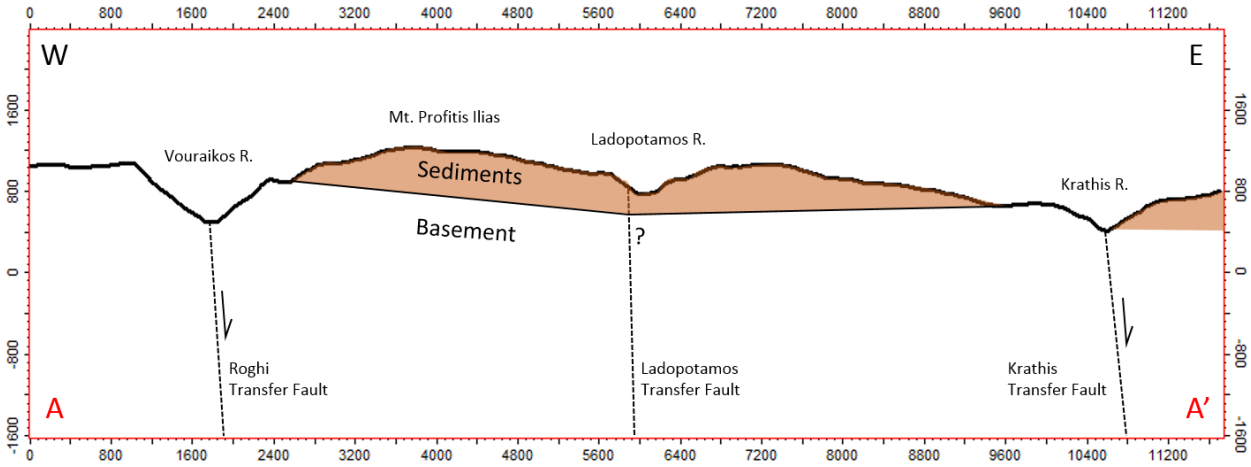

Figure 74: E-W cross section (A-A') showing the relationship between basement and sedimentary infill across proposed transfer faults. The location of the cross section is marked on Figure 73.

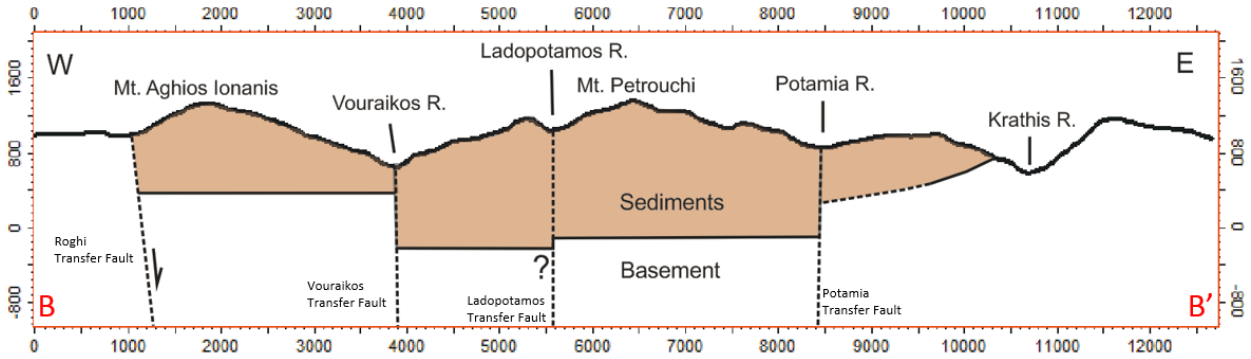

Figure 75: E-W cross section (B-B') showing the relationship between basement and sedimentary infill across proposed transfer faults. The location of the cross section is marked on Figure 73.

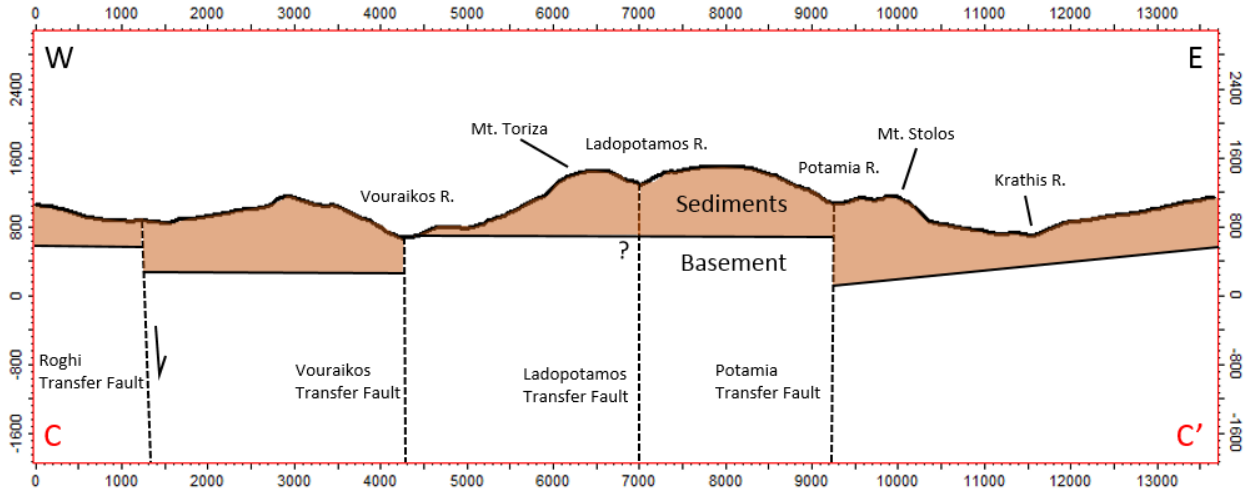

Figure 76: E-W cross section (C-C') showing the relationship between basement and sedimentary infill across proposed transfer faults. The location of the cross section is marked on Figure 73.

5.2 Structural evolution

The effort to understand the structural evolution is primarily focused on the area limited by Vouraikos and Krathis Rivers (highlighted in Figure 77). The evolution of the area is complex, as each segment bounded by transfer faults have evolved individually. The factors controlling the development of the transfer faults are poorly understood, and the evolution model proposed in this sub-chapter is based on the assumption that the transfer faults are controlled by pre-existing features in the underlying Pindos Basement.

Based on the proposed stratigraphic relationship between the different lithologies, the structural evolution of the study area can be broken down to four main stages:

1. Deposition of Basal Alluvial Conglomerates
2. Deposition of Fluvial Conglomerates
3. Deposition of Upper Alluvial Conglomerates
4. Recent faulting resulting in the present structural configuration, and deposition of deltaic sediments (Middle Group, Ford *et al.* (2013)) in the hangingwall of the Mamoussia-Pirgaki Fault

Each stage (illustrated with simplified structural maps, (Figure 78) and chronostratigraphic diagram (Figure 79)) will be further discussed in this sub-chapter. A western, central and eastern N-S cross section, (Figure 80, Figure 81 and Figure 82) are presented for each evolution stage in order to visualize the differences between individual segments. The Grey Breccia/conglomerate is not included in the model, both because of its limited extent, and the fact that it is poorly understood.

Stage 1: Large volumes of Basal Alluvial Conglomerates, sourced from the uplifted footwall of the active Kalavryta Fault, are transported northwards across the rift. It extends all the way to (or beyond) the present-day Mamoussia-Pirgaki Fault, onlapping pre-existing rotated basement blocks in the northwest. During this stage, the easternmost part of the Kerpini-Tsivlos Fault is active, evident by growth strata in its hangingwall. To the west of the Potamia Transfer Fault, the fault is less active or inactive. The Valimi Fault is also active during this stage, allowing the easternmost Kerpini-Tsivlos Fault Block to rotate.

Stage 2: The South and North Graben Faults become active, creating accommodation space for Fluvial Conglomerates (NE-flowing rivers) in the developing graben. East of the Ladopotamos Transfer Fault, the South Graben Fault Block rotates along the Valimi Fault, evident by growth strata within the Fluvial Conglomerates. The footwall of the Valimi Fault is significantly uplifted in the easternmost section, and acts as a barrier for the rivers. The western graben is eventually overfilled, and Fluvial Conglomerates are continuously deposited northwards.

During this stage, the central and western part of the Kerpini-Tsivlos Fault become more active, and the Kalavryta and Kerpini-Tsivlos Fault Blocks are south-rotated. The pre-existing Prinos Fault rotates along with the latter fault block, explaining its low present day dip of 20°N.

Stage 3: A sudden increase in transport energy (likely a major deglaciation event) initiates deposition of the massive Upper Alluvial Conglomerates, sourced from the uplifted footwall of the Kerpini-Tsivlos Fault. The unit onlaps the rotated Basal Alluvial Conglomerates in the Kerpini-Tsivlos Fault Block, before being transported further north to deposit conformably on top of the Fluvial Conglomerates. The unit is believed to transition into more of a fluvial facies somewhere south of the present-day Mamoussia-Pirgaki Fault. During this stage, activity along the Kalavryta Fault ceases.

Stage 4: Fault activity migrates northwards, as activity along the Kerpini-Tsivlos and South Graben Faults ceases and the Mamoussia-Pirgaki Fault initiates. The Mamoussia-Pirgaki Fault marks the boundary between non-marine and marine/transitional environments (Lower and Middle Groups, Ford *et al.* (2013)), as major Gilbert-type deltas are deposited in its hangingwall.

In the west, the graben sediments between the South and North Graben Faults rotate northwards towards the still active North Graben Fault, while being displaced by four south-dipping faults (MFS1 - MFS4). East of the Ladopotamos Transfer Fault, significant displacement along the Valimi Fault takes place, rotating the Valimi Fault Block along the Mamoussia-Pirgaki Fault. No south-rotation occurs to the west of this transfer fault, likely because of the absence of an active north-dipping fault south of the Mamoussia-Pirgaki Fault.

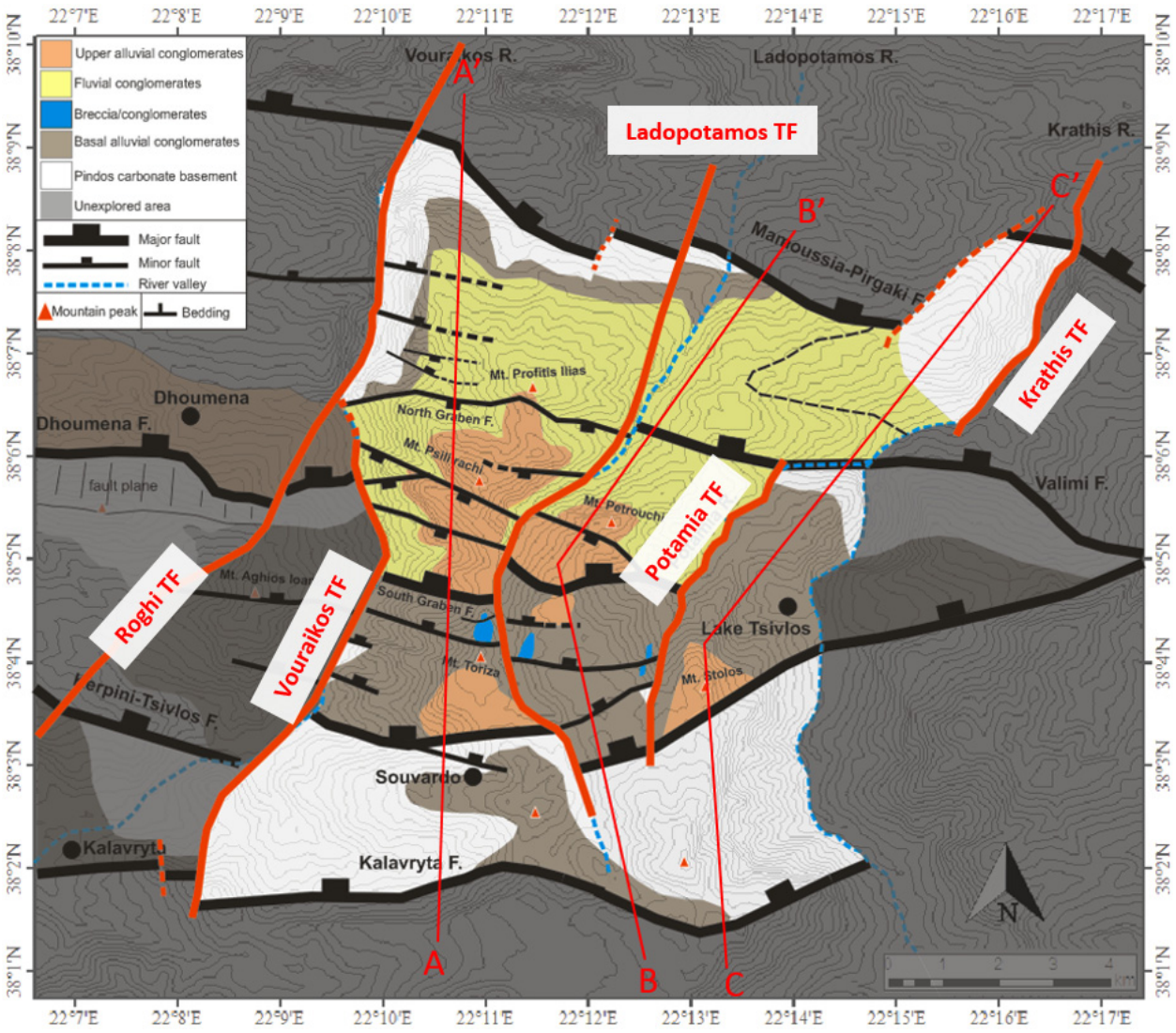

Figure 77: Structural map highlighting the area of the proposed evolution model, and the location of the three cross sections discussed in this sub-chapter.

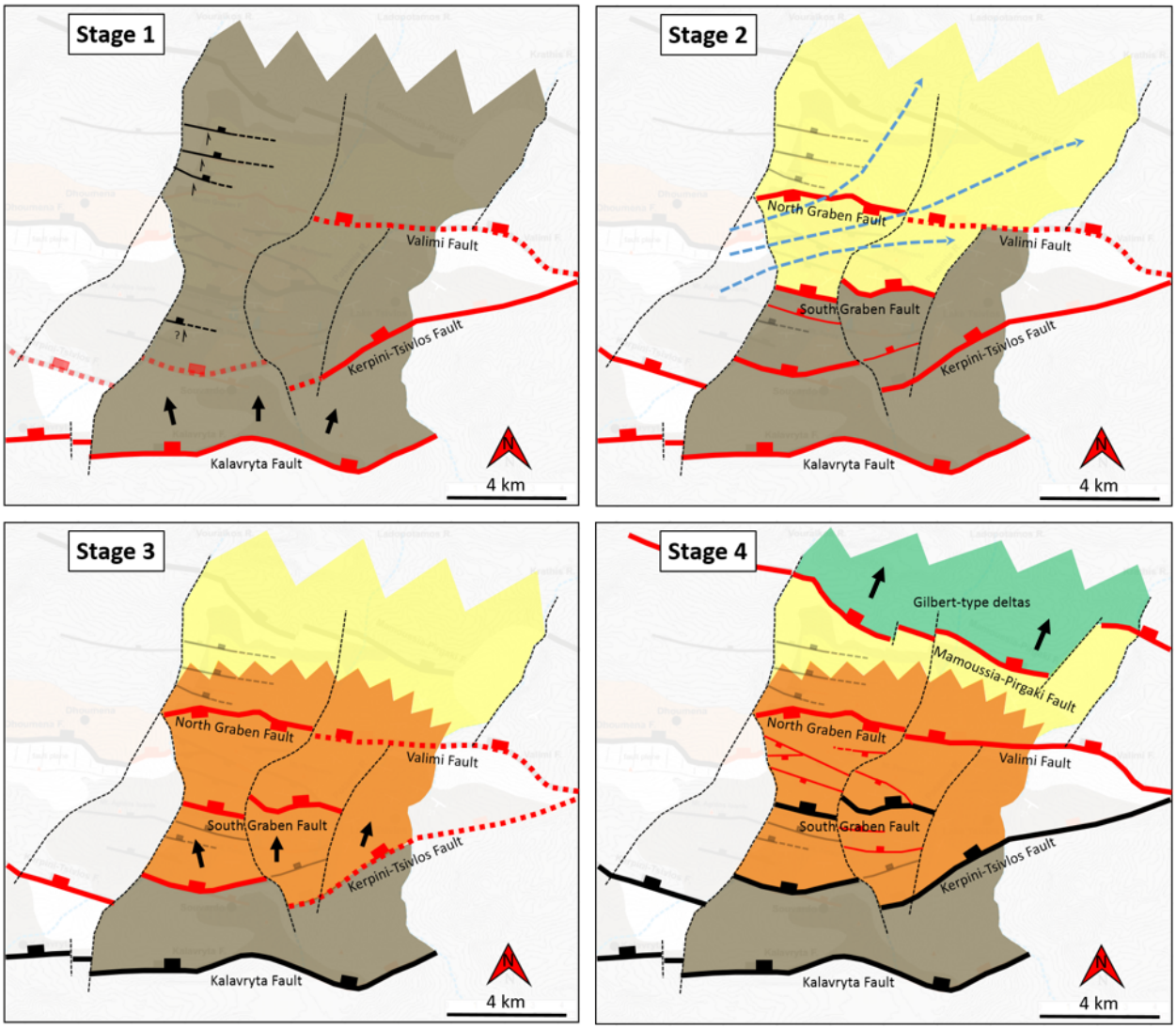

Figure 78: Simplified structural maps illustrating the proposed four-stage evolution of the study area. Solid red lines: active faults. Dashed red lines: active faults pre/post period of maximum displacement. Solid black lines: inactive faults. Dashed black lines: transfer faults. Dashed blue lines: rivers.

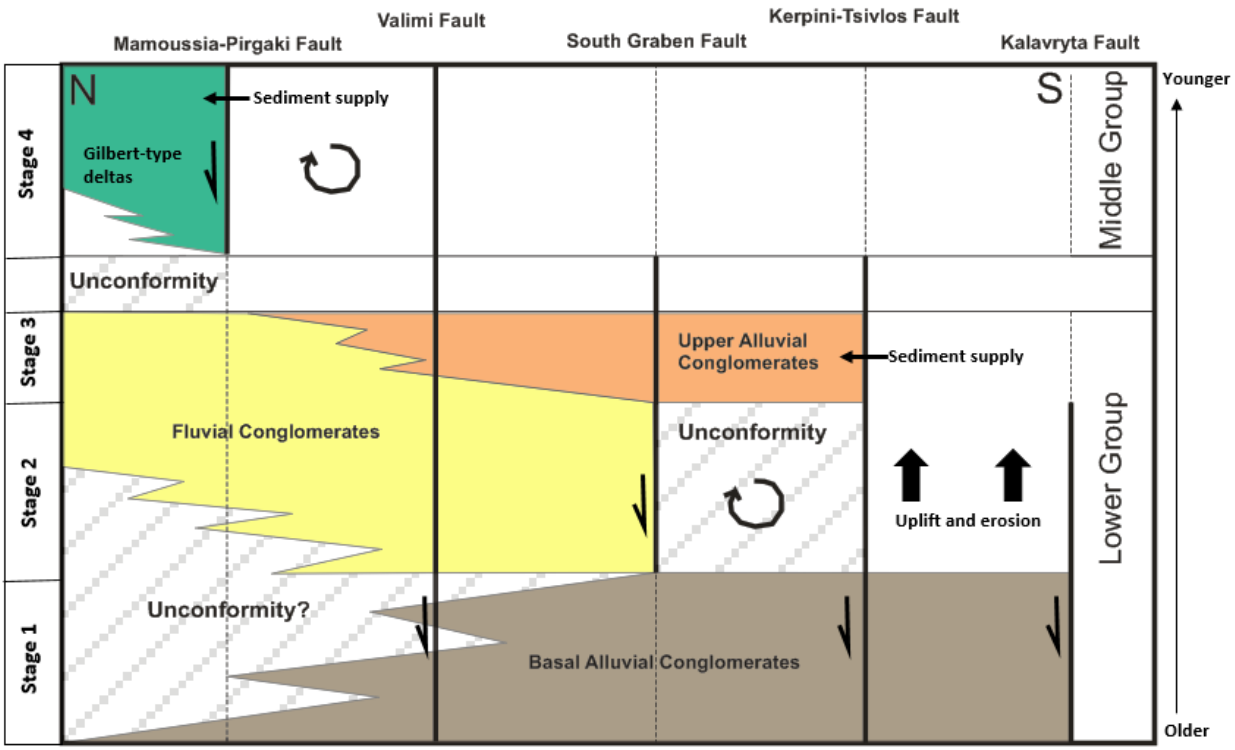

Figure 79: Generalized chronostratigraphic diagram showing the relative timing of faulting and sedimentation, and the four stages of evolution. Active faults are shown as thick solid lines.

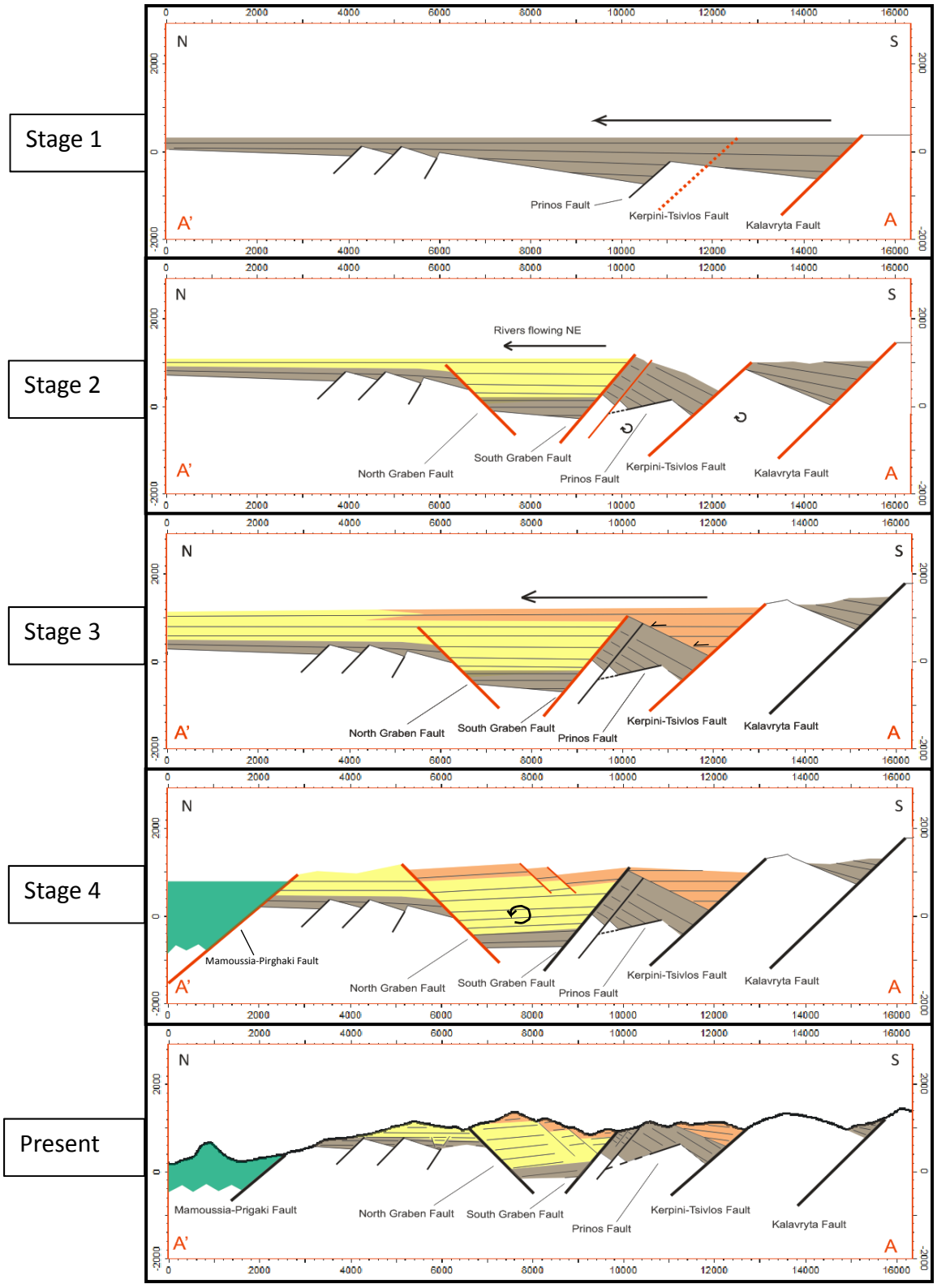

Figure 80: Proposed evolution of the western part of the study area. Solid red lines: active faults. Dashed red lines: active faults pre/post period of maximum displacement. Black lines: inactive faults. The location of the section is marked on Figure 77.

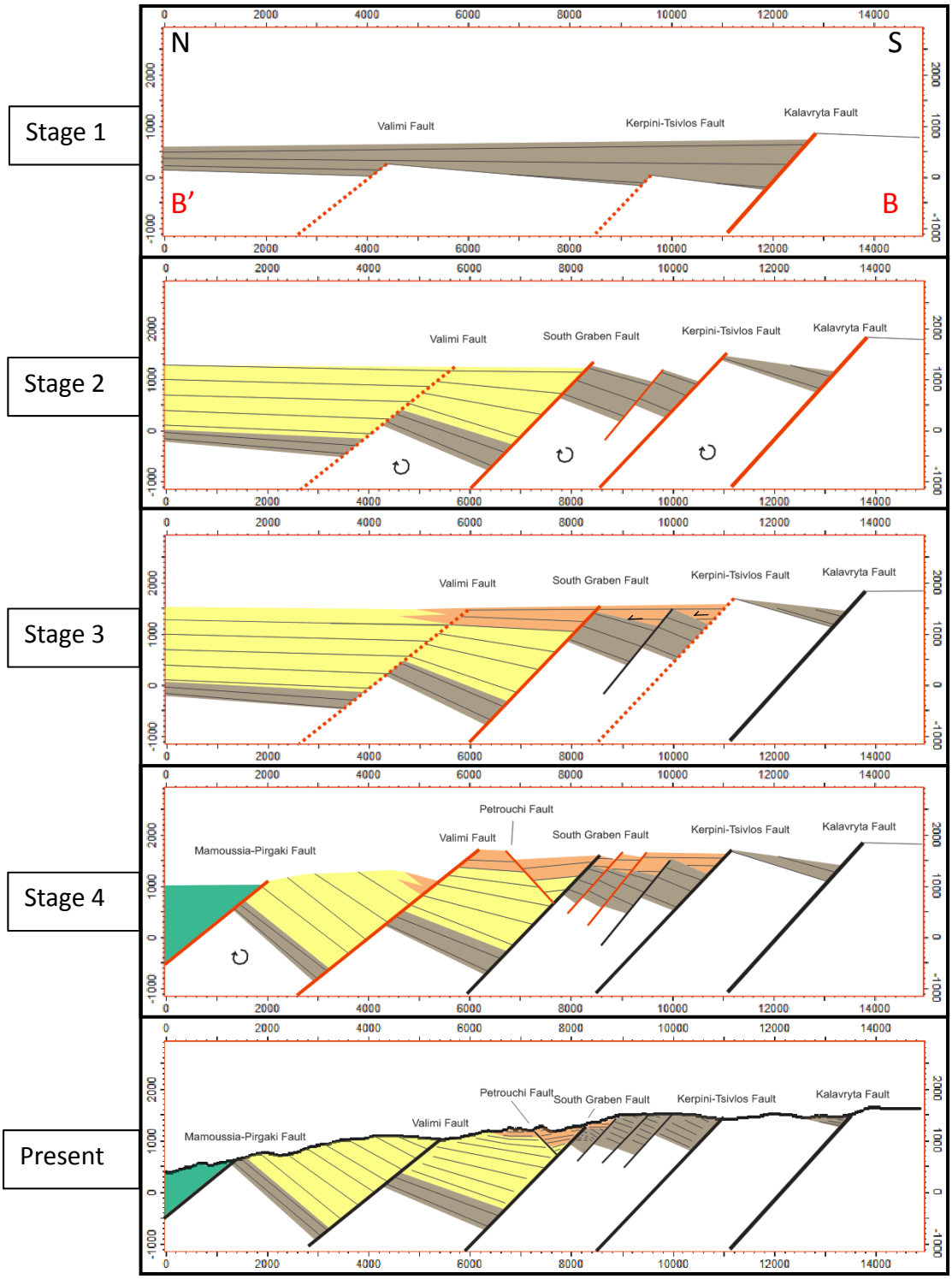

Figure 81: Proposed evolution of the central part of the study area. Solid red lines: active faults. Dashed red lines: active faults pre/post period of maximum displacement. Black lines: inactive faults. The location of the section is marked on Figure 77.

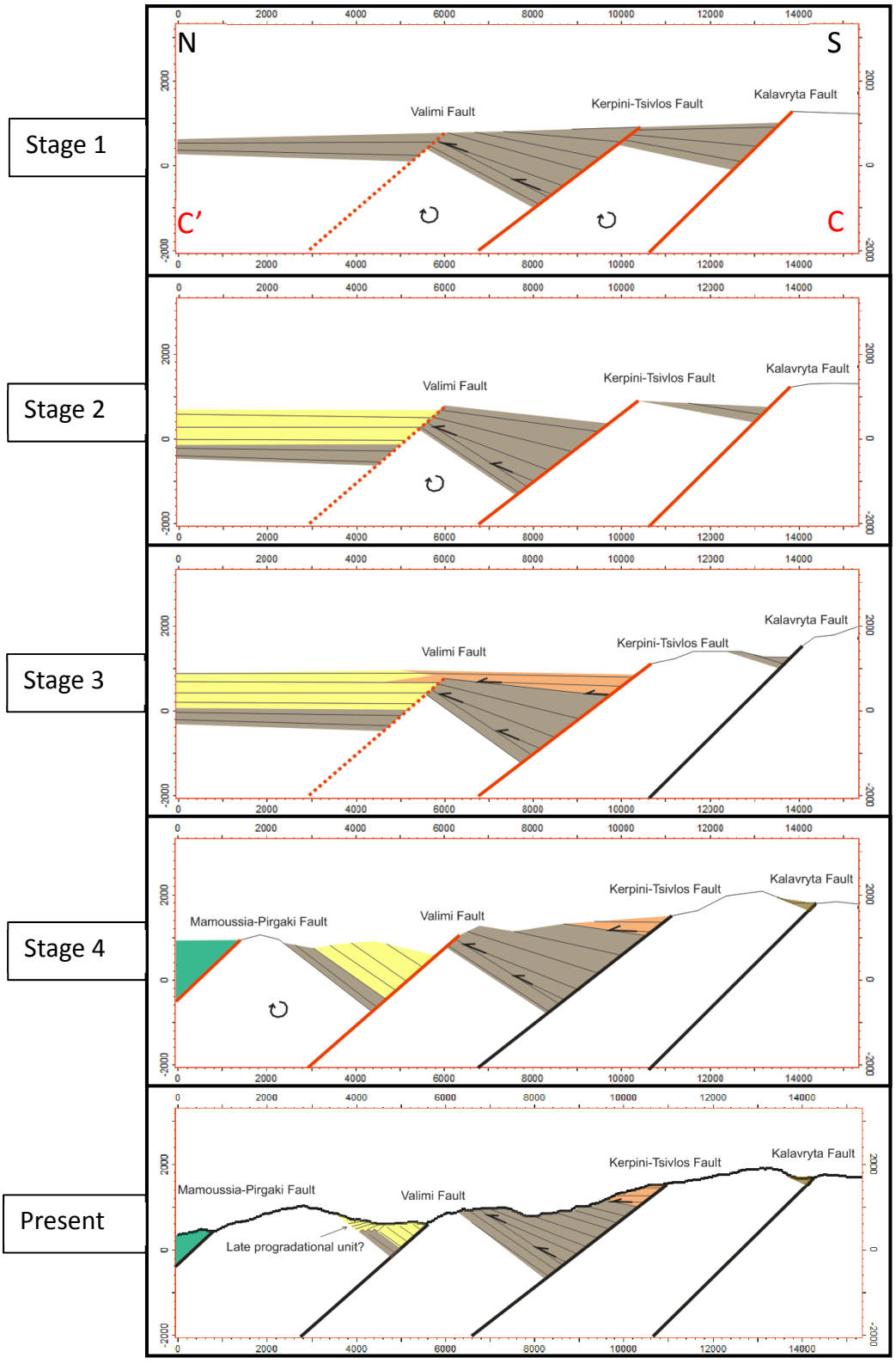

Figure 82: Proposed evolution of the eastern part of the study area. Solid red lines: active faults. Dashed red lines: active faults pre/post period of maximum displacement. Black lines: inactive faults. The location of the section is marked on Figure 77.

Chapter 6 – Conclusion

The study has provided valuable contributions to the understanding of the Corinth Rift. These are the main conclusions drawn:

- There are extensive SSW-NNE trending rift-segmenting structures in the Ladopotamos, Potamia and Krathis Rivers, concurrent to the conclusion by Dahman (2015) in Vouraikos River. These are most likely high-angle transfer faults, and they partially control the present day location of the rivers.
- The transfer faults allowed segments to evolve individually, and the total displacement was distributed across a different number of faults in each segment. The structural evolution is thus more complex than previously recognized, and it resulted in significant variations in basement elevation, lithology and bedding geometry/dip across transfer faults.
- Fault activity during the early rift stages was broadly distributed across a number of faults, whereas the southern rift margin has migrated northwards through time. This is in general agreement with most of the recent evolution models, and it contradicts models involving a simple northwards progression of narrow half-grabens (Sorel, 2000).
- The syn-rift sediments record a dominant supply from the south/southwest.
- The proposed South Graben Fault marks a sharp facies boundary between the southern alluvial succession (in the Kerpini-Tsivlos Fault Block) and the northern fluvial succession. This contradicts previous publications which propose a transitional northward alluvial-fluvial facies change (Ford *et al.* 2016).
- The Kerpini-Tsivlos Fault propagated from east to west, and it was highly active in the east during deposition of the Basal Alluvial Conglomerates.
- The Valimi Fault was active during deposition of the entire Lower Group.

Some aspects of this study remain ambiguous, where the most significant one being whether the northern and southern Basal Alluvial Conglomerates correlate or not. A detailed sedimentological comparison of these deposits are recommended for a future project, as they are critical for understanding the earliest rifting stage.

References

Anders, M. H., Dawers, N. H., & Scholz, C. H. (1993). Growth of normal faults: Displacement-length scaling. *Geology, 21*, 1107-1110.

Armijo, R., Meyer, B., King, G. C. P., Rigo, A., & Papanastassiou, D. (1996). Quaternary evolution of the Corinth Rift and its implications for the Late Cenozoic evolution of the Aegean. *Geophysical Journal International, 126*, 11-53.

Athmer, W., Groenenberg, R., Luthi, S., & Willingshofer, E. (2010). Relay ramps as pathways for turbidity currents: A study combining analogue sandbox experiments and numerical flow simulations. *Sedimentology, 57*, 806-823.

Causse, C., Moretti, I., Eschard, R., Micarelli, L., Ghaleb, B., & Frank, L. (2004). Kinematics of the Corinth Gulf inferred from calcite dating and syntectonic sedimentary characteristics. *Comptes Rendus Geosciences, 336*, 281-290.

Chery, J. (2001). Core complex mechanics: from the Gulf of Corinth to the Snake Range. *Geology, 29*, 439-442.

Collier, R., & Jones, G. (2004). Rift Sequences of the Southern Margin of the Gulf of Corinth (Greece) as Exploration / Production Analogues. *AAPG Search and Discovery, 5007*.

Dahman, A. (2015). *The Vouraikos Valley: an example of rift segmentation in the Corinth Graben, Greece.* (Msc), University of Stavanger.

Doutsos, T., & Piper, D. J. W. (1990). Listric faulting, sedimentation, and morphological evolution of the Quaternary eastern Corinth rift, Greece: First stages of continental rifting. *Geological Society of America Bulletin, 102*, 812-829.

Doutsos, T., & Poulimenos, G. (1992). Geometry and kinematics of active faults and their seismotectonic significance in the western Corinth - Patras rift (Greece). *Structural Geology, 14*, 689-699.

Flotté, N., & Sorel, D. (2001). Structural cross-sections through the Corinth–Patras detachment fault-system in northern Peloponnesus (Aegean arc Greece). *Bulletin Geological Society Greece, XXVI*, 235-241.

Ford, M., Hemelsdaël, R., Mancini, M., & Palyvos, N. (2016). Rift migration and lateral propagation: evolution of normal faults and sediment-routing systems of the western Corinth rift (Greece). *The Geometry and Growth of Normal Faults, 439*. doi:10.1144/SP439.15

Ford, M., Rohais, S., Williams, E. A., Bourlange, S., Jousselin, D., Backert, N., & Malartre, F. (2013). Tectono-sedimentary evolution of the western Corinth rift (Central Greece). *Basin Research, 25*(1), 3-25.

Ford, M., Williams, E., Backert, N., Malartre, F., & Rohais, S. (2010). Rivers and Rifting: Interaction of Normal Faulting, Erosion and Sediment Dispersal in the Corinth Rift. *Search and Discovery, 30136*.

Gautier, P., Brun, J. P., Moriceau, R., Sokoutis, D., Martinod, J., & Jolivet, L. (1999). Timing, kinematics and causes of Aegean extension: a scenario based on a comparison with simple analogue experiments. *Tectonophysics, 315*, 31-72.

Ghisetti, F., & Vezzani, L. (2005). Inherited structural controls on normal fault architecture in the Gulf of Corinth (Greece). *Tectonics, 24*(4), 1-17.

Hadland, S. (2016). *Geological Mapping and Investigation into a proposed Syn-rift Alluvial Fan Deposit in the Kerpini Fault Block, Greece.* (Msc), University of Stavanger.

Jackson, J. (1994). Active tectonics of the Aefean region. *Annual Review of Earth and Planetary Sciences, 22*, 239-271.

Jolivet, L., Brun, J. P., Gautier, P., Lallemant, S., & Patriat, M. (1994). 3D-kinematics of extension in the Aegean region from the early Miocene to the Present, insight from the ductile crust. *Bulletin de la Societe Geologique de France, 165*, 195-209.

Jolivet, L., Labrousse, L., Agard, P., Lacombe, O., Bailly, V., Lecomte, E., . . . Mehl, C. (2010). Rifting and shallow-dipping detachments, clues from the Corinth Rift and the Aegean. *Tectonophysics, 483*(3-4), 287-304.

Krumbein, W. C., & Sloss, L. L. (1956). Stratigraphy and Sedimentation.

Le Pichon, X., & Angelier, J. (1979). The Hellenic Arc and Trench System: A key to the neotectonic evolution of the Eastern Mediterranean Area. *Tectonophysics, 60*, 1-42.

Leeder, M. R., Mack, G. H., Brasier, A. T., Parrish, R. R., McIntosh, W. C., Andrews, J. E., & Duermeijer, C. E. (2008). Late-Pliocene timing of Corinth (Greece) rift-margin fault migration. *Earth and Planetary Science Letters, 274*(1-2), 132-141.

Lister, G. S., Etheridge, M. A., & Symonds, P. A. (1986). Detachment faulting and the evolution of passive continental margins. *Geology, 14*, 246-250.

Mack, G. H., & Seager, W. R. (1995). Transfer zone in the southern Rio Grande Rift. *Journal of the Geological Society, 152*, 551-560.

McNeill, L. C., Cotterill, C. J., Henstock, T. J., Bull, J. M., Stefatos, T. J., Collier, R. E. L., . . . Hicks, S. E. (2005). Active faulting within the offshore western Gulf of Corinth, Greece: Implications for models of continental rift deformation. *Geology, 33*(4), 241-244.

Milani, E. J., & Davison, I. (1988). Basement control and transfer tectonics in the Reconcavo–Tucano–Jatoba rift, Northeast Brazil. *Tectonophysics, 154*, 41-70.

Moretti, I., Sakellariou, D., Lykousis, V., & Micarelli, L. (2003). The Gulf of Corinth: An active half graben? *Journal of Geodynamics, 36*(1-2), 323-340.

Morley, C. K., Nelson, R. A., Patton, T. L., & Munn, S. G. (1990). Transfer zones in the East African Rift System and their relevance to hydrocarbon exploration in rifts. *American Association of Petroleum Geology, 74*, 1234-1253.

Moustafa, A. R. (1996). Internal structure and deformation of an accommodation zone in the northern part of the Suez rift. *Journal of Structural Geology, 18*, 96-107.

Ori, G. G. (1989). Geological history of the extensional basin of the Gulf of Corinth (?Miocene-Pleistocene), Greece. *Geology, 17*, 918-921.

Papazachos, C. B. (1999). Seismological and GPS evidence for the Aegean-Anatolia interaction. *Geophysical Research Letters, 26*, 2653-2656.

Richter, D. (1976). Das Flysch-Stadium der Helleniden - Ein Uberblick. *Zeitschrift Dt. Geol. Ges., 127*, 96-128.

Rietbrock, A., Tiberi, C., Scherbaum, F., & Lyon-Caen, H. (1996). Seismic slip on a low angle normal fault in the Gulf of Corinth: Evidence from high-resolution cluster analysis of microearthquakes. *Geophysical Research Letters, 23*, 1817-1820.

Rohais, S., Eschard, R., Ford, M., Guillocheau, F., & Moretti, I. (2007). Stratigraphic architecture of the Plio-Pleistocene infill of the Corinth Rift: Implications for its structural evolution. *Tectonophysics, 440*(1-4), 5-28.

Scott, B. (1981). The Eurasian-Arabian and African continental margin from Iran to Greece *Journal of the Geological Society of London, 138*, 719-733.

Sigmundstad, E. (2016). *Detailed Structural Mapping and Correlation of a Thick Syn-Rift Sequence in the Kerpini Fault Block, Greece.* (Msc), University of Stavanger.

Skourlis, K., & Doutsos, T. (2003). The Pindos Fold-and-thrust belt (Greece): Inversion kinematics of a passive continental margin. *International Journal of Earth Sciences, 92*(6), 891-903.

Skourtsos, E., & Kranis, H. (2009). Structure and evolution of the western Corinth rift, through new field data from the northern Peloponnesus *Geological Society Special Publication* (Vol. 321, pp. 119-138).

Stuvland, M. E. (2015). *Kalavryta and Kerpini Fault Block: Investigation into correlation and nature of sub-horizontal layers; Corinth Graben, Greece.* (Msc Master Thesis), University of Stavanger.

Syahrul, R. A. (2014). *Fault Controlled Sedimentation: A case study of the Kerpini Fault, Greece.* (Msc Master Thesis), Universiy of Stavanger.

Taymaz, T., Yilmaz, Y., & Dilek, Y. (2007). The geodynamics of the Aegean and Anatolia: Introduction. *The Geological Society of London, 291*, 1-16.

Westaway, R. (2002). The Quaternary evolution of the Gulf of Corinth, central Greece: coupling between surface processes and flow in the lower continental crust. *Tectonophysics, 348*, 269-318.

Wood, A. M. (2013). *The influence of fault geometric uncertainty on hydrocarbon reservoir and simulation models.* (Ph.D. Doctoral thesis), University of Leeds. Retrieved from http://etheses.whiterose.ac.uk/id/eprint/5885